Acoustic Emission Technology for Engineering Health Monitoring of a Wave Energy Converter

Submitted by

Jodi Walsh

to the University of Exeter as a thesis for the degree of

Doctor of Philosophy in Renewable Energy

In April 2018

I certify that all material in this thesis which is not my own work has been identified and that no material has previously been submitted and approved for the award of a degree by this or any other University.

Signature: .....

Abstract

Marine renewable energy has the potential to produce up to 20% of the UK's current electricity demand, leading to extensive research and development activities in this area. As the industry of wave energy progresses toward commercialisation, a number of barriers still limit its potential, including the cost of energy. A significant portion of this is the cost of operation and maintenance activity due to the challenging environments in which wave energy devices reside. Maintenance activity as it stands can include vessel activity and skilled workers including divers. Condition monitoring techniques designed for the wave energy industry and utilising the water that surrounds the devices could reduce maintenance costs by decreasing human intervention and the early detection of faults and degradation.

This thesis looks to explore the feasibility of underwater Acoustic Emission (AE) monitoring as a method of condition-based maintenance for wave energy converters and other marine energy devices. This is achieved through three strands of work: sea trials, component testing and propagation modelling.

Eighteen months of acoustic data from the *Lifesaver* wave energy converter, deployed at Falmouth Bay Test Facility in Falmouth Bay, UK, are re-assessed for evidence of component AE signatures. Signatures are identified and presented from the power-take-off and generator of the device.

Novel testing is conducted through submerged marine component testing adapted to include AE monitoring. Three 12-strand double braided synthetic mooring ropes undergo cyclic fatigue testing and AE signals detected can be classified by amplitude and frequency range, with increasing severity as the component loading is increased before sample failure.

Finally, propagation modelling is used to understand the effect of AE from engineering components on the local soundscape. To enable a comparison between devices, a new efficiency ratio is presented that compares the underwater acoustic energy emitted through the life cycle of the wave energy converter to the useful electrical energy produced by the device.

This thesis presents the first steps toward a novel method of condition monitoring in an ocean environment, potentially adaptable for arrays of devices.

Acknowledgements

While my PhD has been a personal journey of knowledge, discovery and determination, I can in no way claim I was alone. I was supported by academic staff, colleagues and loved ones everyday. Be it intellectual, practical or emotional support, the people I would like to mention here, and many more, have made this PhD thesis possible.

With three academic supervisors I thought that I would struggle to find a balance between them, but each one has brought unique advice and support for which I am truly grateful. Dr Phillip Thies, my primary supervisor at the University of Exeter, has been supportive, understanding, and the guide I needed to keep me focused. His knowledge of marine engineering enabled me to transition from a pure physics background to Renewable Energy and I am forever grateful for his support when difficult decisions had to be made. Dr Philippe Blondel, at the University of Bath has not only been an academic supervisor, but a friend. From his encouragement through periods of doubt, to his thorough feedback, to his refreshing view on academic work – life balance, thank you for the last 8 years! Finally, Prof. Lars Johanning, from the University of Exeter, thank you for your strategic view of my work and its context within the Marine Energy Group and the field in general, which enabled me to grow as an academic.

This work would not have been possible without its funders, the Natural Environmental Research Council, for which I was part of the first cohort of Doctoral students at the Great Western 4+ Doctoral Training Partnership. Thank you to NERC, the GW4+ DTP and its students, especially those who started this journey with me in 2014.

I would also like to acknowledge and thank my external examiner, Prof. Ian Masters (Swansea University) and my internal examiner, Dr Steve Simpson (University of Exeter) for their work and refreshing discussion of this thesis.

Thank you to my industrial supervisor, Darren Puckey of SEA (formally J+S Marine), for his technical guidance at the start of this journey and for the loan of vital equipment.

Dr Imran Bashir and Dr Joanne Garrett from the Renewable Energy Group at the University of Exeter Falmouth Campus, thank you for all the guidance, advice and support you gave. It would not have been possible without you. A special

thank you to David (Dinx) Raymond, for your help with splicing the rope samples. Dr Helen Smith, thank you for being my mentor and generally enabling me to feel empowered as a female scientist. To all others in the Renewable Energy Group, thank you for accepting me into the field.

Thank you to my Mum and Dad, Sue and Tony Walsh for teaching me the value of hard work, kindness, honesty and humour! I will always be grateful for your support and wish you both a very happy retirement just as my working life is beginning!

Finally, David Hooper, my partner in every way. Your love and devotion has been incredible. We may never understand each others PhD work but you have supported me in every way through this process. Your patience, understanding and thoughtfulness I will never forget.

Contents

Acronyms

AcTUP	Acoustic Toolbox User interface and Post processor
AE	Acoustic Emission
AET	Acoustic Emission Testing
AIS	Automatic Identification System
AMAR	Autonomous Multichannel Acoustic Recorders
COE	Cost of Energy
CSV	Comma Separated Values
DMaC	Dynamic Marine Component Test facility
EIA	Environmental Impact Assessment
EMEC	European Marine Energy Centre
FaBTest	Falmouth Bay Test facility
FFT	Fast Fourier Transform
GHG	Greenhouse Gas
GPS	Global Positioning System
MBL	Minimum Breaking Load
MRE	Marine Renewable Energy
O&M	Operation and Maintenance
PSD	Power Spectral Density
PV	Photovoltaic
RL	Received Level
RMS	Root Mean Square
SL	Source Level

SPL	Sound Pressure Level
STFT	Short Time Fourier Transform
TL	Transmission Loss
TSD	Tidal Stream Device
WEC	Wave Energy Converter

List of Figures

List of Tables

Chapter 1

Introduction

1.1 Research Context

In 2010 the energy supply sector was responsible for 35% of global anthropogenic greenhouse gas emissions (IPCC 2014), highlighting the impact that this sector has upon annual emissions and climate change. Renewable energy technologies have the potential to mitigate these emissions as acknowledged by UK (DECC 2014) and international (European Commission 2010) policy. Wind and solar energy are the most mature of the renewable energy technologies. An emerging, less mature energy technology is Marine Renewable Energy (MRE) including Wave Energy Converter (WEC) and Tidal Stream Device (TSD).

MRE has the potential to produce up to 20% of the UK's current electricity demand (DECC 2013). This has led to extensive research and development activities regarding MRE, however this industry is still in its infancy. An increasing number of WECs have reached full-scale device testing and TSDs are now being deployed as arrays of devices in a number of instances (EMEC 2017). Both WECs and TSDs are looking toward commercial availability in the near future, but there are a number of challenges to overcome before this is possible.

One of those challenges, and perhaps the largest, is to reduce the Cost of Energy (COE) in order to make the technology economically viable. The cost of Operation and Maintenance (O&M) activities are anticipated to be high because of a number of factors. MRE devices are designed to operate in energetic environments, making marine intervention difficult and costly. Specialist vessels, equipment and trained staff are required for either in-situ O&M or the recovery of devices for onshore O&M. Such energetic environments also result in short weather windows for appropriate access to devices, resulting in the scheduling of maintenance to also be challenging (O'Connor et al. 2013). This can lead to extended periods of costly device downtime.

Condition-based maintenance within the wind industry has shown to reduce device downtime, improve the operational safety of devices and reduce O&M activity costs (García Márquez et al. 2012). It is therefore important to establish reliable,

remote condition monitoring techniques as a vital tool for the implementation of condition based maintenance scheduling within the MRE industry.

1.2 Aim of the Research

This research aims to assess the feasibility and develop a method of underwater acoustic emission monitoring of MRE devices to enable a reduction in cost of O&M costs associated with WECs. This can be split into a number of objectives outlined as:

1. To assess the feasibility of using AE techniques in an underwater environment for engineering monitoring.
2. To identify AE signatures from an operational WEC that relate to the engineering of the device.
   (a) Can signatures of AE from an operational WEC be detected and distinguished?
   (b) Can AE signatures be linked to the degradation and therefore health of the device?
3. To develop and conduct laboratory testing methods to identify AE signatures relating to the components condition.
   (a) Will the use of multiple hydrophones enable the localisation of the AE source and hence component location?
4. To compare the underwater acoustics of a WEC during different periods of its lifetime.
   (a) What is the overall effect of the WECs underwater AE over its lifetime?
   (b) Are there significant variations during different periods of its lifetime?
5. To assess the propagation of underwater AE from a WEC in its environment.
6. To develop a means of comparing the underwater AE from WECs and other submerged structures.

The funders of this work are the UK National Environmental Research Council (NERC). Their vision is: "To place environmental science at the heart of responsible management of our planet." The work presented in this thesis complements the NERC vision through responsible management of the sound pollution we are adding to our waters, while still developing renewable energy which will help in the reduction of global warming.

1.3 Contribution to Knowledge

This thesis makes the following contributions to knowledge in the field of Underwater Acoustics of Marine Renewable Energy:

- Review of in-air AE health monitoring and its application to submerged MRE devices and underwater acoustic signatures relating to MRE device engineering and components
- Development and application of experimental methods for submerged AE component testing
- Original characterisation of AE signals for 12 strand double-braided synthetic mooring rope in controlled conditions
- Identification of failure location through data processing techniques
- Detailed appraisal and scrutiny of AE field measurements and feasibility of acoustic failure detection through propagation modelling methods in shallow water environments

Appendix A contains a list of publications associated with this thesis.

1.4 Content and Structure

The aim of the research presented in Section 1.2 is pursued through three methodologies around which this thesis is presented. They are shown in Figure 1.1. Each element of this cycle is interlinked to the others, and this research could have started with any one of the three. All three of these elements are needed to complete the cycle, and this framework could be transferred to other applications, devices and installations. For simplicity, this thesis follows the chronological order in which they were conducted.

Chapter 1 has introduced the motivation for this research and explicitly specified the contributions to knowledge that are discussed throughout the thesis.

Chapter 2 reviews literature relevant to the research around renewable energy, AE monitoring and underwater acoustics monitoring. Thorough scrutiny of this literature has led to a defined list of research questions that have been raised to be answered in this thesis.

Chapter 3 outlines the methods used in conducting this research. This includes tools used within underwater acoustics, component testing and the sea trials of *Lifesaver* at FaBTest, Falmouth Bay, UK. Finally in Chapter 3 the novel methodology of underwater AE monitoring of synthetic mooring rope is presented in full.

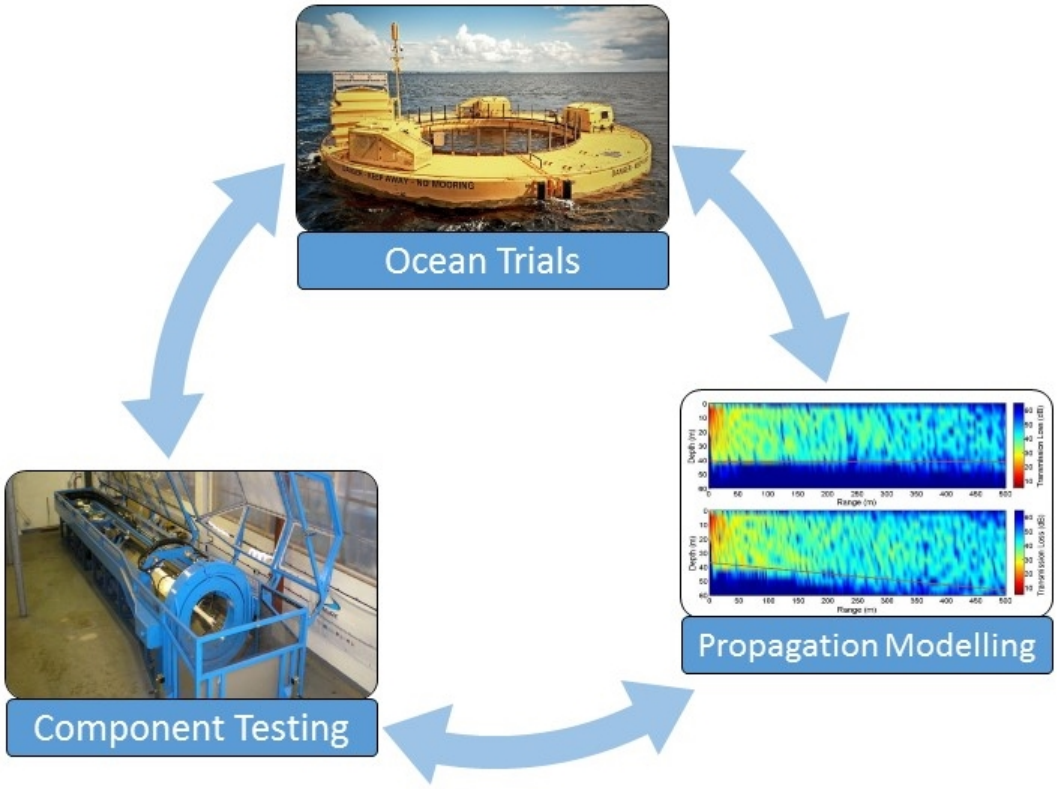

Figure 1.1: Main three strands that form the content of the thesis.

Chapter 4 is the first of three result chapters. It presents the relevant findings from the sea trials conducted on *Lifesaver* WEC at FaBTest, Falmouth Bay, UK. This body of work is one of the first deployments of long term underwater acoustic monitoring of a WEC and the first to directly link the underwater acoustics to the engineering health of the device. The chapter questions the feasibility of such a method through component signature identification.

Chapter 5 presents the results of the novel methodology presented in Section 3.4 for a 12-strand double-braided polyester mooring rope. This laboratory experiment successfully identifies a number of individual underwater acoustic signals and analyses the progression of these signals across increased tension loading.

Chapter 6 assesses the use of propagation models such as Bellhop for use with AE condition monitoring. It looks to compare the propagation of underwater AE across the periods of the *Lifesaver's* life cycle and a novel ratio is presented that considers the amount of underwater AE energy compared to the useful energy output of the WEC in question.

Chapter 7 concludes the thesis with a synoptic discussion of the results, a conclusion and identifies areas of potential further work.

Chapter 2

Background and Literature Review

2.1 Renewable Energy Technologies

In the effort to mitigate the negative effects of climate change, renewable sources of energy have the largest potential to reduce Greenhouse Gas (GHG) emissions and increase energy security world wide. In 2010 the energy supply sector was responsible for 35% of the total anthropogenic global GHG emissions (IPCC 2014). International policies recognise the need for support and investment in renewable energy (UNFCCC 2015), setting challenging targets for governments to strive towards. In the EU, the 2020 package sets the target that 20% of EU energy should be from renewable sources (European Commission 2010). In the UK, nearly 20% of electricity needs were met by renewable energy at the end of 2014 (DECC 2014).

Renewable energy is a diverse term that encompasses a number of technologies and energy generation methods. These can be broken into categories such as solar, biomass, hydroelectric, geothermal, wind, wave and tidal (Figure 2.1).

Hydropower is the action of turbines being rotated by flowing water (e.g. water mills and dams) and is the world's largest and most mature renewable energy source, representing 85% of the global renewable electricity production (IRENA 2012; Pazheri et al. 2014). However, the production of hydro power is at risk during times of drought and the production varies annually and seasonally, depending on rainfall levels, which limits the predictability of the resource (Brown et al. 2011).

Wind power harnesses the energy of moving air currents which are caused by air pressure differences (Clarke 2016). Prof James Blyth of Anderson's College, Glasgow built the first wind turbine used for the production of electricity in July 1887 (Price 2005). Now, wind power is the most developed technology after hydropower and is dominated by three-blade horizontal-axis wind turbines. It is now also the most commercially developed with more than 80 countries using wind power commercially (Pazheri et al. 2014). The cost of new wind turbines has decreased by 25% since 2010 (IEA 2017), realising economies of scales and continued improvements. Turbines are located onshore and (more recently) offshore with a capacity ranging from tens of

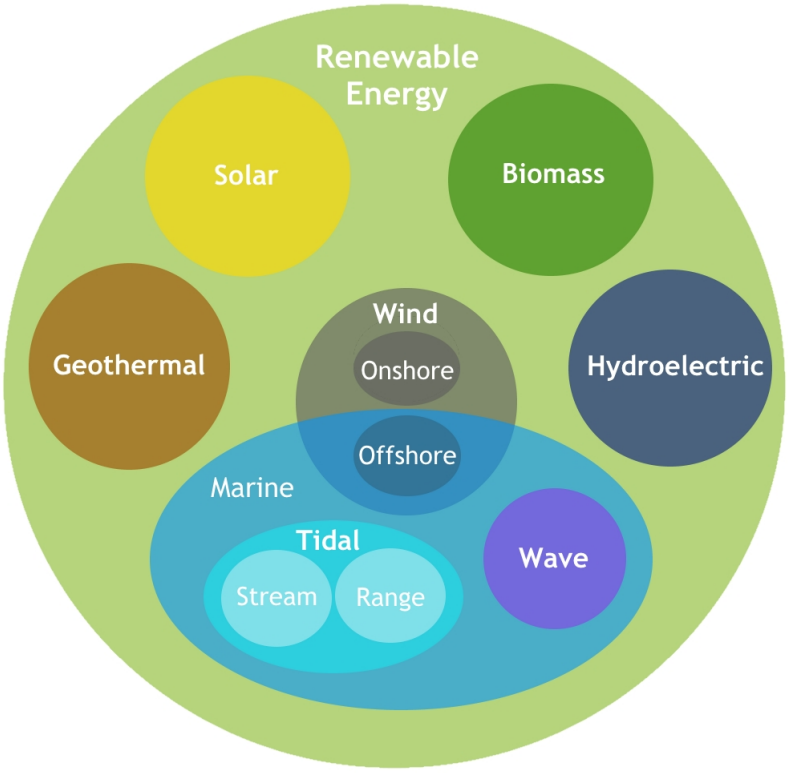

Figure 2.1: Types of renewable energy, highlighting the relationships between the MRE sectors

Watts at micro-scale to several Megawatts (Twidell and Weir 2006). Opposition to the installation of turbines is concerned with protecting the visual landscape of an area, noise pollution near residential areas and bird collisions (Twidell and Weir 2006). The industry in an attempt to both increase the size of turbines and move away from opposition, developed an increasing number of offshore projects (Clarke 2016).

Solar power, despite being a very low power option (maximum intensity at the Earth's surface is 1 kW m^{-2} (Clarke 2016)) is a well used form of renewable energy. Large collector areas are needed to gather significant quantities of power. Solar power includes the world's most rapidly growing technology in the world, Photovoltaic (PV), with a growth rate of 35% - 40% per year (Tyagi et al. 2013). While PV is a potential solution for powering rural communities, there is reduced power during peak times, and hence storage must be considered. While there are no emissions or noise pollution to consider while PV is in place, the manufacturing of the PV uses energy and noxious chemicals (Gerbinet et al. 2014; Twidell and Weir 2006).

Biomass is the material of plants and animals (including waste and residues). The use of these organic materials as a renewable energy source is biomass energy where, by burning the biomass, heat is released which can be used to generate electricity (Twidell and Weir 2006). The use of biofuel in the form of wood etc. for

cooking is still critical for about 50% of the world's population (Twidell and Weir 2006). The global operating biomass plant capacity was around 72 GW at the end of 2011 (Pazheri et al. 2014). Potential environmental effects from biomass energy include a reduction in biodiversity, water requirements and competition for food production to name but a few (Clarke 2016; Sims et al. 2007).

Geothermal power is a mature technology with established markets in several countries (Sims et al. 2007). This form of renewable energy uses the heat from the Earth's interior and is very site-specific, concentrated mainly around volcanic and plate margin areas (Clarke 2016; Pazheri et al. 2014), but provides power continuously. Geothermal power can only partially be thought of as renewable, given that the replenishment of the heat resource in the rocks takes longer than the geothermal power plant lifetime (Sims et al. 2007). Environmental impacts include use of space, noise, emissions and subsidence.

Figure 2.1 also shows MRE which encompasses those technologies found in the marine environment including offshore wind, tidal energy (tidal stream and tidal range) and wave energy. The available resource for wave and tidal energy around the UK amounts to 20% of the UK's electricity consumption at 70 TWh/yr (Carbon Trust 2011). This, combined with the added benefits of increased energy security and diversity, make MRE an attractive option for the UK's energy mix, as well as worldwide. Worldwide growth in the wave and tidal energy generation is expected to reach on average 15.2% annually until 2030 (Krewitt et al. 2009).

The offshore environment provides some unique challenges to overcome. The harsh and risky environment that MRE devices reside in are subject to high wind and waves resulting in difficult access for both installation and maintenance. Devices must have high survivability and reliability while still being cost effective and not over-engineered to profit in these difficult locations. This has been an issue for a number of developments. The *Oceanlinx* wave energy device sank during transportation to its site in South Australia (Esteban and Leary 2012) and *Wave Dragon's* mooring broke during a storm, stranding the platform near a beach in Denmark (Christensen et al. 2005). These offshore devices become unreachable during the worst weather conditions, and only accessible during clear weather windows for maintenance or transportation (O'Connor et al. 2013). However, the reward for taking energy generation offshore is the availability of larger devices (in the case of wind energy), and a large untapped resource.

Offshore wind has two advantages over onshore wind - public perception and capacity. Higher average wind speeds and less turbulence than onshore allows for greater energy capture offshore (Crabtree et al. 2015). Visual and noise concerns from residents are mitigated but there is still a concern over the environmental impacts, for example, on marine life. It is accepted that O&M costs are the largest barrier to a reduction in the cost of energy for offshore wind. O&M activity accounts

for up to 30% of the total cost of energy for offshore wind turbines (Crabtree et al. 2015). Onshore wind turbines experience faults which are easy to resolve with little effect upon the related downtime. Because offshore wind is derived from the same technology, it is expected that they will experience similar faults but due to their remote location the downtime is expected to be much longer and therefore more costly (Carroll et al. 2016; Faulstich et al. 2009, 2011; Pfaffel et al. 2017).

Tidal energy can be harnessed in two different forms: tidal range and tidal stream. Tidal range energy involves the trapping of high tide water (up to 17 m in the Bay of Fundy, Canada) and allowing it to run through a turbine at low tide (Lewis et al. 2011; Twidell and Weir 2006). Studies have estimated the UK's total theoretical tidal range resource is enough to supply around 12% of current UK electricity demand (DECC 2013). The Swansea Bay Tidal Lagoon project is currently the most advanced tidal lagoon project in the UK (Waters and Aggidis 2016). It plans to provide 320 MW, supplying approximately 155,000 homes with power. The tidal range at Swansea Bay is one of the best in the UK with an average of 6.5 m (Fijen 2017). The estimated cost of the project is substantial and risky, at £1.3 billion. There is however an injection into the economy expected from the project through jobs, tourism and UK manufacturing contracts. The environmental concerns regarding fish passage are less likely to be important, as the lagoon does not block the estuary completely. Overall, the project is set to lead the way internationally for large-scale tidal range power (Fijen 2017; Waters and Aggidis 2016).

Tidal stream energy works through similar principles to wind power. Turbines are positioned in the flow of tidal currents (horizontal movement of water), like underwater wind turbines (Lewis et al. 2011). Also like wind power, they are envisaged to be in large submerged "farms" of turbines.

Both tidal range energy and tidal stream energy rely upon highly predictable general tides which allow for forward planning and (near) certainty in power output. Locally however tidal flow is difficult to model and hence predict. Environmental concerns still exist for TSD around the impact upon underwater habitats and especially around noise pollution, specifically during the installation process of pile-driven systems (Polagye et al. 2011). Tidal range developments have impact upon the estuaries in which they would reside, for example reducing the exposure of mud flats for feeding birds (Twidell and Weir 2006). Tidal range developments come with large financial risks as the entire system must be complete before any power can be produced, whereas tidal stream allows for a small number of turbines to be producing power while others are being installed (Twidell and Weir 2006).

The work presented in this thesis focuses on wave energy but is also applicable to other offshore technology such as tidal devices. The total world resource of deep water wave energy has been estimated at 1 - 10 TW (World Energy Council 2007).

Large wave resources depend upon wind speed, duration of wind, length of fetch, and proximity to the shore (near shore waves loose much of their energy to friction with the seabed, causing the waves to break) (Clarke 2016). The most energetic wave climates are therefore coasts with exposure to the prevailing wind direction and long fetch, such as the western coasts of North and South America, Europe, South Africa and Australia (World Energy Council 2007). It was reported in (Thorpe 1999) that the economically exploitable wave resource of the world could rise to 2000 TWhr/yr if improvements to the existing devices (of 1999) were made. However, wave energy is still a pre-commercial industry and the cost of energy remains high compared to both non-renewable and other renewable energy sources (Carbon Trust 2006; Catapult Offshore Renewable Energy 2014).

Wave energy is an attractive option to create energy, given its large resource potential in specific areas and the predictability of the waves (Twidell and Weir 2006). Also, the increased energy demand during winter months is matched by an overall increased wave resource reducing the need for long-term energy storage solutions (World Energy Council 2007).

Wave energy, although still an emerging technology today, is not a new concept. Techniques for exploiting the energy from waves was first patented in the nineteenth century, and by 1981 over 1000 ideas were patented across Japan, North America, and Europe (McCormick 2007). Progress since this date has been intermittent, mainly due to inconsistent support from governing bodies (Clarke 2016).

Within the industry today, there are 8 types of WEC that are summarised by the European Marine Energy Centre (EMEC) (EMEC 2012). Each of these devices is shown in Figure 2.2 and described below.

- **Attenuators** are devices that float parallel to the wave direction. Energy is captured through the relative movement of 2 arms as waves pass them. An example of an attenuator device is *Wavepiston* from Denmark (WavePiston 2013).

- **Point Absorbers** are also made from a floating structure whose relative movement to the base is converted into energy. Examples include *Wave Star* from *Wave Star Energy ApS* in Denmark (Marquis et al. 2010), *Oceanus 2* from *Seatricity* in the UK (Tidal Energy Today 2016) and *Wave Catcher* from *Marine Energy Corporation* in the USA (Marine Energy Corporation 2016).

- **Oscillating Wave Surge Converters** harness energy from wave surges and the movement of the water particles within. An arm oscillates as a pendulum mounted on a pivoted joint in response to the movement. An example of this device type is *Wave Roller* from *AW Energy* in Finland (AW Energy 2012).

- **Oscillating Water Columns** are a partially submerged hollow structure that is open to the sea below the waterline. Within the hollow structure there

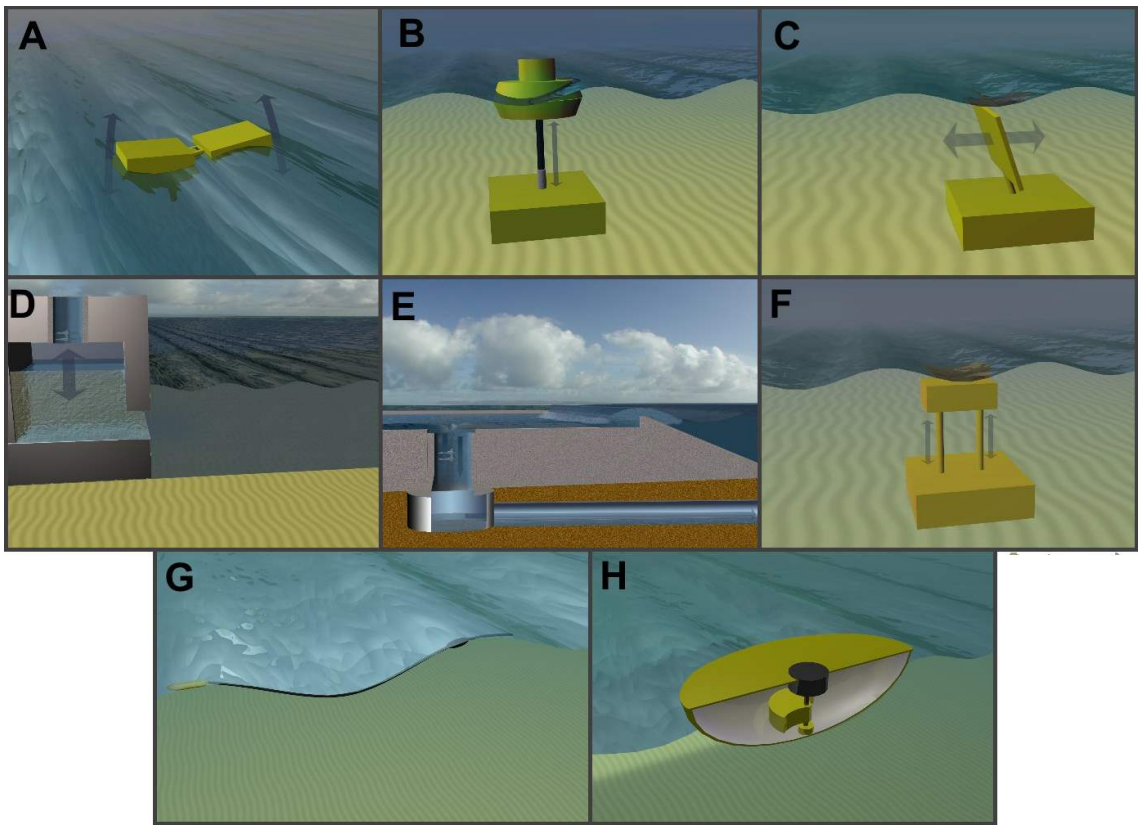

Figure 2.2: Illustrations of the 8 major types of WEC devices as described by EMEC (EMEC 2012). A: Attenuator, B: Point Absorber, C: Oscillating Wave Surge Converter, D: Oscillating Water Column, E: Overtopping or Terminator Device, F: Submerged Pressure Differential, G: Bulge Wave, H: Rotating Mass. Illustrations from (Aquaret 2009)

is water and an enclosed column of air, is compressed and depressed by the waves. This compressed air is released through a turbine. An example of this device type is *PicoOWC* from *Pico* in Portugal (Monk 2012).

- **Overtopping or Terminator Devices** use the working principle that waves break into a storage reservoir where water is collected. The water is then simply returned to the sea through a turbine. A working example of this device type is *Wave Dragon* from Denmark (Russel et al. 2016).

- **Submerged Pressure Differentials** are devices located near-shore and attached to the seabed. The motion of the waves causes the sea level to rise and fall which induces a pressure differential. An example of this device is *mWave* from *Bombora Wave Power* in Australia (Bombora Wave Power 2016).

- **Bulge Wave devices** are a rubber tube parallel to the wave direction. As a wave passes, water enters the stern, causing pressure variations along the length of the tube and creating a bulge. This bulge gathers energy along the length of the tube and exits through a turbine at the bow. The *Anaconda* by *Checkmate Seaenergy UK Ltd* is an example of a Bulge WEC (Carbon Trust

2009).

- **Rotating Mass devices** use both the heaving and swaying of the device to capture energy. The movement drives either a weight or a gyroscope to power a generator. The *Penguin* WEC from *Wello OY* based in Finland is an example of a Rotating Mass WEC (Wello 2017).

Within wind energy, the industry has a dominant device design: the three-blade horizontal axis turbine. Overall agreement on a device design has not yet happened within the wave energy industry and all device designs are developed concurrently and built by companies all over the world. Figure 2.3 shows the popularity of each device design, both worldwide and in the UK. There seems to be a general trend toward the attenuator and point absorber designs, however there are a number of undisclosed device designs within this dataset (EMEC 2017).

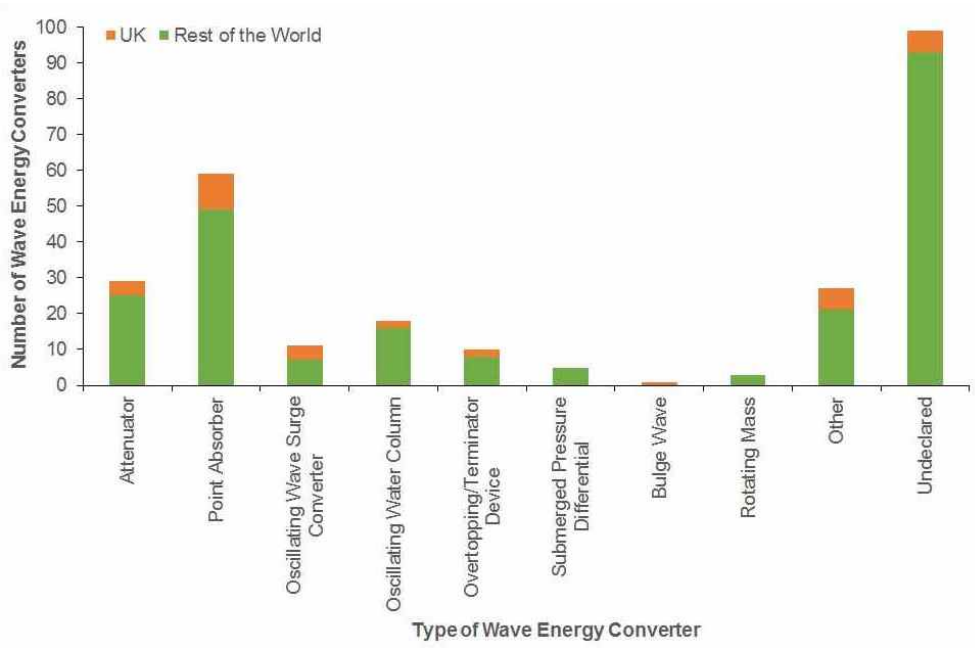

Figure 2.3: Distribution of WEC types being developed in the UK and worldwide as of January 2017, from (EMEC 2017)

A number of significant challenges still face the wave energy industry. As already described for tidal and offshore wind energy, the three main challenges are delivering cost-effective energy, the reliability and the survivability of the devices.

WECs are by design located in the sea and experience harsh conditions. While, the majority of the time, sea conditions are relatively calm, storm conditions test prototypes to their very limits of survivability, not always successfully (Thies et al. 2013). It is thought that exposed moving parts are more susceptible to damage, and therefore devices like *mWave* (Submerged Pressure Differential) are more likely to survive (Bombora Wave Power 2016). However, moving parts are unavoidable. Some devices have developed a "Storm Mode" where a defensive configuration is triggered

during worse than normal conditions. This could be through further submerging a device below the harsh surface waves of a storm like, for *Cycloidal* WEC (Atargis Energy Corporation 2012), or locking moving parts to restrict motion like for *Oyster* (Coe and Neary 2014; Whittaker et al. 2007).

Whether a device survives or not, during its lifetime, maintenance will need to be conducted. It can be expected that O&M costs will contribute a considerable amount to the overall cost of energy for wave energy. There are existing monitoring and maintenance techniques applied in offshore engineering and offshore wind in particular that can be adapted for marine renewable energy in order to reduce O&M cost.

2.2 Condition-Based Maintenance: Acoustic Emission Monitoring

Maintenance strategies can be defined by the cost of conducting a failure repair relative to the cost of preventing a failure (García Márquez et al. 2012). Reactive maintenance is the operation of a machine until a failure occurs, and reacting to that failure once it has happened. It has low costs for preventing a failure, but high repair costs for a large number of failures. Preventative maintenance involves the periodic repair and replacement of parts regardless of condition, usually dependant upon manufacturers' recommended lifetimes. This strategy has high preventative costs but very low failure repair costs. Most system maintenance strategies are a combination of these two methods finding the optimum point at which a balance between these two costs is at its minimum (Figure 2.4).

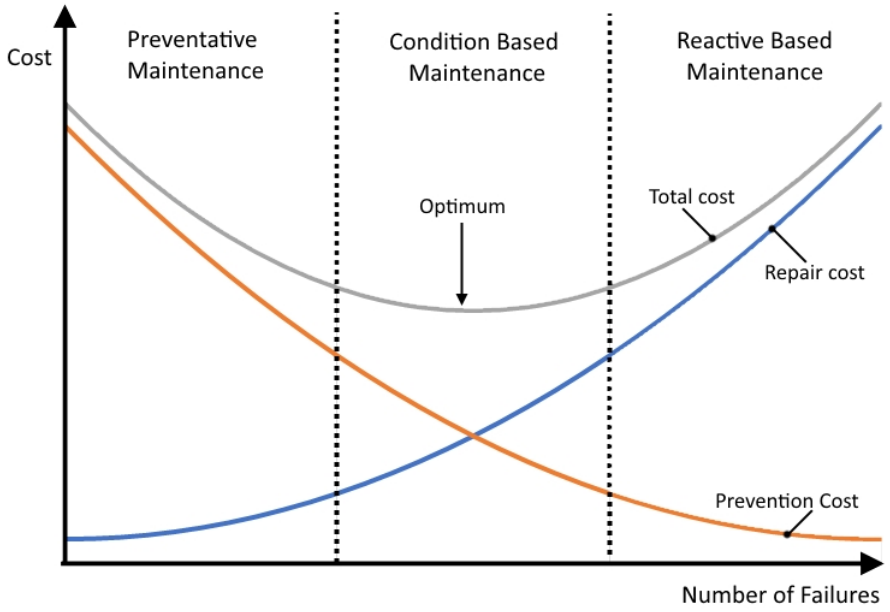

Figure 2.4: Illustration showing relative cost of maintenance strategies and the optimum point of condition based maintenance.

The costs of both maintenance strategies are increased in an offshore environment. Preventative maintenance is costly due to the expensive equipment and labour needed to conduct the maintenance. Reactive maintenance in an offshore environment results in long periods of downtime where the failure cannot be fixed due to weather conditions or short-term vessel availability.

This has been highlighted in the offshore wind industry, presently facing high O&M costs for offshore wind turbines. This is mainly due to the large downtime associated with failures. Data from 750 onshore wind turbines in Sweden during the period 1989-2005 show that 75% of annual downtime was caused by only 15% of failures (Fischer et al. 2012). Studies have shown that these failures usually originate within subsystems centred on the drive train, including the main shaft and bearings, gearbox, rotor brake, blades and generator (Carroll et al. 2016; Lu et al. 2009).

As shown in Figure 2.4 the optimum point for maintenance when considering the overall cost is found in the "condition based maintenance" sector. There are a number of methods of condition based maintenance where system parts are continually monitored and inspected to predict the onset of a failure, and determine the necessary maintenance before the failure occurs. It has been shown to improve operational safety, reduce the number and severity of system failures and minimise O&M costs (García Márquez et al. 2012). This could provide large savings - e.g. for an offshore wind turbine, O&M costs are estimated to be 20-25% of the total income (Lu et al. 2009).

Condition based maintenance is achieved with condition monitoring techniques that use sensors and signal processing to detect onsets of degradation. Examples include vibration analysis, strain measurements, oil analysis and Acoustic Emission (AE) (Al-Ghamd and Mba 2006; Mba and Rao 2006; Park et al. 1999).

AE is the sound produced by friction or the release of potential energy within a material. Within the context of condition monitoring, AE is defined as transient waves generated by a sudden release of energy caused by damage to a material, and occurs within the high frequency ranges of 100 kHz to 1 MHz (Mba and Rao 2006). Lower frequencies are generally investigated with vibration analysis. AE can produce two types of signals: i) impulsive (distinct acoustic signals, separate in time) or ii) continuous signal(s) (i.e. impulsive waveforms are not individually distinguishable). These are shown in Figure 2.5.

Although AE was originally developed for non-destructive testing of static structures, it has been adapted to monitor the health of rotating machines, including bearings, gearboxes and pumps (Mba and Rao 2006). In rotating machinery, AE can be caused by cyclic fatigue, friction, material loss and cavitation. Commercially available AE sensors are usually piezoelectric transducers, placed directly on, or close to the part to be monitored, as currently used within the wind energy sector.

AE has had a number of successes over the years. It can detect early defects

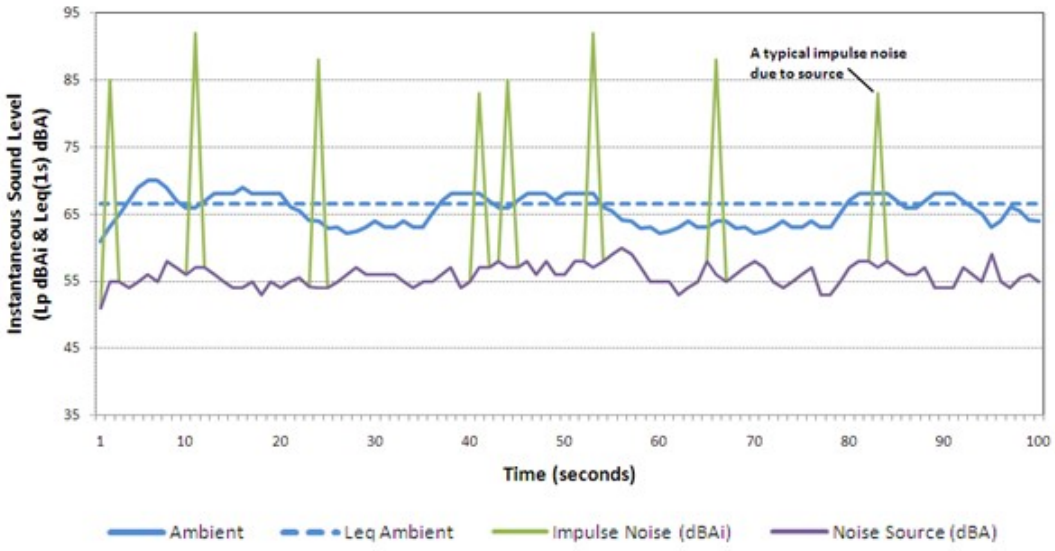

Figure 2.5: Typical time series of impulsive and continuous sources of noise (from railway noise measurements to illustrate types of signals). The green peaks are short bursts of high amplitude sound (impulses) and the purple line shows the continuous source noise. The blue lines are related to the ambient sound of this signal due to the combination of impulsive and continuous noises. Taken from (Canadian Transportation Agency 2011).

within bearings (Al-Ghamd and Mba 2006) and gearboxes (Tan et al. 2007), using a variety of signal processing techniques. For the operation of pump machinery, it is accepted that best efficiency occurs with minimal flow turbulence in the system, i.e. minimum AE activity (Alfayez et al. 2005). For moorings, direct correlations between AE and breaks of fibres (Park et al. 1999) or steel wire cables (Gaillet et al. 2009) have been reported. These studies and others (detailed in (Mba and Rao 2006) and later in Table 2.1) show the potential of this technology for a wide variety of components within the MRE sector, if it can be adapted for an underwater environment.

AE offers a number of advantages in underwater environments where there is often a large amount of low frequency (<10 kHz) ambient noise, especially with local shipping which can be intermittent. AE primarily focuses on the higher frequencies as a way of monitoring a system with less interference. The frequency ranges of interest will become clearer once specific components have been tested, but it can be conservatively assumed that all frequencies in the range 1 Hz to 1 MHz could provide useful information.

Another advantage is that sound does not attenuate as quickly in water as in air. In air, attenuation (1 kHz, 50% humidity) is 4.7 dB km^{-1} compared to attenuation in water (1 kHz, 10°C) of 0.07 dB km^{-1} (Kaye & Laby Online 2005). Sensors can be placed away from a WEC, where they can monitor multiple parts of a system at once. The use of water as a "connecting medium" in (Casey et al. 1987) was very successful in detecting wire breaks with no reduction in signal amplitude at a distance of 100

mm. Some information (e.g. shear waves, evidently not transmitted through water) was lost, or reduced to specific components. AE associated to wire fracturing was also investigated in air (Alfayez et al. 2005), showing a direct correlation between wire breaks and AE counts. Similar results were obtained for fibres, also in air (Casey et al. 1985). Impulsive AE would be expected to follow the same principles underwater.

Experiments with other components in air give indications of what to expect underwater. Rolling element bearings can produce both impulsive and continuous emissions across a wide frequency range (up to 2 MHz), and it can be related to the geometry and speed of the bearing. Signal processing techniques such as ringdown counts, energy, Root Mean Square (RMS) and peak amplitude have all shown events to increase with the size of different types of defects (Choudhury and Tandon 2000; Elforjani and Mba 2010; Li et al. 1999). In James Li and Li (1995), faults were detectable 0.3 m from the bearing, whereas within all other investigations, sensors were placed onto or very close to bearings.

Evidence of degradation within gearboxes produces similar acoustic results. High frequency (up to 1 MHz) impulsive and continuous-type components would therefore be expected. Amplitude, RMS and ringdown counts all increased with defect size in e.g., (Price et al. 2005; Tan et al. 2007; Tandon and Mata 1999) and it was also found that RMS increased with misalignment of gears (Toutountzakis and Mba 2003). In these studies, sensors were placed upon gears or on the gearbox.

Although pumps are not always found in WEC systems, there have been investigations in air and in water into the detection of incipient cavitation. Cavitation in air corresponds to a continuous broadband spectrum (20 Hz to 20 kHz) (Al Thobiani 2011), and incipient cavitation produced an increase in RMS and peak amplitude (Al Thobiani 2011; Alfayez et al. 2005). Similar results underwater were found within a similar frequency range (20 Hz – 20 kHz) (Al Thobiani 2011).

Table 2.1 summarises these results and provides a quality matrix of acoustic properties, faults and expected frequency ranges, emission types and general findings of studies in air (unless otherwise stated). These are useful when considering similar faults and mechanisms underwater. It is important to note that frequency analyses were conducted in some references e.g. (Casey et al. 1987; Price et al. 2005), but as it is not directly transferable to an underwater situation, it is not included in Table 2.1.

Table 2.1: Quality matrix of AE for components relevant to underwater AE techniques (Walsh et al. 2017a).

Mechanical Part	**Fault Details**	**Frequency Range**	**Emission**	**General Findings**
Rolling element bearing (ball bearing and cylindrical bearing)	Natural and seeded defects located in multiple locations of bearings	In air 100 kHz to 2 MHz	Impulsive and continuous components	Increase in ring down counts and energy with defect size. SPL_{RMS} and peak amplitude increased with defect size for rough, point and line defects. Ability to detect faults 0.3 m from bearing.
				Choudhury and Tandon (2000), Elforjani and Mba (2010), James Li and Li (1995), Li et al. (1999), and Tan et al. (2007)
Gearbox	Pitting and scuffing of gear tooth	In air 100 kHz to 1 MHz	Impulsive and continuous components	Increase in SPL_{RMS} with defect size and due to misalignment. Increase in (wideband) amplitude and ring down counts with defect size.
				Price et al. (2005), Tan et al. (2007), and Tandon and Mata (1999)
Pump	Incipient and developed cavitation	In air 5 Hz to 20 kHz	Continuous	Minimum noise at best-efficiency point of the pump, due to minimal flow turbulence. Cavitation produces broadband acoustic spectrum. Increase in SPL_{RMS} and peak amplitude cavitation onset.
		Underwater 0.1 Hz to 100 kHz	Continuous	Frequencies less than 8 kHz contained mechanical noise. Noise signal was a better parameter to sense the occurrence of cavitation (than traditional methods).
				Al Thobiani (2011), Alfayez et al. (2005), and Christopher and Kumaraswamy (2013)
Rope	Fibre and wire rope fractures and breaks	In air 100 kHz to 600 kHz	Impulsive	1-to-1 correlation between AE events and broken fibres/wires.
	Wire rope breaks	In air *through* water 1 kHz to 200 kHz	Impulsive	Wire breaks detected remotely. No information at frequencies < 25 kHz due to non-propagation of shear waves in water.
				Casey et al. (1987, 1985) and Park et al. (1999)

Table 2.2: Quality matrix of underwater AE for devices and components of Marine Energy devices.

Device name	**Mechanical Part & Fault Details**	**Frequency Range**	**Emission**	**General Findings**
Lysekil WEC	Incorrect assembly of device	Broadband up to 20 kHz	Impulsive	1-s high-amplitude pulses that saturated the recorder Haikonen et al. (2013)
Pelamis P2 WEC	Various components	100 Hz to 5 kHz	Impulsive	Clanking from chains, received levels 139 dB re 1 $\mu Pa^2/Hz$ power spectral levels at 1 kHz. Rattle, received level of 120 dB re 1 $\mu Pa^2/Hz$ power spectral levels at 2.5 kHz. Squeak with a slight sweep in frequency over a narrow band centred on 900 Hz. Received levels of 127 dB re 1 $\mu Pa^2/Hz$ with duration of > 0.5 s. Banging with received levels of 150 dB re 1 $\mu Pa^2/Hz$ at 100 Hz with durations of 0.5 - 1 s. Lepper et al. (2012)
Searay WEC	Fore generator identification	Above 800 Hz	Continuous (periodic)	Could identify WEC if no shipping. Increases in spectral levels that are consistent with the WEC torque and shaft speed in the fore generator. Bassett et al. (2011)
Wavestar WEC	Hydraulic pump	150 kHz	Continuous (tonal)	During pump start-up and shut-down a tonal noise was detected at 150 kHz with SPL 121 - 125 dB re 1 μPa Robinson and Lepper (2013) and Tougaard (2015)
Scotrenewables Tidal Power Ltd. tidal turbine	Anchor block and clump weight identification	Undisclosed	Impulsive	Sounds with "effective peak-peak source level" estimated 154 - 173 dB re 1 μPa Robinson and Lepper (2013)
Verdant Tidal Turbines	Turbine blade fault	Not disclosed	Continuous	More noise generated than expected Reported source level of up to 145 dB re 1 μPa referred to 1 m. Robinson and Lepper (2013)

2.3 Underwater Acoustic Monitoring

Underwater acoustics is the method of choice in assessing the environmental impact of the sound radiated by WECs and other underwater operations (Lepper et al. 2014). Generally these studies inspect Sound Pressure Level (SPL) averaged over a broad frequency band and variations, e.g. SPL_{RMS}, to investigate the impact that the SPL created by the WEC could have upon the behaviour and health of marine wildlife (Robinson et al. 2014).

For example, the underwater acoustics from *Wavestar* WEC was recorded for just 57 minutes at a distance of 25 m. It was found that the broadband SPL was 123 dB re 1 μPa, irrespective of its operational status, therefore being unlikely to affect marine mammals (Tougaard 2015). A $1/7^{th}$-scale prototype of *SeaRay* WEC was recorded for a total of 4 hours at distances from 10 m to 1500 m. Broadband SPLs ranged from 132 dB re 1 μPa at <100 m to 116 dB re 1 μPa at 1100 m (Bassett et al. 2011). In this case, a source level could not be determined due to significant amounts of anthropogenic noise. The *Pelamis P2* device was recorded for 30 hours at average distances between 250 - 350 m. Lepper reports a maximum increase in the sound levels in the range of 10 to 20 dB re 1 μPa when *Pelamis P2* device is present (Lepper et al. 2012).

These studies and others (see Austin et al. 2009; Robinson and Lepper 2013), carried out for environmental purposes, have already revealed a number of engineering events and faults. These are summarised in Table 2.2 and described below. Table 2.2 is constructed with similar information included as is in Table 2.1 in order to draw a parallel between the established field of AE in air and the relatively new underwater AE.

Tonal elements of WECs have been noted in a number of studies. For the *Wavestar* WEC, the tonal noise of the hydraulic pump during start-up and shut-down was discernible (Robinson and Lepper 2013; Tougaard 2015). The *SeaRay* WEC induced increases in spectral levels consistent with the torque and shaft speeds in the fore generator (Bassett et al. 2011). These cases provide evidence that WEC engineering processes are detectable, even when data collection is not specifically designed for their detection.

Impulsive signals have also been recorded from MRE devices. Impulses with an effective peak-peak source level estimated as 154 to 173 dB re 1 μPa were recorded from the *Scotrenewables Tidal Power Ltd* WEC and attributed to the anchor block and clump weight (Robinson and Lepper 2013). The *Pelamis P2* WEC was associated to a "clanking" sound 333 m from the device, with no discussion as to its possible source (Wilson et al. 2014). This particular signal lasted ca. 1 s, within a frequency range of 0 to 6 kHz, strongest around 1 kHz.

Two other studies revealed unexpected acoustic signals, later attributed to device faults. *Verdant* tidal turbines generated "more noise than was expected" (Robinson

and Lepper 2013), and it was later found that a blade on one of the six turbines was broken and another was subject to an incipient failure. Measurements of two point absorber WECs at *Lysekil* (Haikonen et al. 2013) reported a number of 1-s high-amplitude impulses that saturated the recorder (up to 20 kHz). These impulses were found to be due to impacts on the end stop within the WECs. At the times of recording, the significant wave height was 0.5 m, below the 2-m peak-to-peak wave height expected to fully activate the end stop. It was later found that the device closest to the hydrophone (20 m away) was incorrectly assembled and causing these acoustic emissions. These measurements were taken from a distance of 20 m and 40 m. The duty cycle was recording 5 minutes of every 30 minutes over 39 days, but this did not prevent detecting these acoustic emissions.

The opportunity presented by this literature review is the combination of AE and underwater acoustic monitoring of MRE devices. By monitoring the AE of MRE devices for engineering faults as well as for environmental purposes, the costs of O&M can be reduced, in turn reducing the overall cost of energy. Figure 2.6 shows how the two fields presented here can be combined to explore underwater AE condition monitoring of MRE.

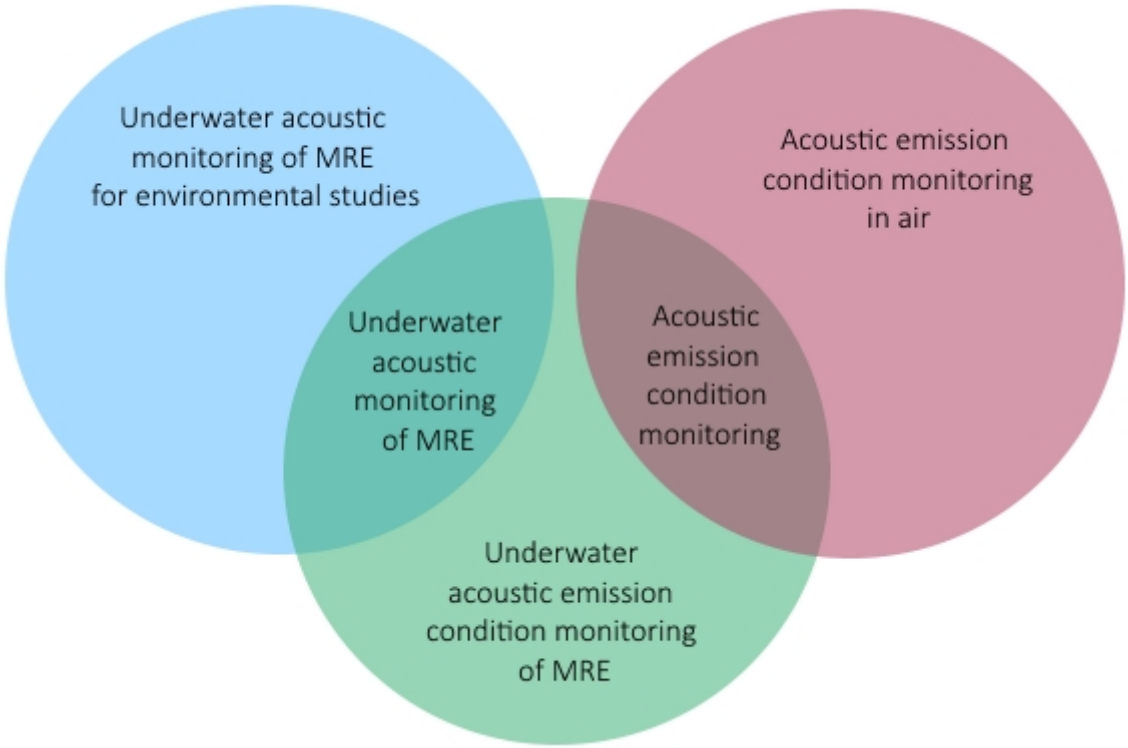

Figure 2.6: Venn Diagram to highlight the research in relation to already established fields.

2.4 Fatigue Theory

When a single load is applied to a structure that is far less than the static strength of the structure, no damage is done. However, if that same low load is repeatedly applied many times it can induce complete failure. This is called fatigue (Schijve 2009).

Fatigue lifetime (from the first load application to failure due to fatigue) can be split into 2 periods - crack initiation period and crack growth period - and is shown in Figure 2.7. The crack initiation period is a surface phenomenon. It starts with a repeated load application on the structure leading to crack nucleation occurring on the < 1 μm sale. Microcrack growth then occurs in the scale of 1 μm to 1 mm scale. Finally, the crack growth period occurs with macrocrack growth on the > 1 mm scale until complete failure of the structure. The crack growth period is a bulk material phenomenon.

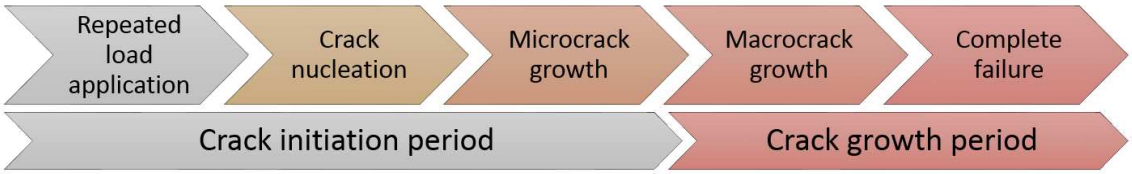

Figure 2.7: Overview of the stages of fatigue life

Because the crack initiation period is a surface phenomenon the things that effect it are surface effects such as roughness, surface damage and treatments and environmental effects. Because the crack growth period is a bulk phenomenon the material bulk properties and environment effect this period.

In order to test the fatigue mechanisms of a structure, cyclic loading must be applied up to a maximum force that is lower than the strength of the structure.

2.5 Research Questions Raised

There are 2 main areas in which this raises a number of research questions that have not yet been addressed by the scientific community; underwater AE component testing and the effect upon the local soundscape around WECs.

- What AE is emitted underwater by individual components of WECs?
  - Can this be linked to the degradation and therefore health of the device?
  - Is it possible to do this testing in a laboratory setting?
  - Will the use of multiple hydrophones enable the localisation of the AE source and hence component location?
- How does the AE from WECs propagate in a shallow water environment?

- What is the best way to calculate this for condition monitoring purposes?
- What is the overall effect of the WECs underwater AE over its lifetime?
- Are there significant variations during different periods of its lifetime?
- Can this be directly compared between WECs and other offshore devices?

Chapter 3

Methodology: Acoustic Tools and Engineering Tests

The content of this Chapter draws from two peer- reviewed journal publications, (Bashir et al. 2017; Walsh et al. 2017a), as well as one publication to be submitted which is developed from a combination of the conference papers (Walsh et al. 2016, 2017b).

3.1 Underwater Acoustics

While astronomers and astrophysicists seek to understand stars and planets light years away, underwater acousticians consider the underwater realm that covers over 70% of the planet Earth. Underwater acoustics has been used since World War I for the detection of submarines using passive acoustics. Active acoustics saw a jump in success during World War II with the development of sonar systems (Lurton 2002). During much of the 20^{th} Century, underwater acoustics was a priority for naval defence development but fast forward to the turn of the millennium and the understanding of climate change leads scientists to want to quantify the effect of excessive underwater noise on marine wildlife.

Today renewable energy technologies reside in offshore locations, and the once quiet oceans of the world are being filled with machines. By understanding the link between these machines and the underwater acoustics produced, the effects upon the environment can be mitigated, and improved underwater machine systems can be developed. In order to carry this out, a number of metrics, methodologies and tools must be utilised as outlined in this section.

3.1.1 Acoustic Quantities

Sound is a physical pressure wave that travels through a medium by the oscillation of its particles. It is described by the variable pressure, p, measured in Pascals

$[Pa]$, that is a deviation in the ambient pressure caused by a sound wave. This longitudinal wave can be continuous or impulsive and has a number of properties as shown in Figure 3.1.

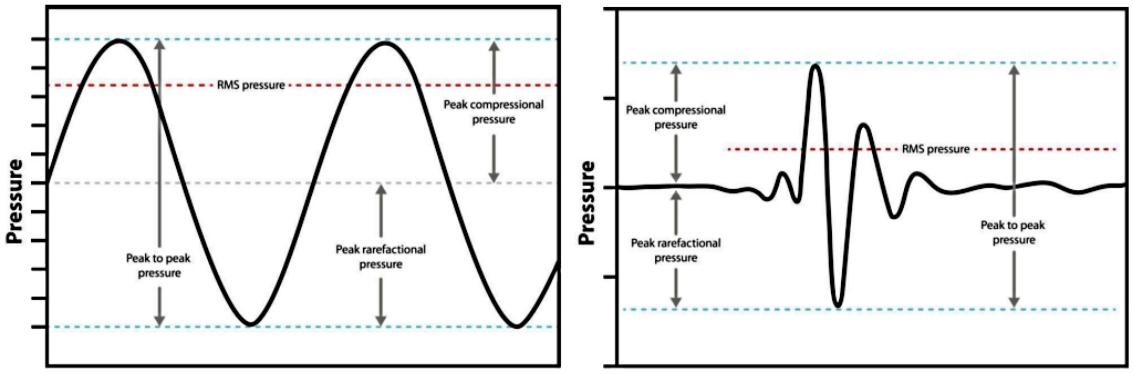

Figure 3.1: Properties of a continuous sound wave (left) and sound pulse (right) from (Robinson et al. 2014).

A pressure wave has a number of properties, as shown in Figure 3.1. This includes peak-to-peak pressure, the difference between the highest and the lowest measured pressures, and RMS pressure which is calculated as

$$p_{RMS} = \left\{ \frac{1}{t_2 - t_1} \int_{t_1}^{t_2} p(t)^2 dt \right\}^{\frac{1}{2}} \tag{3.1}$$

where t_1 and t_2 are the start and end of the time interval to be averaged over. This is true for both continuous and impulsive sound waves, but as can be seen from Figure 3.1 these properties will differ due to the shape of the wave.

3.1.2 Acoustic Metrics and Visualisation

It is common to express acoustic quantities in terms of levels, with the units decibels, $[dB]$. A level expresses the magnitude of a quantity as a logarithmic ratio to a reference value, which for acoustics is the ambient pressure of the medium the sound wave is travelling in. The most basic of these metrics is the SPL given by,

$$SPL = 10log_{10}\left(\frac{p^2}{p_0^2}\right) = 20log_{10}\left(\frac{p}{p_0}\right), \tag{3.2}$$

where p_0 is the reference pressure of the medium. In air $p_0 = 20$ μPa and in water $p_0 = 1$ μPa. This means that an SPL in air and an SPL in water cannot be directly compared. To make the reference pressure clear, the unit of SPL (in water) is dB re 1 μPa.

The average SPL can be calculated using the SPL_{RMS} where p in Equation 3.2

is substituted for p_{RMS}.

$$SPL_{RMS} = 20log_{10}\left(\frac{p_{RMS}}{p_0}\right), \tag{3.3}$$

To understand the frequency characteristics of a sound pressure signal, it is converted into the frequency domain using the Fast Fourier Transform (FFT). The signal is divided into small segments of time. Each segment undergoes FFT to understand the amplitude of each frequency component. This is called a Power Spectral Density (PSD), with frequency, f, on the x-axis and SPL on the y-axis, giving the amplitude of each frequency component. This is particularly helpful when looking for individual frequency components within a signal.

To fully visualise the data, the PSD for each segment is aligned next to each other on a time scale (x-axis), with the frequency component on the y-axis and a colour coded surface representing the amplitude of the signal. An example of this is shown in Figure 4.14 and is called a spectrogram. It is particularly helpful to assess how a signal changes, both with amplitude and frequency, over a given time period.

An acoustic signal can also be understood in terms of power and energy (Polagye 2017). The SPL (or SPL_{RMS}) can be considered as the amount of power being entered into a system. Consider an SPL received at a distance r from a source. This can be converted to the power output of the source by considering the area, A, over which the sound is emitted. If the SPL is expressed in dB re 1 μPa then the SPL can be expressed in the power unit [Watts] as,

$$SPL[W] = \frac{Ap^2}{\rho c} = \frac{4\pi r^2}{\rho c}(10^{-6}\times 10^{\frac{SPL[dB]}{20}})^2, \tag{3.4}$$

where ρ is the density of the water and c is the speed of sound in water. In a well mixed medium these variables can be considered constant, $\rho = 1024\ kgm^{-3}$ and $c = 1490\ ms^{-1}$ (Bassett et al. 2012).

The total energy produced from n number of different sources can be described as,

$$E[J] = \sum_{i=1}^{n} SPL_i[W]\times t_i[s], \tag{3.5}$$

where t_i is the time period that source i is active for (Bassett et al. 2012). The resulting energy, E is the total energy emitted by n sources of sound and enables an understanding of the energy input into the ocean by a source or multiple sources.

3.1.3 Sound in the Ocean

The ocean is a noisy place, with numerous natural and anthropogenic sources of ambient noise. These sources of noise were compiled by Wenz and visually described in what is commonly referred to as Wenz Curves shown in Figure 3.2 (Wenz 1962).

He concluded that ambient noise in general is a composite of three sources: i) turbulent-pressure fluctuations, ii) noise from bubbles and spray and iii) ocean traffic. Figure 3.2 shows the frequency and spectrum level characteristics of each source of noise including earthquakes, precipitation and sea states. The graph clearly shows that more ambient noise is concentrated at the lower frequencies, while it is less dominant at high frequencies.

At low frequencies (< 300 Hz) ambient noise is dominated by shipping (Chapman and Price 2011). Since the 1960s, vessel traffic in the ocean has doubled and the vessels occupying the ocean have increased in size and power. Perhaps unsurprisingly, this has led to an increase in the ambient noise levels in the ocean. The European Commission's Marine Directive has a goal to achieve "Good Environmental Status" of EU marine waters by 2020 in which Descriptor 11 is "Introduction of energy (including underwater noise) does not adversely affect the ecosystem" (European Commission 2010).

Natural sources of underwater noise come from sea state, precipitation, and marine life (communication and movement). Anthropogenic sources of underwater sound include ships (naval, fishing, cargo, recreation, construction etc.), seismic exploration, sonars, industrial activity (e.g. drilling, trawling, dredging), explosions and low-flying aircraft (Erbe 2010). Shipping noise has already been described as the largest contributor to underwater noise, and it is made up of two main components: machine noise and hydrodynamic noise (Erbe 2010). Even the noise not produced underwater will radiate through the ship's hull into the ocean. Another increasing source of anthropogenic noise in the ocean is pile driving (Tougaard et al. 2008). Offshore wind turbines are now installed in large numbers offshore and often require noisy pile driving as structural foundation. Mitigation methods to reduce the effect on the marine life are used such as bubble curtains to reduce sound levels and warning blasts to move suseptible animals away (Nedwell and Howell 2004).

Sound in the ocean propagates further than in air. The amplitudes of sound waves do not diminish as quickly, allowing them to travel further. This means that increased shipping in a port could have a large effect on the ambient sound level in the deep ocean. In general, this is because the density of the medium (water) is much higher than in air, allowing for the transfer of energy from particle to particle to happen much faster. The speed of sound in air is 343 m s^{-1} and in water is around 1,500 m s^{-1}.

In reality, it is a little more complicated as a number of variables affect the velocity of sound in the ocean. The main variables are temperature, hydrostatic pressure (related to depth) and salinity (Lurton 2002). A typical depth sound velocity profile is shown in Figure 3.3. The profile is split into a number of layers. In each layer a different variable dominates to determine the sound velocity which will vary between 1,450 m s^{-1} and 1,600 m s^{-1}.

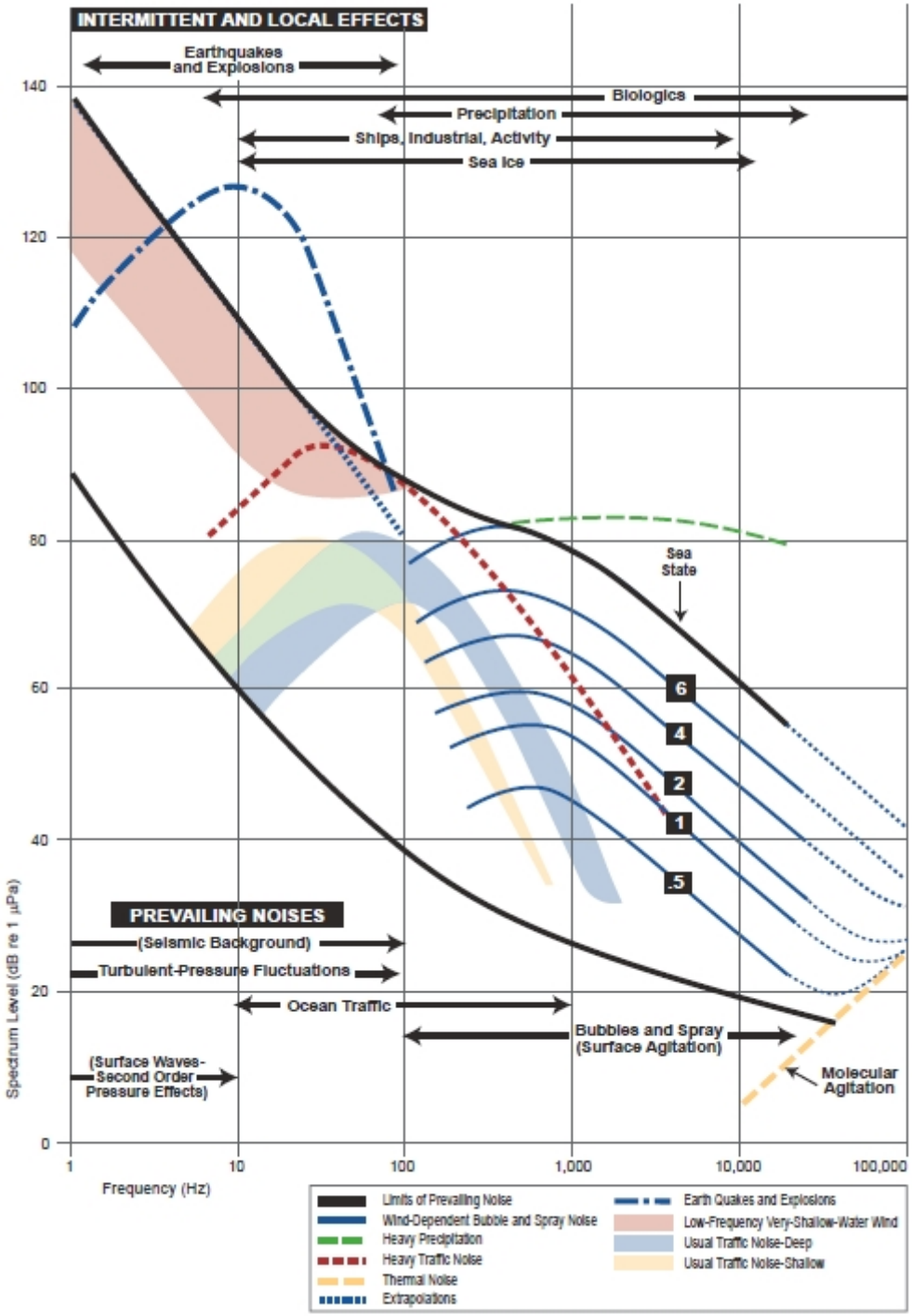

Figure 3.2: Wenz curves: Ambient noise spectra detailing both natural and anthropogenic sources of underwater noise (Wenz 1962).

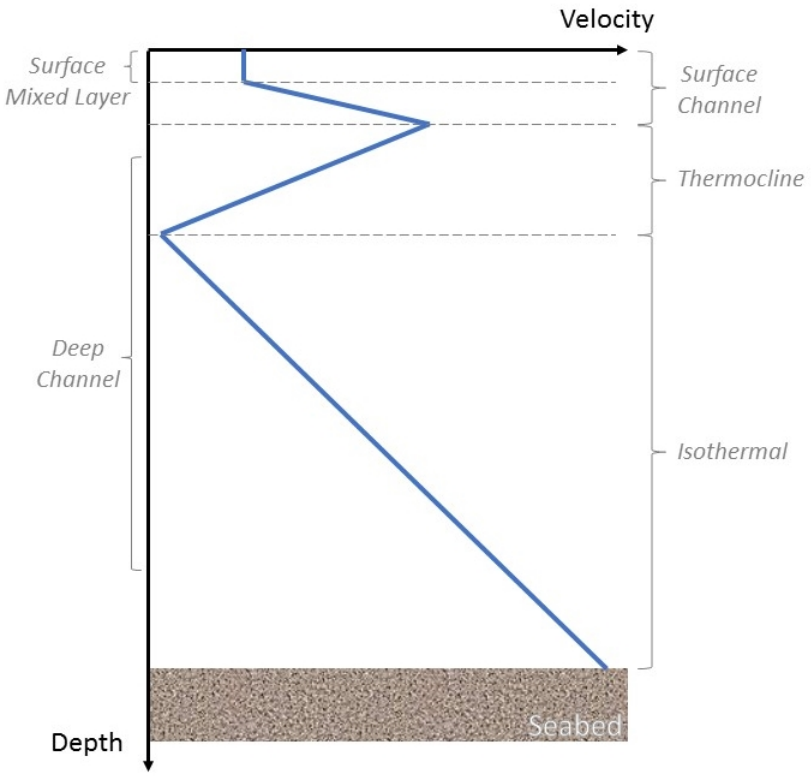

Figure 3.3: Illustration of the sound velocity profile for the ocean. The x-axis represents the sound velocity and the y-axis represents depth (sea surface at the top, sea bed at the bottom). Adapted from (Lurton 2002).

The very surface of the ocean is the surface mixed layer, where wave action creates mixing of the particles and hence a constant sound velocity that is dependant upon external factors such as season and precipitation. At a depth beyond this, but still within the surface channel, the hydrostatic pressure is the dominating variable and the sound velocity increases with increasing hydrostatic pressure. The sound velocity then decreases as temperature becomes the dominant variable. This is called the thermocline where a significant drop in temperature with depth causes the sound velocity to fall to its lowest. At the end of the thermocline, the temperature then stays relatively constant and the hydrostatic pressure dominates again. This causes an increase in sound velocity in the deepest isothermal layer down to the seabed. This is only an example sound speed profile and factors such as location, boundaries, bathymetry and depth will adjust this profile in specific locations. For example, the sound speed profile in the summer for the North Atlantic Ocean near 23°N, 70°W ranges from 1,540 m s^{-1} at the surface, to a minimum of 1,490 m s^{-1} at 1.2 km to 1,525 m s^{-1} at the seabed at 4 km depth (Etter 2013).

3.1.4 Sound Propagation

As an acoustic wave propagates through a medium, it loses energy becoming quieter the further it travels from the source. This is called the Transmission Loss (TL).

There are two components of energy that make up TL: spreading loss and absorption loss.

Spreading loss is a geometric property where the acoustic energy from a source is spread over an increasing surface area hence the intensity of the sound decreases. The simplest of these scenarios is spherical spreading loss (assuming an homogeneous infinite medium with a point source) as shown in Figure 3.4. The decreased acoustic energy between surface 1 and surface 2 is inversely proportional to the ratios of the surface areas of the spheres which allows us to consider the TL over the distance $R = R_2 - R_1$. The reference distance the transmission loss is considered over is usually $R_{ref} = 1\ m$.

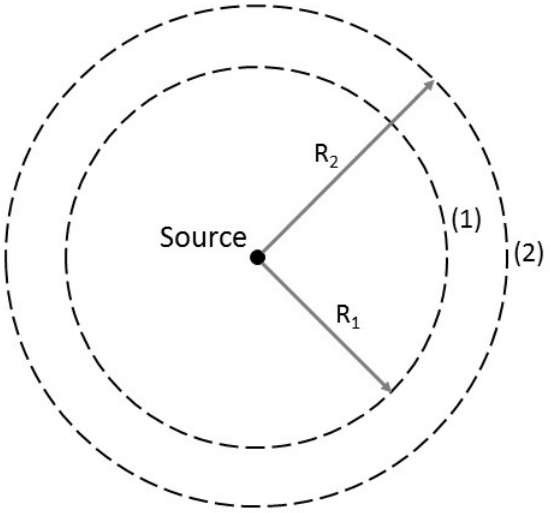

Figure 3.4: Spherical spreading from a point source.

The TL is then most commonly expressed as,

$$TL = 20log\left(\frac{R}{R_{ref}}\right) = 20log(R). \tag{3.6}$$

Absorption losses are due to sea water absorbing part of the transmitted acoustic energy and dissipating it in other ways, hence sea water is a dissipative propagation medium. The decrease in amplitude at any point is proportional to the amplitude itself. This is most commonly accounted for as an attenuation in the TL estimation as,

$$TL = 20log(R) + \alpha R \tag{3.7}$$

where α is the absorption coefficient, usually expressed in the unit of dB km^{-1}.

Absorption is highly dependant upon the frequency of the sound, f. In seawater absorption comes from three factors: pure water viscosity (increases with squared frequency), the relaxation of $MgSO_4$ molecules (below 100 kHz) and the relaxation of $B(OH)_3$ molecules (below 1 kHz). This is accounted for using the well-known model by Francois-Garrison (Lurton 2002). The absorption coefficient is made up of

3 terms, one for each contribution of absorption. They are dependant upon depth, z, temperature, T and salinity, S enabling a relationship to be found between α and f. In Figure 3.5 the relationship between each component and f is shown as well as the overall absorption coefficient, α for $T = 15$ °C, $S = 35$ p.s.u. and $z = 0$ m. As can be seen in Figure 3.5, for frequencies below 1 kHz absorption losses are less than 0.1 dB km^{-1} and therefore are not significant.

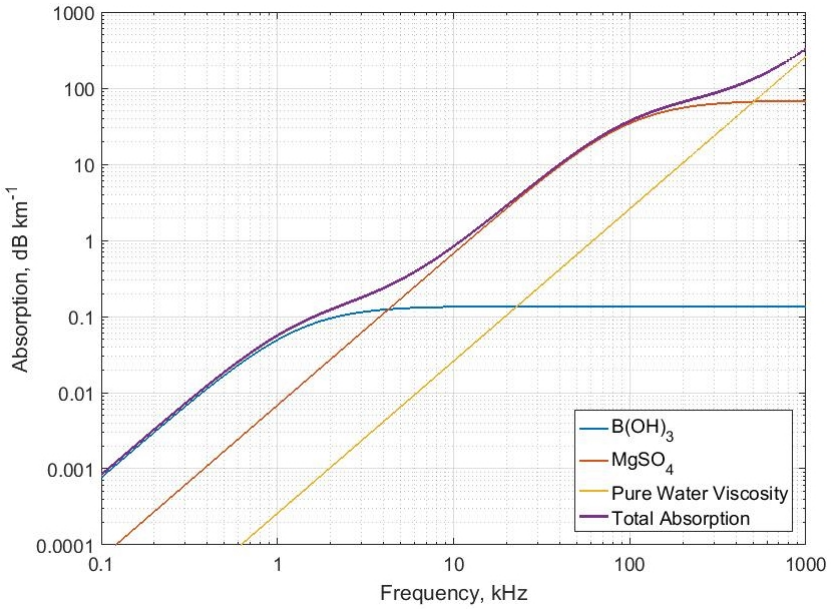

Figure 3.5: Absorption coefficient calculations using the Francois-Garrison model accounting for the absorption from $MgSO_4$, $B(OH)_3$ and Pure Water Viscosity from 0.1 kHz to 1000 kHz.

The Received Level (RL) from a source at a point can be estimated at any other point in space using the TL. This can be estimated further from the source (forward propagation) or closer to the source (back propagation). It is often convenient to consider the sound level of the source at a distance of 1 m - a well used estimation called the Source Level (SL). To calculate the SL, a RL of a source is back propagated to 1 m from the source. When absorption is not significant, this is calculated as,

$$SL = RL + TL = RL + 20log(R) \tag{3.8}$$

with the units of dB. This is useful for simple comparison with other sources of sound. For example, a WEC with a RL measured at 200 m can be easily compared with another WEC with a RL measured at 800 m. However, this calculation does assume spherical spreading which, in the shallow water WECs often reside in is not accurate as the spreading is affected by surface reflections, bathymetry and other boundaries (Etter 2013).

One way to estimate the effects of surface reflections from the sea bed and sea surface is to use cylindrical spreading. This assumes the propagation of the sound forms a cylindrical shape from the point source as shown in Figure 3.6, of a height

d which is the depth of the water column.

Following the same process as above for calculating spherical spreading loss, the estimation for TL via cylindrical spreading is given by,

$$TL_{(cylindrical)} = 10log(R) \tag{3.9}$$

where TL is measured in dB referenced to 1 m. Note how the TL does not depend on the depth of the water column due to the cancellation with the reference term.

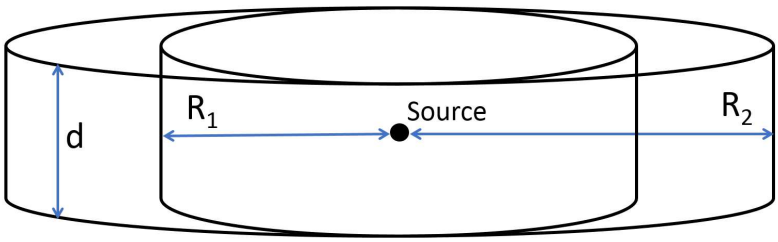

Figure 3.6: Cylindrical spreading from a point source.

3.1.5 Sound Propagation Modelling

To be able to describe the propagation of sound with specific boundaries and properties a more rigorous method is needed than the estimation of spreading and absorption losses. Propagation modelling is based upon the wave equation, with the assumption that the force term and pressure are harmonic, leading to the Helmholtz equation,

$$\nabla^2 p(\mathbf{r}) + \frac{\omega}{c(\mathbf{r})}(\mathbf{r})^2 p(\mathbf{r}) = f(\mathbf{r}) \tag{3.10}$$

where p is the pressure, $\mathbf{r}$ is the position, w is the angular frequency, c is the speed of sound in the medium and f is the forcing term that represents the acoustic sources (Duncan and Maggi 2006). There are a number of different models available to use, as summarised in Table 3.1. The propagation models all have ideal conditions of use that solve this equation with different assumptions and have all been extensively benchmarked and tested (Wang et al. 2014).

The Normal Mode method is a full-field solution that solves the equation for separate horizontal and vertical components. It works best in the far field, in shallow water at low frequencies, however, the fully range dependent model (allowing the input of range dependent variables such as bathymetry) is computationally expensive. The models that use this method include Kraken and C-SNAP (Wang et al. 2014).

The Wave Number Integration method is an exact solution at close range only using a numerical approach of spectral wave number integration (Wang et al. 2014). This model only supports range-independent environments and works best with

Table 3.1: Propagation modelling methods and their properties (Duncan and Maggi 2006; Wang et al. 2014). LF = low frequency, HF = high frequency.

Method	**Model Name**	**Shallow Water**		**Deep Water**		**Range Dependant**	**Pros**	**Cons**
		LF	HF	LF	HF			
Ray Tracing	Bellhop	No	Yes	Yes*	Yes	Yes	Computationally efficient	Accuracy limited at low frequencies
Normal Mode	Kraken, C-SNAP	Yes	Yes*	Yes*	No	Yes	Full field solution	Computationally expensive
Wave Number Integration	SCOOTER, OASES and SAFARI	Yes	Yes	Yes	Yes*	No	Exact Solution	Close range only and range dependant version not freely available
Parabolic Equation	RAM, IFD, MMPE, P-CAN, HAMMER	Yes	No	Yes	Yes*	Yes	Discontinuous sound speed profiles supported	Computationally expensive at f $>$ 1 kHz

*with specific limitations

deep-water, high-frequency problems. The models that use this method include OASES and SAFARI (Wang et al. 2014).

The Parabolic Equation Method is a one-way propagation solution that neglects back-scattered rays. It is a range-dependent code, with the ability to support discontinuous sound speed profiles. However at frequencies higher than 1 kHz it is computationally extensive. This method is coded within RAM and derivative models like RAMGeo (Wang et al. 2014) and HAMMER (HR Wallingford 2015). The HAMMER model (Hydro-Acoustic Model for Mitigation and Ecological Response) combines acoustic propagation modelling, hydrodynamics and ecological response models.

The Ray method calculates the path of individual rays coming from the source at different angles and the acoustic field level is calculated by summing up the rays near the receiver (Wang et al. 2014). It allows for range-dependent environments including bathymetry and sea surface, however, the accuracy of this model is limited at low frequencies (<200 Hz), where diffraction and sea bed penetration occur. Interactions of rays with the sea floor are considered via the calculation of a reflection coefficient. The model used to implement the Ray method is Bellhop (Dong and Dong 2014; Porter and Liu 1994) in conjunction with Bounce for reflection coefficients (Porter 2011b).

Other modelling methods include the Energy Flux Method, a hybrid solution between ray solutions and mode solutions and the Finite Difference/Finite Element methods, a common computational approach to physical problems, but incredibly computationally expensive (Wang et al. 2014).

Acoustic Toolbox User interface and Post processor (AcTUP) (V2.2L Maggi and Duncan 2016) is a Matlab toolbox that allows for a consistent user interface between multiple propagation models. This includes Bellhop, Bounce, Kraken, and RAM. This toolbox will be used within this thesis due to its ease of use, the incorporation of multiple models and well documented use in the research community.

3.2 *Lifesaver* at FaBTest, Falmouth Bay, UK

In order to evaluate the potential for detecting AE, an initial study was conducted based on data previously collected for the purpose of assessing the effect of WEC noise on the underwater soundscape in Falmouth Bay, UK (Garrett 2015). The work presented in this section summarises the conditions under which this data was collected and presented by (Garrett 2015) and published in (Walsh et al. 2017a).

3.2.1 The WEC and its environment

Falmouth Bay (Cornwall, UK) is a large and deep natural harbour at the western entrance to the English Channel. It is close to busy shipping lanes and also welcomes

considerable local commercial shipping and recreational boating activity, whose noise contributions were presented in Merchant et al. (2012). Figure 3.7 is a density map of Automatic Identification System (AIS) data from the vicinity around Falmouth Bay throughout the year 2016. Heavy shipping lanes are clearly shown in an E-W direction, N-S direction (north coast of Cornwall) and the main English Channel shipping lane in the bottom right corner from SW-NE.

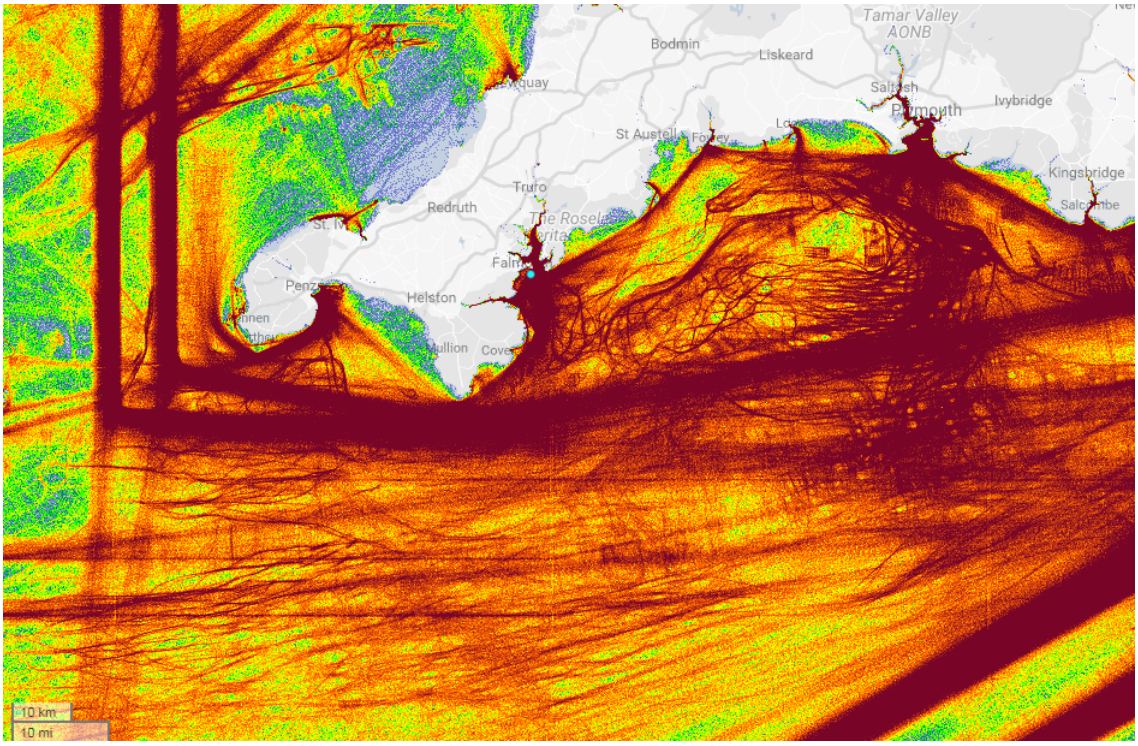

Figure 3.7: AIS density map for 2016 within the vicinity of Falmouth Bay, UK. Red is high density, blue is low density. From (MarineTraffic 2016)

Falmouth Bay Test facility (FaBTest) (FaBTest 2014) is a 2.8-km^2 test area supported by the University of Exeter. It is situated within Falmouth harbour, 3-5 km offshore as shown in figure 3.8. By being in the lee of the Lizard Peninsula, it is sheltered from the prevailing SW wind and swell, and exposed to long-fetch waves from the E-SE. This moderate wave climate, with peak tidal surface currents of 0.8 m s^{-1}, makes it an ideal "nursery" site to test MRE devices and in particular WECs (Garrett et al. 2014).

In March 2012, Fred. Olsen Ltd. deployed and trialled an electro-mechanical WEC at the FaBTest site (Sjolte 2014) to gain operational experience of the device and to investigate its performance over a total period of more than 2 years. This WEC, named *'Bolt-2 Lifesaver'*, is a doughnut-shaped floating device, shown in figure 3.9. The floatation platform has a 10-m inner diameter, 16-m outer diameter and 1-m height with a mass of 55 tons. The floatation platform has the capacity to install five PTO systems, but only three were installed during the trials. During operation, the PTOs were moored to the seabed and a five-point secondary mooring system was attached to the device. The PTO was realised with a winch, gearbox

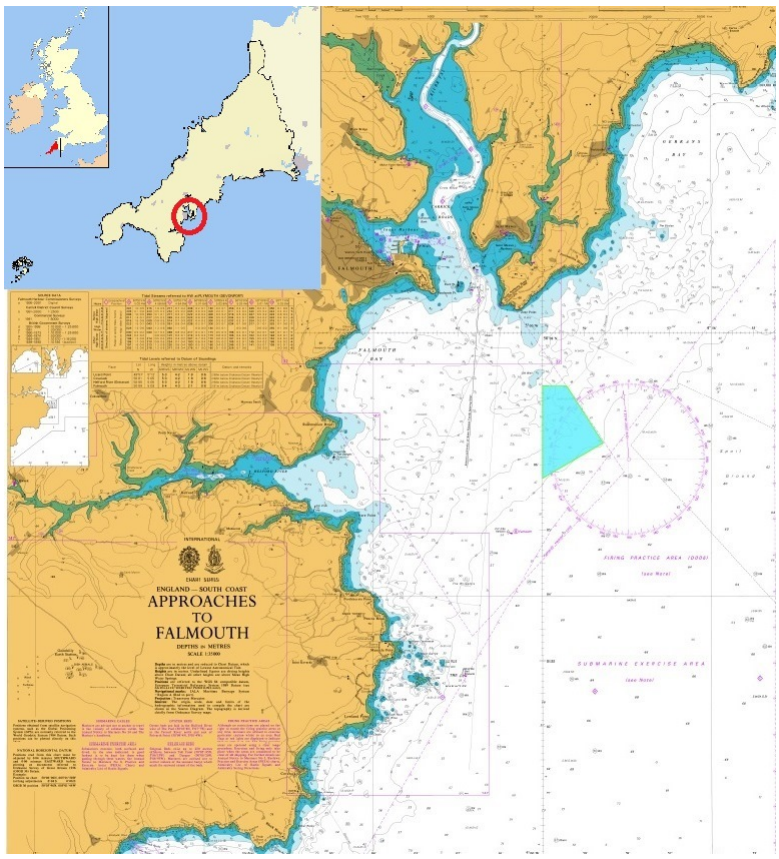

Figure 3.8: Map of the FaBTest facility location in Cornwall, UK from (FaBTest 2014). The test area is indicated by the aqua coloured area.

and generator as schematically shown in figure 3.10. The WEC was redeployed to Hawaii in March 2015.

3.2.2 Acoustic Monitoring

Passive acoustic monitoring of the WEC and its environment has been continuous during all stages of installation and operational activities of the WEC (Garrett 2015; Garrett et al. 2016). Autonomous Multichannel Acoustic Recorders (AMAR) (Generation 2, from Jasco Applied Sciences) were used, due to their high storage capacity (1 TB) (Jasco Applied Sciences Ltd. 2014), suitable for long periods of recording, and for their ease of deployment. Two AMARs were used in turn: when one was recovered and uploading data, the other was deployed in its place, ensuring continuous monitoring during successive 90-day deployments between 13 June 2012 and 4 November 2013 (the data between 9 April 2013 and 4 June 2013 was however lost during recovery).

The WEC was located in the South Western corner of the FaBTest Facility as shown in figure 3.11. It was located in 40 m of water depth and so each AMAR deployment aimed to follow the 40 m contour for continuity of the data. As can be seen in figure 3.11 each of the 8 deployments of the AMAR were in a slightly different location. Averaging these locations shows that across the 8 deployments

Figure 3.9: *Lifesaver* WEC on site at FaBTest, Falmouth, UK. Credit: Duncan Paul, Falmouth Harbour Commissioners, 2013

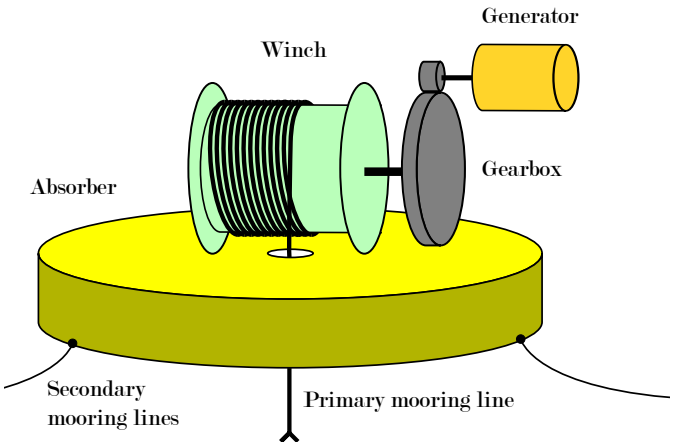

Figure 3.10: Schematic for PTO system and primary mooring line (Sjolte 2014). Reproduced with permission from the author.

the AMAR was located around 200 m from the WEC.

Figure 3.11 also shows a wave buoy, at which wave heights were measured. This Seawatch Mini II directional wave buoy (Fugro 2010) was deployed approximately 150 m from the AMAR location (Ashton et al. 2013). Its measurements were sampled at a frequency of 2 Hz for 1024 s (17 min 4 s) every 30 min and used for assessment of environmental contributions to noise and for comparison with WEC operational activity (Garrett 2015; Garrett et al. 2016, 2014).

The AMARs measured ambient sound levels for the first 30 min of every hour, sampling at 96 kHz (and therefore accessing a frequency range of 10 Hz - 48 kHz). However, during deployment 1 only, the sampling rate was at 64 kHz. Each AMAR was based around an omni-directional hydrophone (GeoSpectrum M8E), with nominal sensitivity of 165 $\pm$ 5 dB re 1 V/μPa and 24-bit dynamic resolution.

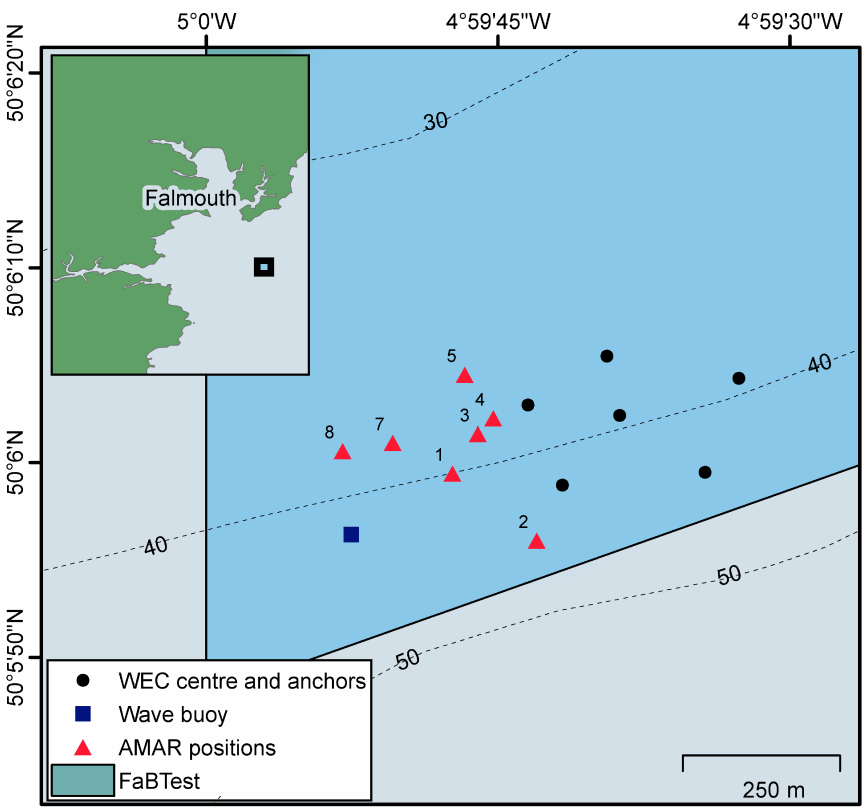

Figure 3.11: Location of the WEC, moorings, AMAR deployments and wave buoy. From (Garrett 2015)

Each hydrophone was calibrated by the manufacturer before deployment (2012) and upon return for servicing (2014), and after the last deployment with a pistonphone (GRAS type 42AC). Accuracies were ± 1.32 dB and ± 0.70 dB respectively, very close to the ± 1 dB operational accuracy expected in typical conditions and fully in line with good practice recommendations from (Robinson et al. 2014).

The device developers allowed access to the engineering log book, which detailed times the WEC was operational or non-operational. Operational activity was considered to occur when one or more PTO systems were active and producing power (Garrett 2015). Across all eight deployments of the AMAR, periods of pre-installation (baseline), installation, operation and non-operation were recorded. Figure 3.12 shows this graphically with the number of PTOs active at the time.

3.3 Marine Component Testing

The development of a new technology (eg. computers and motor cars) generally begins in the early stages with frequent breakdowns, low reliability and unexpected downtime, and MRE has not been immune as already described in Chapter 2. It is therefore crucial to prove the survivability and reliability of MRE devices including WECs. Instead of testing full scale prototypes, which is expensive and time consuming, individual component testing allows the reliability testing to be

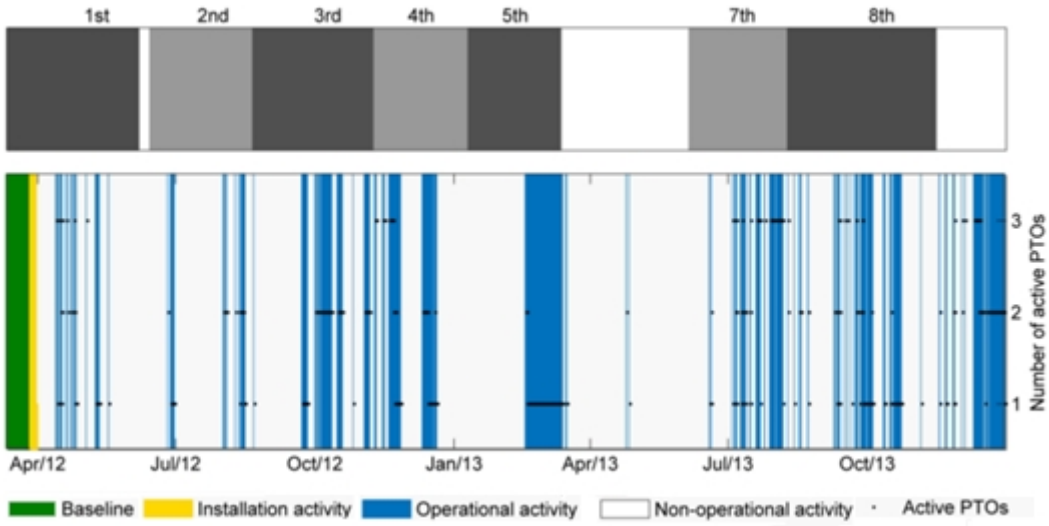

Figure 3.12: Operational status of *Lifesaver* WEC and recording equipment at FaBTest.The top chart shows the time periods and number of each AMAR deployment where white spaces indicate no recording. The bottom chart shows the time periods of different activity periods at the FaBTest site including baseline, installation activity and operational periods from 29th March 2012 to 30th December 2013. The number of PTOs active for each operational activity period are also shown. Adapted from (Garrett 2015)

broken up into more manageable and achievable segments. This could be the case for both brand new components to the industry and also developed components being used under different operating conditions.

3.3.1 DMaC Test Rig Specification

Dynamic Marine Component Test facility (DMaC) is a purpose-built test rig with the ability to replicate the forces and motions that components are subjected to in offshore applications. It was built at the University of Exeter after a gap was identified in the industry for such a test rig (Thies 2012). Components that can be tested in the rig include cables, mooring ropes, PTOs and shackles. DMaC is shown in Figure 3.13 as both a technical drawing and a photograph.

The linear actuator (left side of Figure 3.13a) and the headstock (right side of Figure 3.13a) allow the dynamic testing of large scale components in a fully controlled environment by applying realistic motion and load time series. By tensioning or compressing components in 3 degrees of freedom, the forces and motions that offshore components are subjected to can be replicated in this test rig. The rig can test component specimens of up to 5 m in length (with up to 1 m extension) and has the capability of carrying out immersed (underwater) component testing.

The linear actuator (Z-ram) is a hydraulic system providing axial loading in the z direction. A movable trolley allows for the Z-ram to be positioned according to

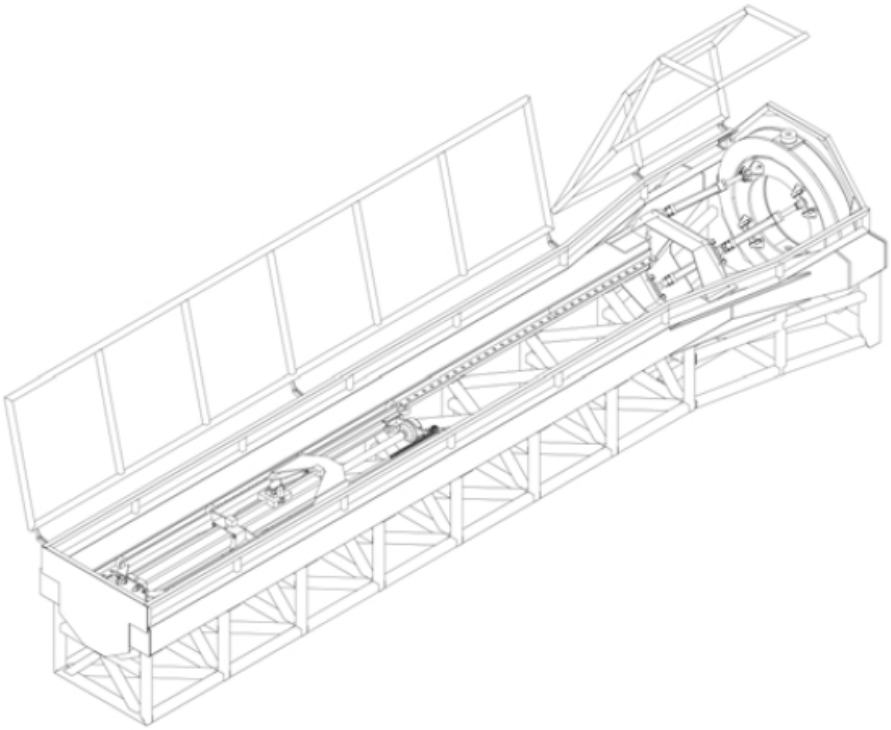

(a) Technical drawing of the elevated view of DMaC test facility.

(b) Photo of DMaC test facility.

Figure 3.13: DMaC test facility, allowing for the testing of components up to 5 m long.

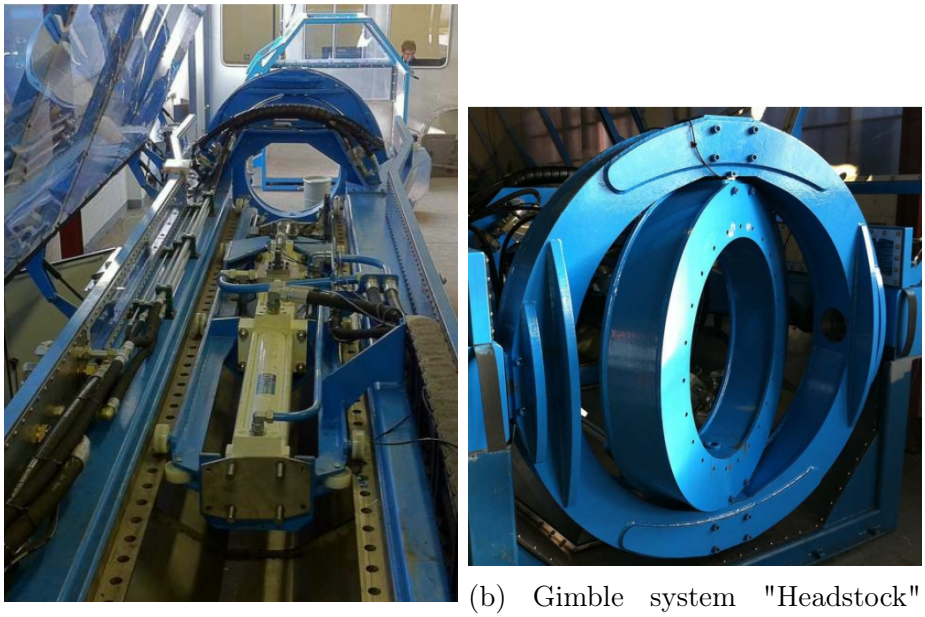

(a) Linear actuator "Z-Ram".

(b) Gimble system "Headstock" with tilted inner ring.

Figure 3.14: Load application points of DMaC test facility.

specimen size. The Z-ram is shown in Figure 3.14a and its functional parameters are shown in Table 3.2.

The moving head stock is made of a two plane gimble system as shown in Figure 3.14b where the inner gimble ring is pivot mounted to the outer gimble ring which is in turn pivot mounted to the main frame. The inner gimble ring provides the vertical x axis bending and the outer ring provides the horizontal y axis bending. This is controlled and monitored by an angle encoder fitted to each axis. The rings are driven by four hydraulic actuators and the maximum angular displacement of the two gimbles is $\pm 30°$. The maximum diameter of the test specimen is constrained by the brace at the headstock of $D_{max} = 800$ mm. More detailed explanation of the functionality of the DMaC test rig is available in Thies (2012) and Thies et al. (2011).

Table 3.2: Functional parameters and dimensions of the hydraulic actuator (Z-ram) of the DMaC test facility.

Parameters	**Value**
Maximum stroke	1 m
Maximum dynamic force	30 tonnes
Maximum static force	45 tonnes
Pre-load force	14 tonnes
Maximum specimen length	6 m
Maximum specimen diameter	800 mm
Maximum specimen weight	1000 kg

3.3.2 Loading Regimes

DMaC was designed to replicate the forces and motion that a component would experience in an offshore environment. As described in Thies (2012), simulations can be used to create test signals of what a component would experience in the ocean depending on a number of parameters. Using this type of loading schedule is classified as a performance test as it aims to understand how a component performs under realistic conditions.

Although DMaC is designed to be as realistic as possible, there are other loading schedules that can be applied to a specimen in order to tailor the test. DMaC can be operated in 2 distinct modes where either the force exerted on the specimen is the control parameter or the displacement of the specimen is the control parameter.

Two types of testing can be carried out on a sample depending upon what the purpose of the test is. A performance test will question if the component performs as is intended (Luxmoore et al. 2016). A reliability test is used to investigate failure mechanisms or rates and can be done either through a simple pull test or fatigue testing (Gordelier et al. 2015; Thies et al. 2016).

The simplest test that can be conducted in DMaC is a simple pull test to determine the strength of the specimen, also called a load to failure or break test (Weller et al. 2014). By extending the specimen to complete failure in displacement mode, the testing is more stable than if it had been conducted in force mode. This is because displacement mode does not include the specimen's response to the force exerted.

Fatigue testing is carried out to determine fatigue properties of materials and components, and the phenomenon behind degradation. In force mode, a cyclic loading schedule is applied where the loading placed upon the specimen oscillates between a minimum and maximum in a sinusoidal motion. Cyclic loading enables a quantification of repeated loading which could lead to fatigue and degradation (Schijve 2009). In Weller et al. (2014), a synthetic mooring rope with a parallel-stranded sub-rope construction (MBL = 466 kN) was subjected to simple harmonic loading schedules (maximum loading 40% MBL) to investigate the effect of loading history on the immediate dynamic properties of the rope. The author reports the outcome of the work to be that previous load history (in this case, bedding in) has a significant influence on the performance of the rope.

3.3.3 Bedding In

If the specimen in question is a rope, a process called "bedding-in" should be conducted to ensure the true performance of the rope is tested by conditioning the rope from its manufactured state to a settled state. Newly manufactured ropes need to be bedded-in to allow all fibres and terminators to have aligned in the direction

of stress (Weller et al. 2014). To do this the rope should be extended to 20% - 40% of the Minimum Breaking Load (MBL) (minimum ultimate strength when tested to failure) as outlined in Weller et al. (2014), held at that tension and then relaxed back to a minimum loading. The MBL of a rope is the minimum breaking force needed to break the rope completely as defined by the manufacturer.

A bedding-in loading schedule is shown in Figure 3.15 from 5 kN to 20 kN with 20 s hold at minimum and maximum, and 20 s ramping between the two.

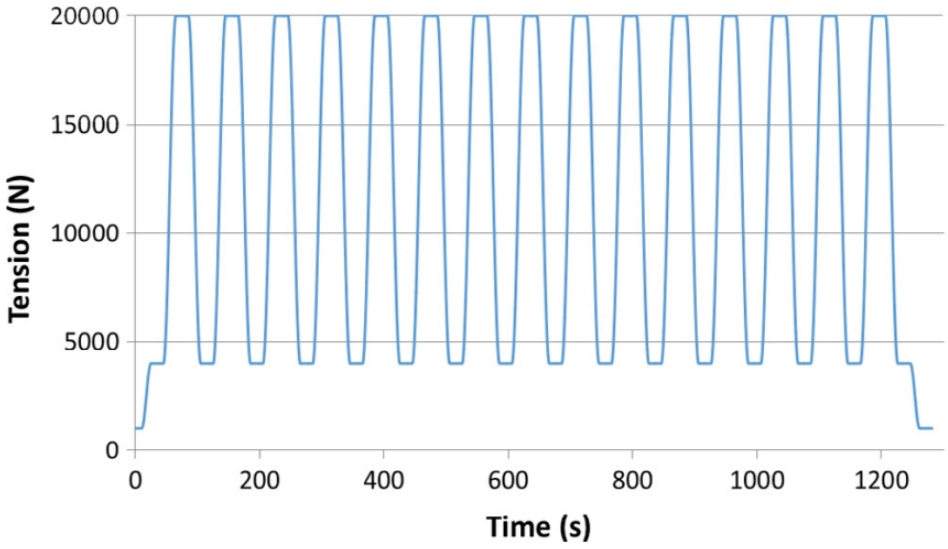

Figure 3.15: Twenty minute bedding-in time schedule for 12 strand double-braided polyester rope (MBL = 129 kN), 20 s hold and ramping, minimum load = 5 kN, maximum load = 20 kN.

3.3.4 DMaC Test Procedure

After the specimen has been fixed in place within DMaC and the safety top has been put in place, there is a procedure for collecting the data. As described by (Thies 2012), the test procedure is generally as follows:

1. Define the test signal, specify displacement or force parameters for each of the three axis.

2. Save and import test signal as Comma Separated Values (CSV) file format.

3. Choose displacement and force parameters, sampling rate, interpolation method for the time series, control parameters and data logging channels and time steps.

4. Send test data to the rig controller and write to the input file of the controller.

5. Start the test.

6. Observe test through visual control, camera recording and real time data streaming of the output signals.

7. Download and archive logged data file.

3.4 Underwater Acoustic Monitoring of Synthetic Mooring Rope

Underwater acoustic monitoring of a submerged component test within DMaC had not previously been done. This section is based on the methodology presented in (Bashir et al. 2017) and was conducted jointly between I. Bashir, a post-doctoral researcher at the University of Exeter, and Walsh in 2015 with assistance from the other co-authors.

Underwater acoustic testing to study the AE of synthetic fibre mooring ropes is a novel experiment. The aim of the testing was to detect the release of acoustic waves or energy in response to applied loading regimes, informing remote monitoring options for reliability and durability assessment of polyester ropes. It was predicted to be of importance after empirical observations of high amplitude acoustic emissions preceded failure of a synthetic mooring rope during a pull to failure test.

3.4.1 Sample Specimens

The rope type chosen for the experiments was a representative 12-strand double-braid polyester rope with a nominal diameter of 24 mm. The rope has six right-hand laid strands and six left-hand laid strands that produce a torque balanced rope. It is a double braided rope with a core enclosed by an outer braid cover. The internal and external core construction are both laid in a braided assembly. This 12-strand double-braid rope construction offers high strength and very good abrasion resistance and as such is well suited to MRE mooring applications (Weller et al. 2014).

Acoustic testing was carried out on three polyester rope samples from the same manufacturer's batch, referred to as R1, R2 and R3. The rope sample properties are given in Table 3.3 as stated by the manufacturer (Bridon 2011). Figure 3.16 provides a schematic of the construction of the double-braided rope.

Table 3.3: Sample rope properties and specification (Bridon 2011).

Material	High tenacity polyester multifilament fibre
Construction	12 strand double braid
Nominal diameter	24 mm
Nominal mass in water	0.13 kg m^{-1}
MBL	129 kN

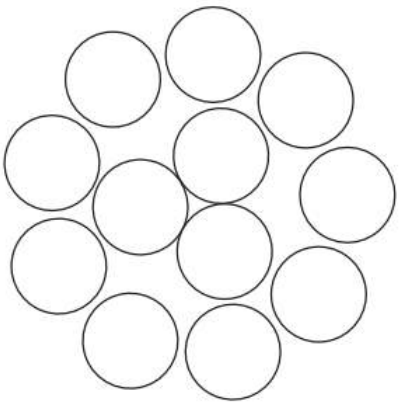

Figure 3.16: Construction of the 12 strand double-braid polyester rope sample.

Figure 3.17: Finished eye splices of R1 (splice 1 and 2) and R2 (splice 3 and 4) specimens.

The three samples were eye-spliced by hand in order to connect them into the test rig using mooring shackles. Appendix A shows step by step instructions on creating an eye splice (NewEnglandRopes 2010).

The four splices of sample R1 and R2 are shown in Figure 3.17. The total eye-to-eye length of the three spliced ropes before loading into DMaC was measured to be R1 = 3.53 m, R2 = 3.60 m, R3 = 3.62 m.

3.4.2 Acoustic Set-Up in DMaC

In order to carry out underwater acoustic testing of polyester ropes, a linear array consisting of three hydrophones was installed inside the DMaC test rig. Two of the sensors were SQ26-08 Cetacean cylindrically shaped directional hydrophones with a frequency range of 20 Hz - 50 kHz and a sensitivity of -169 dB re 1 V/μPa. The third hydrophone was a ball-shaped JS-B100-C4DS-PA Integrated Acoustic Sensor with a frequency range of 20 Hz - 50 kHz and a sensitivity of -168 dB re 1 V/μPa.

Full hydrophone specifications are available in Appendix B.

The two cylindrical hydrophones were placed at the two ends of the rope samples close to the splices ('Headstock hydrophone' and 'Z-ram hydrophone') and the third ball hydrophone was placed at the centre of the rope samples ('Centre hydrophone'). The hydrophones were placed at equal distances (1.6 m) along the rope in order to cover the entire length of the rope. A schematic of this configuration and photographs of the mounted hydrophones are shown in Figure 3.18 and Figure 3.19.

The test rig was filled with fresh water and the rope samples were submerged 10 cm deep. The hydrophone array was placed at a distance of 10 cm next to the length of the rope and at the same depth in the water. The hydrophones were enclosed in a wire cage to protect them from damage as shown in Figure 3.20. Similarly, the cables of the hydrophones were passed through PVC pipes for protection. The pipes were filled with self-expanding foam to avoid them acting as acoustic wave-guides. The hydrophones were fixed to the outside of the DMaC rig using G-clamps and timber with the use of protective padding to avoid the transmission of any external vibration. This is all shown in Figure 3.19.

The two cylindrical hydrophones were synchronised through one recorder unit and thus acted as a synchronised hydrophone array. The ball hydrophone was connected to a separate recorder. Both recording devices had a sampling frequency of 96 kHz.

3.4.3 Loading Schedule

All three rope samples were subjected to similar tensile cyclic loading regimes in force mode with the objective to progressively increase the maximum load until failure. Before applying tensile cyclic loading, bedding-in was carried out for all three rope samples. The bedding-in procedure was specified using the rope MBL as outlined in (Weller et al. 2014). However, due to time constraints a shortened procedure was specified with shorter load-hold durations. A twenty minute bedding-in time interval comprising hold and ramp cycles lasting twenty seconds with a minimum and maximum load of 5 kN and 20 kN respectively was used. The time series plot for bedding-in cycles is given in Figure 3.15. It is acknowledged that the samples may not have been completely bedded-in after this process.

The rope samples were subjected to sinusoidal load cycles in force mode, oscillating between a minimum and maximum load. This was considered dynamic enough to excite the sample (similar to that reported in Weller et al. (2014)) while still maintaining relatively low levels of background noise from DMaC.

The minimum loading was set to 5 kN, whilst the maximum loading was stepwise increased from 30 kN until rope failure. The cyclic loading was increased linearly in order to study the acoustic emission for all regimes. Rope sample R1 was tested with slightly larger step-sizes to identify loads of increased acoustic release. Rope

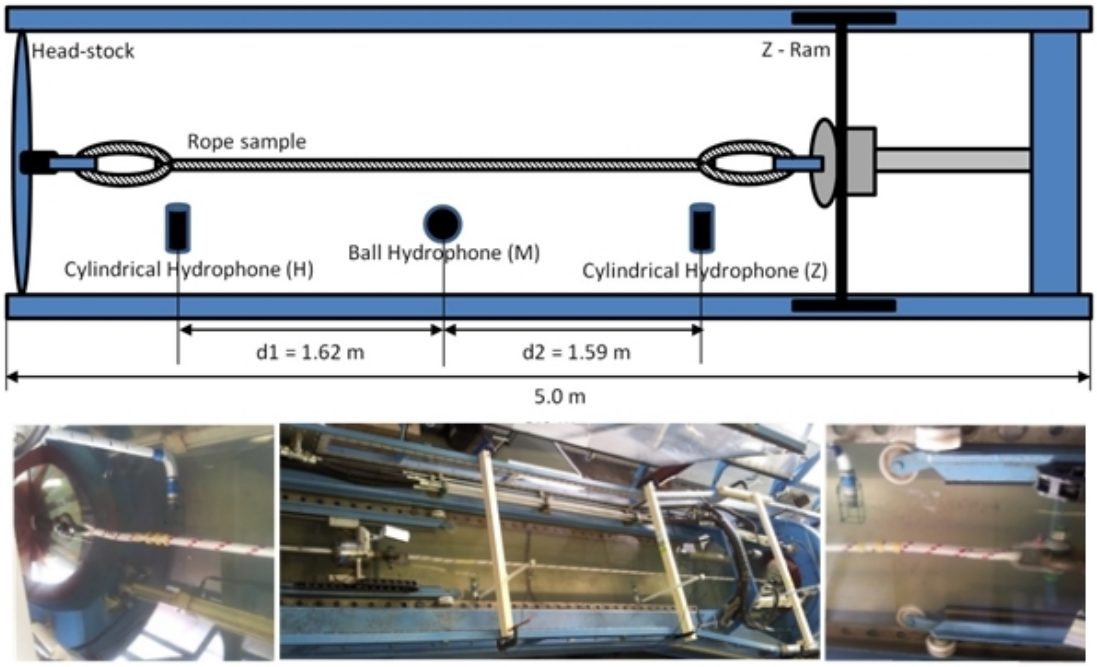

Figure 3.18: Schematic diagram (top view) and associated photographs showing the experimental set up for underwater acoustic rope testing inside the DMaC test facility.

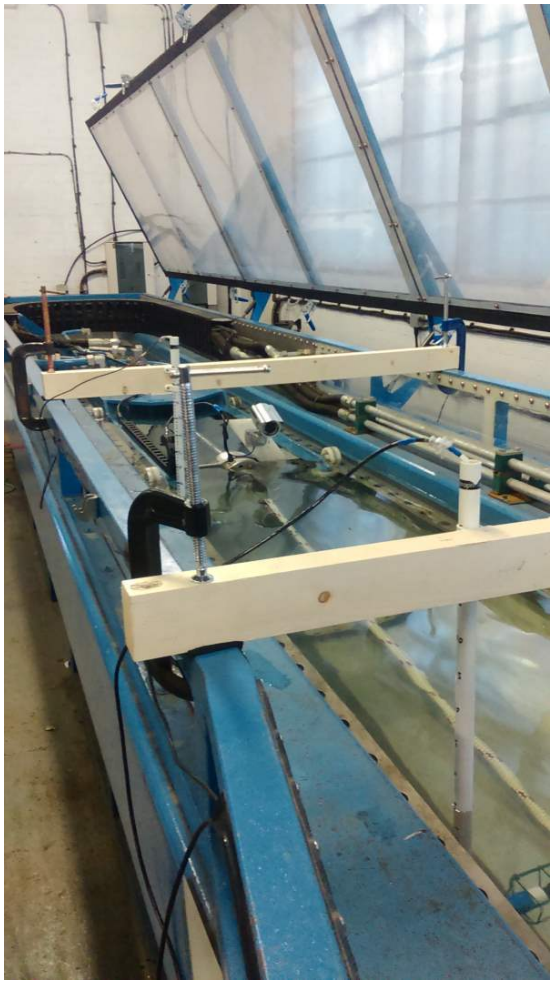

Figure 3.19: Photograph close up of the hydrophone set up within DMaC and supporting visual recording equipment.

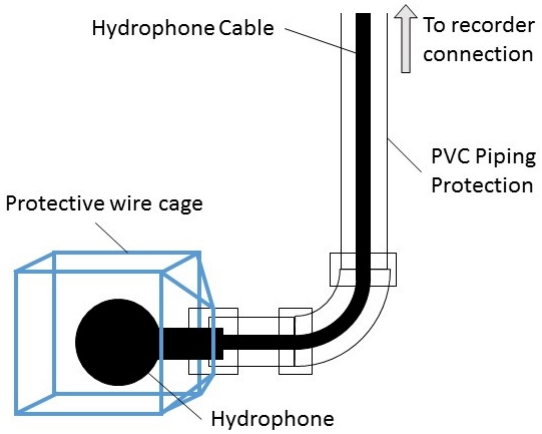

(a) Schematic diagram of the hydrophone casing used to protect equipment.

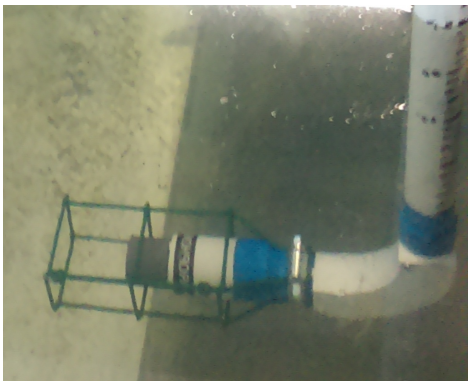

(b) Photograph of a cylindrical hydrophone within the protective casing.

Figure 3.20: Hydrophone set up used within DMaC.

samples R2 and R3 were tested with smaller incremental steps to provide a different load increment. Initially, the rope sample R1 was subjected to load cycles with a time period of 40 s, and this was later increased to 60 s for rope sample R2 and R3 after the background noise of the test rig was determined to be too noisy, offering better conditions at lower speeds. Table 3.4 summarises the individual test cycles experienced by each rope sample.

3.4.4 Underwater Acoustic Monitoring Testing Procedure

DMaC is equipped with a number of measurement instruments, but those relevant to this work included a force load cell measuring the tensile or compressive force that the specimen experiences at the end of the linear cylinder and the linear displacement encoder measuring the stroke position of the linear actuator. The sign convention for the force reading of the load cell considers tensile forces as negative values and compression as positive (against general engineering convention used in this work). Before the experiment, the linear tensile force cylinder was set to a displacement, $D = 0$ m, where 0 m was chosen as the closest possible point to the headstock to allow for as much of the 1 m stroke length as possible to be utilised. Thus, a retraction of the cylinder is defined as negative displacement, while an extension is read as a positive value.

Video recordings were also used to monitor the testing. From the safe location of the cabin, it is difficult to see the details of the testing, therefore small cameras located in a number of locations around the DMaC facility allow for remote visual monitoring of the testing. The tests were not always successfully recorded by the cameras, but the real-time video was used during the testing to visually inspect the rope during the loading schedule. Approaching the machinery would have been dangerous because the safety cover was disabled by the hydrophone support

Table 3.4: Loading regime and time schedule for cyclic loading of R1, R2 and R3.

Rope sample	Total number of cycles	Time period (s)	Total test time (mins)	Minimum load (kN)	Maximum Load (kN)									
R1	22	40	15	5	30	40	50	60	65	70	75	80	82.5	85
					90	91	92	93	94	95	96	97	98	
R2	20	60	20	5	30	40	40	50	60	62.5	65	67.5	70	71
					72	73	74	75	76	77	78	79	80	81
					82	83	84	85	86	87	88	89	90	90.5
					91	91.5	92	92.5	93	93.5	94	94.5	95	95.5
					96	96.5	97	97.5	98					
R3	20	60	20	5	30	40	40	50	60	62.5	65	67.5	70	71
					72	73	74	75	76	77	78	79	80	81
					82	83	84	85	86	87	88	89	90	90.5
					91	91.5	92	92.5	93	93.5	94	94.5	95	95.5
					96	96.5	97	97.5	98	100	102	104	105	106
					108	110	112	112						

structure.

The testing regime was slightly longer than previously described in Section 3.3.4 to account for the extra steps needed to record the AE from the testing as outlined below.

1. Define the test signal, specify force parameters for linear actuator, with headstock stationary.
2. Save and import test signal as CSV file format.
3. Choose displacement and force parameters, sampling rate, interpolation method for the time series, control parameters and data logging channels and time steps.
4. Send test data to the rig controller and write to the input file of the controller.
5. Start the recording of the ball and cylindrical hydrophones.
6. Start the test.
7. Observe test through visual control, camera recording and real time data streaming of the output signals and auditory evaluation. Note any unusual acoustic emissions both from within the test and the external environment.

8. When the test is complete, stop the hydrophone recording and download the data as .wav file format.

9. Download and archive logged data file.

Over a total of 14 days the above testing was repeated 130 times. This included 4 bedding-in cycles per rope sample and the loading regimes outlined in Table 3.4 as well as a background test for environmental noise determination.

Chapter 4

Condition-Monitoring Feasibility Study

To evaluate the feasibility of using AE to monitoring the condition of WECs in the ocean, previously collected data was re-assessed for this purpose. The data, collected by Garrett and presented in Garrett (2015), was available to assess for condition monitoring purposes. It was visually inspected for signals of interest by a post-doctoral researcher at the University of Exeter, I. Bashir, and the author of this thesis (Walsh) contributed to this work through assisting with the signal processing techniques and linking the findings to relevant research as published in Walsh et al. (2017a).

This short chapter is provided to ensure the full context of this data is shown, including relevant outcomes from Garrett (2015) and the results of the condition monitoring feasibility study.

4.1 Environmental Monitoring Results

At the time of data collection, the aim of the original project was to understand the overall effect that the WEC has upon the local soundscape and the mammals within it. These results are presented in full in (Garrett 2015). A short summary of the analysis methods and conclusions will be presented.

To understand if the device had increased noise levels in the area each 30-minute recorded file was analysed. Each file was assigned either operational or non-operational status as in figure 3.12. Each file was processed in 1-minute samples. The raw data was processed to calibrate the data with the frequency dependent hydrophone sensitivity per 1 Hz, interpolated from values provided by the manufacturer. The processing used FFT of 1-s windows, Hann window filter to minimise aliasing and 50% overlap, in line with good practice recommendations (Robinson et al. 2014). This processing yielded median PSD levels per 1 Hz for each 30-minute recorded period.

The highest differences in sound levels in this study were recorded during installation activities, with a median PSD difference of 8.5 dB re 1 μPa^2Hz^{-1} in the frequency range 10 Hz - 5 kHz (Garrett 2015).

The calculated mean difference between operational and non-operational median PSD was 0.04 dB re 1 μPa^2Hz^{-1} in the frequency range 10 Hz - 32 kHz, meaning that average sounds from the WEC are undetectable above background noise, at least at the 200-m range (Garrett 2015). While the WEC does produce distinct sound signatures, the overall PSD between operational and non-operational states when considering long-term averages (as typically performed in environmental assessments) is often masked by other sources.

Comparison of operational and non-operational sound levels in figure 4.1 however shows more important differences in the frequency range 30 - 100 Hz, peaking at 47 Hz (although the peak frequency varied slightly for each deployment). These differences appear small overall (less than 1 dB) but further analyses reveal more significant differences.

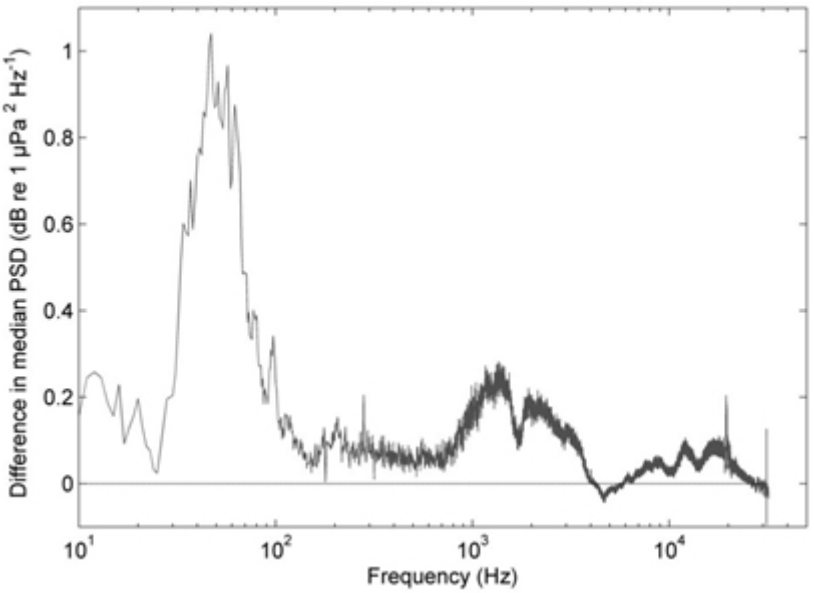

Figure 4.1: Difference in the overall median sound levels (June 2012 to November 2013) between the operational and non-operational activity periods of the WEC. Positive values indicate louder median sound levels during operational activity at that frequency. From Garrett (2015).

The commonly calculated "effective" source SPL_{RMS}, back-propagated to a distance of 1 m from the WEC, were found to be to 155 dB re 1 μPa^2Hz^{-1} (Garrett 2015). This enabled the comparison of the WEC's noise with other studies, and Garrett concluded: "The results of this study indicate that the effect of a single WEC device on the overall sound levels in Falmouth Bay is relatively low considering the substantial presence of shipping in the area." (Garrett 2015).

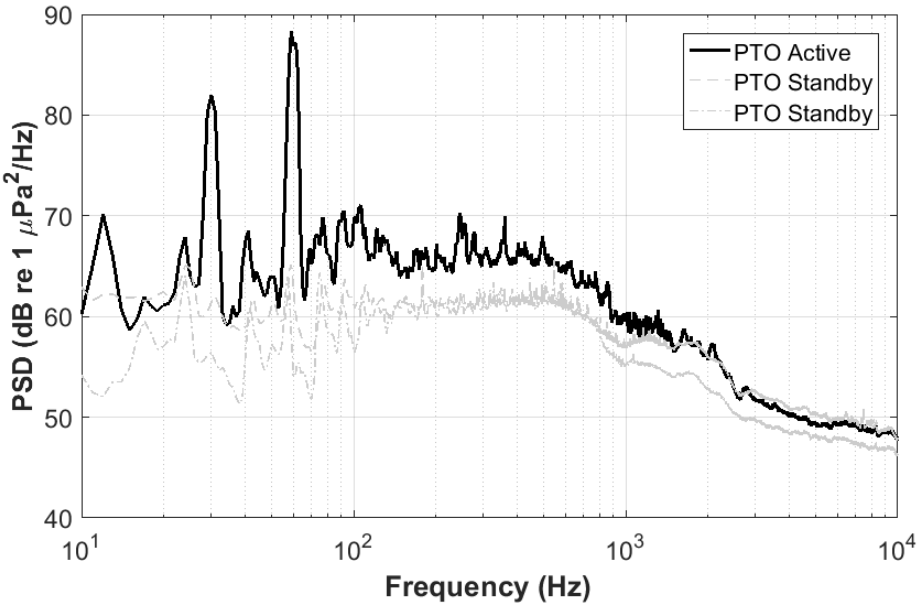

Figure 4.2: PSD (1 Hz frequency resolution) for a typical 30-min acoustic segment when the WEC was operational and the PTO system was active and on standby (device not active). From Garrett (2015).

4.2 AE Monitoring Results

With such a substantial amount of data covering periods of pre-installation, installation, operation and non-operation, it was perceived that by analysing the data on a shorter time scale, information about the minute-by-minute and second-by-second operation of the WEC could be uncovered within the data. Evidence of engineering features and (incipient) faults would test the concept of underwater AE monitoring, even with a data set that was not collected for this specific purpose.

The PSD was considered on a shorter time scale. The operational status from the device developer was matched to 30-minute acoustic segments and tonal noises were regularly identified at multiple frequencies (figure 4.2). The spectrum shows high-amplitude tones at 30 Hz and 60 Hz, respectively 18 dB and 25 dB above the spectrum for conditions when the device was not operational. A marked difference can be observed in comparison to figure 4.1. This is due to the large difference in the time period plotted. Figure 4.1 displays 18 months of averaged data, whilst figure 4.2 shows the operational characteristics of the WEC for a 30-min time period.

AE signals are non-stationary and often comprise overlapping transient waves, with distinct frequency contents varying with time. Short Time Fourier Transform (STFT) were used to produce spectrograms. Time is represented along the horizontal axis, frequency along the vertical axis, and STFT-derived PSD are colour-coded. STFT windows will show different features according to their sizes: large windows provide good frequency resolution but poor time resolution, whereas

small windows provide the opposite. Multiple window sizes were tried during these analyses to best identify and characterise acoustic features related to AE from the WEC.

A number of 30-minutes recordings were considered and are presented in Table 4.1. By matching the operational log book and environmental data, periods of vessel activity could be excluded from the analysis. The observations in Table 4.1 are related to the status of the PTO system, the main component of the WEC, and to the wave parameters. Wave parameters were recorded by a nearby wave buoy (Seawatch Mini II (Fugro 2010)) measuring the Spectral Specific Wave Height, H_{m0} and the Maximum Wave Height (H_{max}). A Figure relating to each entry in this table is also presented.

Figure 4.3 shows the acoustic signature of the WEC when the PTO was active. PTO signatures are indicated in the figure. Tonal noise is also present in this signature at 60 Hz, 100 Hz and higher elements.

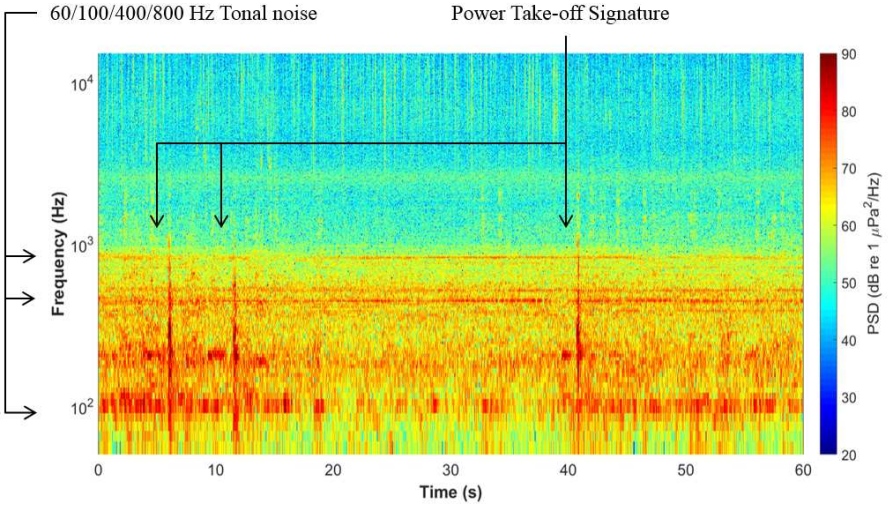

Figure 4.3: Spectrogram of active PTO and tonal noise. 2012-08-11 19:00:00

Figure 4.4 shows the acoustic signature of the WEC when the PTO was active. PTO signatures are indicated in the figure. Tonal noise is also present in this signature at 100 Hz only.

Figure 4.5 shows the acoustic signature of the WEC when the PTO was active. Four PTO signatures are indicated in the figure. Tonal noise is also present in this signature at 100 Hz.

Figure 4.6 shows the acoustic signature of the WEC when the PTO was active. PTO signatures are indicated in the figure. Tonal noise is also present in this signature at 100 Hz along with high shipping noise.

Figure 4.7 shows the acoustic signature of the WEC when the PTO was active, however, no PTO acoustic signature was detected. 100 Hz and 200 Hz tonal noise was detected.

Figure 4.8, figure 4.9 and figure 4.10 show the spectrograms of the WEC when

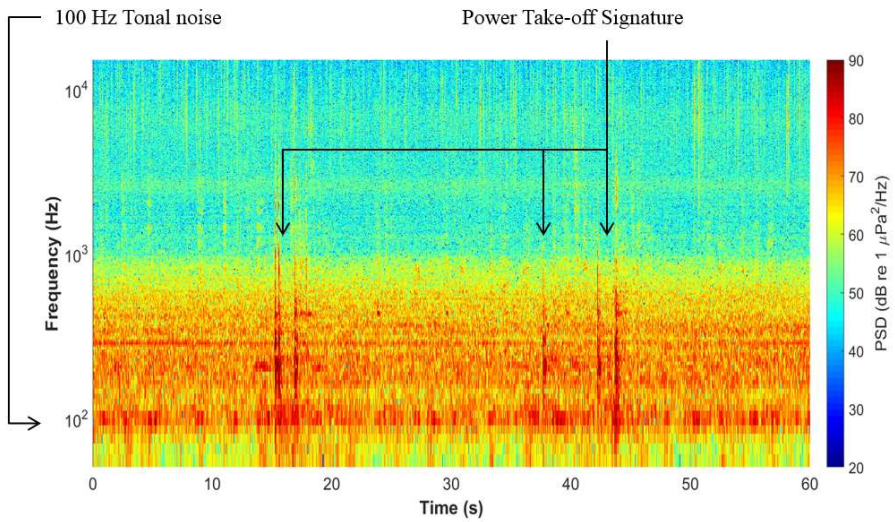

Figure 4.4: Spectrogram of active PTO and tonal noise. 2012-08-11 20:00:00

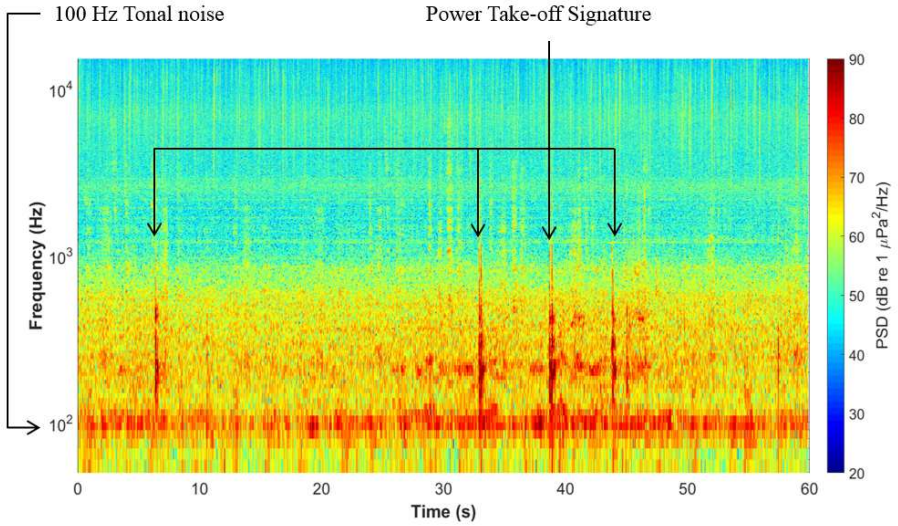

Table 11- A3

Figure 4.5: Spectrogram of active PTO and tonal noise. 2012-08-11 21:00:00

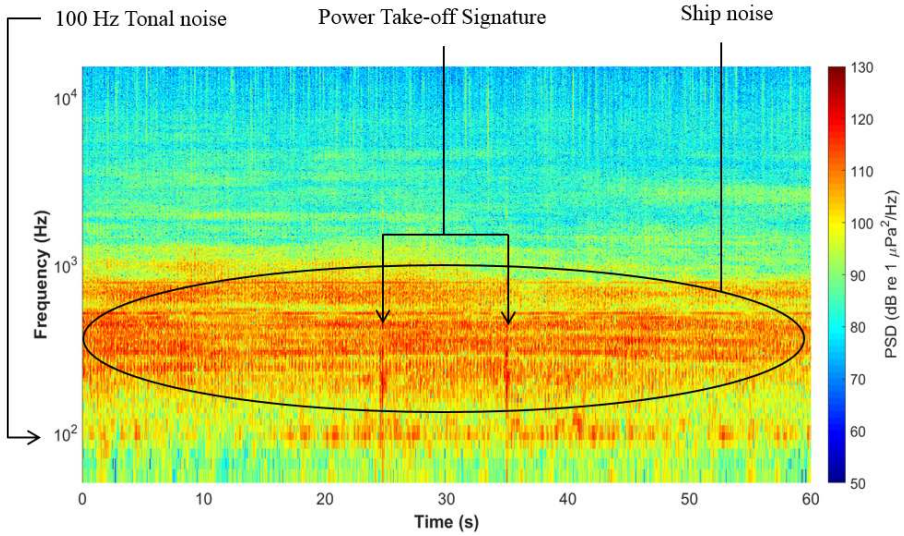

Figure 4.6: Spectrogram of active PTO, tonal noise and high shipping noise. 2012-08-11 22:00:00

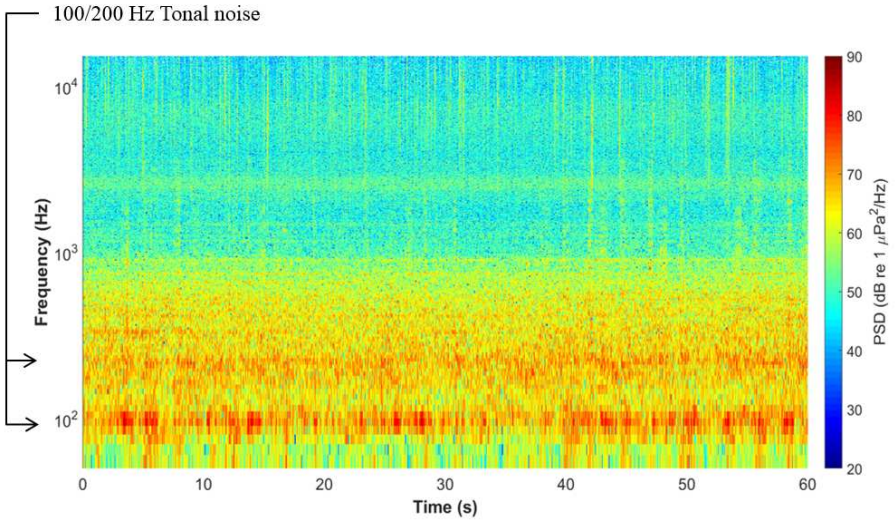

Figure 4.7: Spectrogram of tonal noise and no PTO signature, even though the PTO was active at the time. 2012-08-11 00:00:00

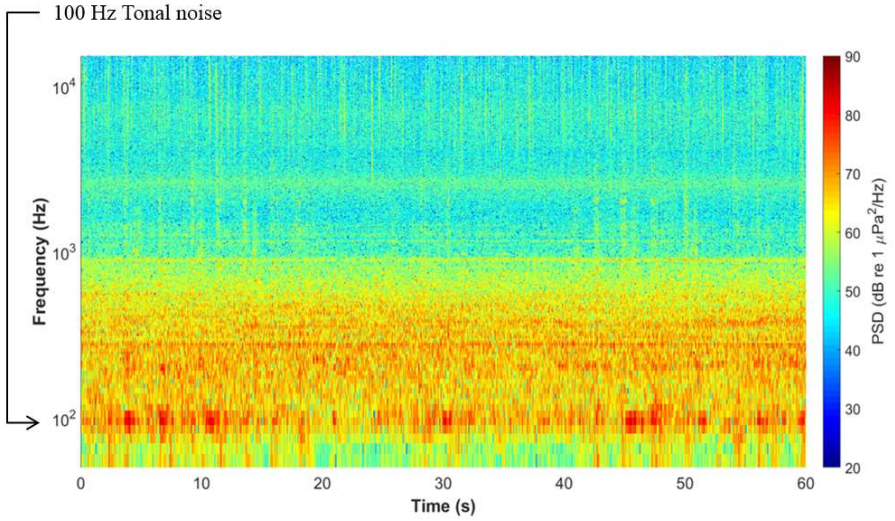

Figure 4.8: Spectrogram of Standby PTO status. 2012-08-11 01:00:00

Table 4.1: Selected acoustic recordings, comparing with the PTO status (Sjolte 2014) and measured wave parameters (Ashton et al. 2013): H_{m0} - Average wave height; H_{max} - Maximum wave height; T_p - Spectral peak period.

Acoustic Recording		PTO Status	Wave Parameters (representative of 30 minutes period)			Observations	Figure
Date	Time		H_{m0} (m)	H_{max} (m)	T_p (s)		
2012-08-11	19-00-00	Active	1.02	1.56	5.96	PTO Signature: Active Tonal Signature: 60, 80 & 100 Hz	4.3
2012-08-11	20-00-00	Active	0.94	1.41	7.32	PTO Signature: Active Tonal Signature: 100 Hz	4.4
2012-08-11	21-00-00	Active	0.94	1.25	5.37	PTO Signature: Active Tonal Signature: 60 & 100 Hz	4.5
2012-08-11	22-00-00	Active	0.86	1.41	5.57	PTO Signature: Active Tonal Signature: 60 & 100 Hz High Shipping Noise	4.6
2012-08-11	00-00-00	Active	0.63	0.94	5.66	PTO Signature: None Tonal Signature: 60 & 100 Hz	4.7
2012-08-11	01-00-00	Standby	0.63	0.94	5.47	PTO Signature: None Tonal Signature: None	4.8
2012-08-11	02-00-00	Standby	0.54	0.94	5.37	PTO Signature: None Tonal Signature: None	4.9
2012-08-11	03-00-00	Standby	0.55	0.94	5.57	PTO Signature: None Tonal Signature: None	4.10
2012-08-11	04-00-00	In-Active	0.55	0.78	5.37	PTO Signature: None Tonal Signature: None	4.11
2012-08-11	05-00-00	In-Active	0.55	0.94	5.57	PTO Signature: None Tonal Signature: None	4.12

the PTO was on standby with no acoustic signatures of the PTO or tonal noises detected.

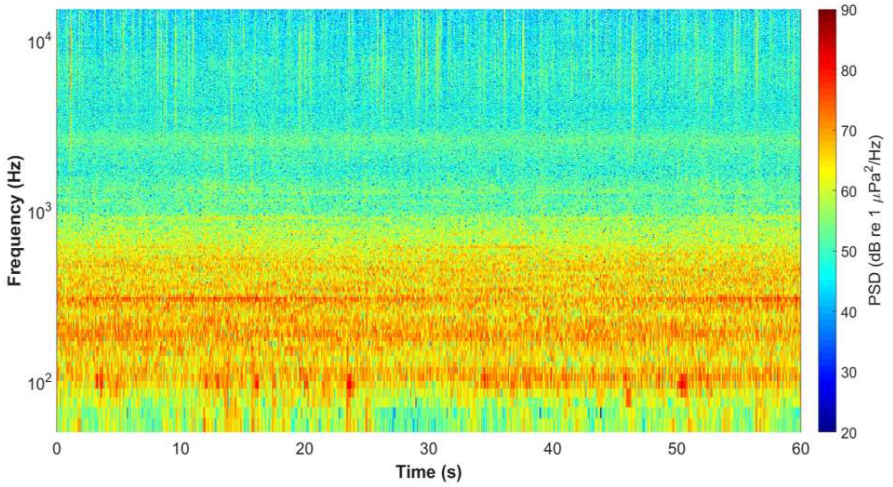

Figure 4.9: Spectrogram of Standby PTO status. 2012-08-11 02:00:00

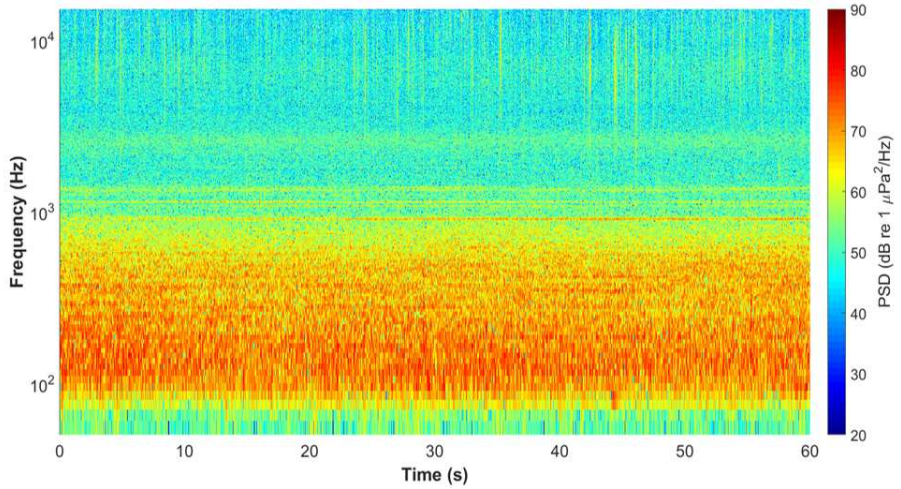

Figure 4.10: Spectrogram of Standby PTO status. 2012-08-11 03:00:00

Figure 4.11 and figure 4.12 show the spectrogram of the WEC when the PTO was in-active with no acoustic signatures of the PTO or tonal noises detected.

Engineering assessments of the PTO showed it operated successfully during the 2-year deployment, although some oscillations were initiated at production saturation level (Sjolte 2014). At high sea states, the PTO winch and floater underwater produced rapid movement. When active, the PTO was tightly moored to the seabed: the floater and primary mooring system exerted forces in opposite directions. When waves were high, the belt-winch hit the end stop, leading the tightly moored belt and floater to produce rapid vibrations a shown in figure 4.13. This is believed to be caused by the dynamic response of the primary mooring, resulting in an aggregate system response (Sjolte 2014).

Spectrograms of individual events further show their acoustic signatures (figure 4.14). This plot was created with a window size of 2048 data points, corresponding

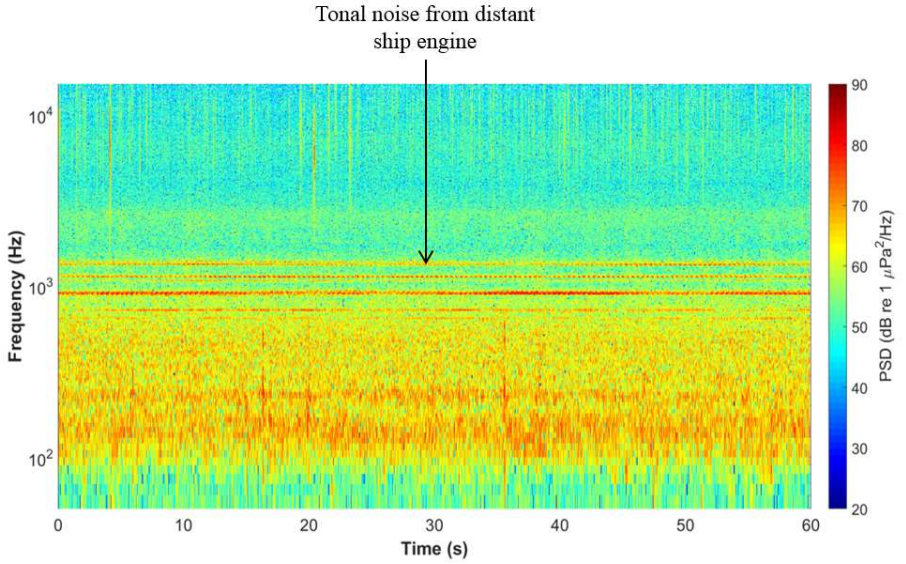

Figure 4.11: Spectrogram of In-Active PTO status. 2012-08-11 04:00:00

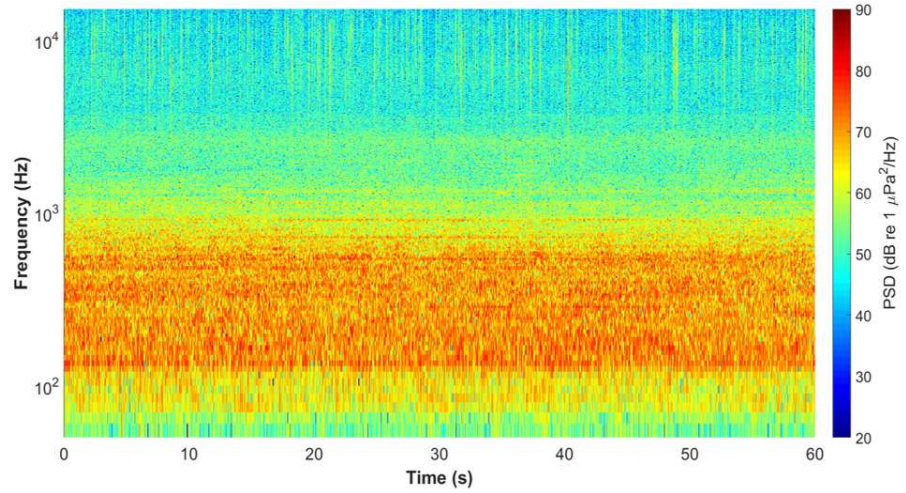

Figure 4.12: Spectrogram of In-Active PTO status. 2012-08-11 05:00:00

to a frequency resolution of 31.25 Hz. High amplitude events (up to 120 dB re 1 μPa) last for approximately 0.5 s, spanning frequencies between 100 Hz and 1 kHz. These events occur regularly, with a period of approximately 6 s matching the periods of oscillations in the primary moorings (Figure 4.13). The regular, small variations in force are directly visible as distinct AE signatures (figure 4.14). They are attributed to the belt-winch hitting the end stop of the WEC at high sea states. Full analysis (Table 4.1) shows this PTO signature is only detected when averaged measured wave heights reach above 0.9 m, as this is the 'cut-in' wave height of the device.

Tonal components were also found to be at 60 Hz with a harmonic at 30 Hz as shown in Figure 4.15. The spectrogram in Figure 4.15a does show high amplitude signals at both 30 Hz and 60 Hz, as indicated in the figure. However, the tonal components become clearer in the PSD in Figure 4.15b where there are clear peaks in the spectrum of 109 dB re 1 μPa at 30 Hz and 115 dB re 1 μPa at 60 Hz.

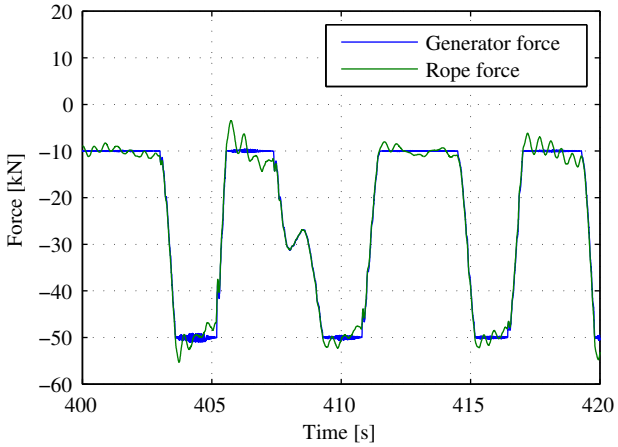

Figure 4.13: Oscillations encountered in primary moorings due to system dynamics (Sjolte 2014). Reproduced with permission from the author.

Spectrograms such as Figure 4.14 also show tonal components centred on 100 Hz and intermittently between 200 and 300 Hz. This acoustic behaviour has been observed throughout the data recordings (Table 4.1) and is understood to be the acoustic signature of the PTO generator (Walsh et al. 2017a).

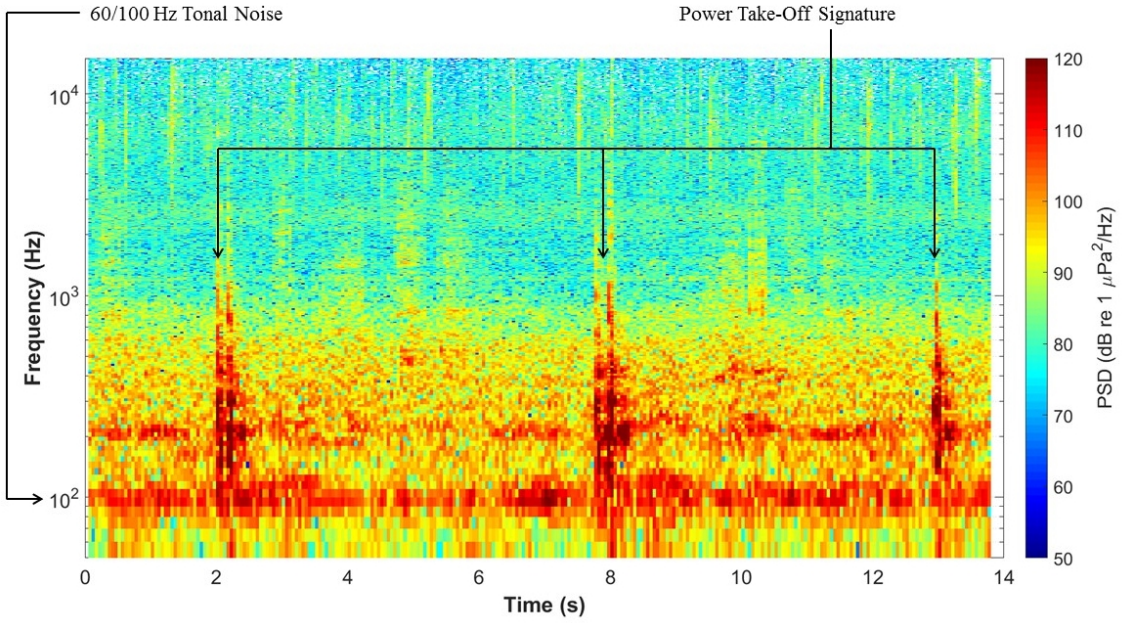

Figure 4.14: Typical acoustic signature identified due to the PTO of *Lifesaver*. The STFT plot (31.25 Hz frequency bandwidth, 50% overlap, flat shading) shows variations in frequencies with time, and the colour coding details the relative magnitude of the power spectrum.

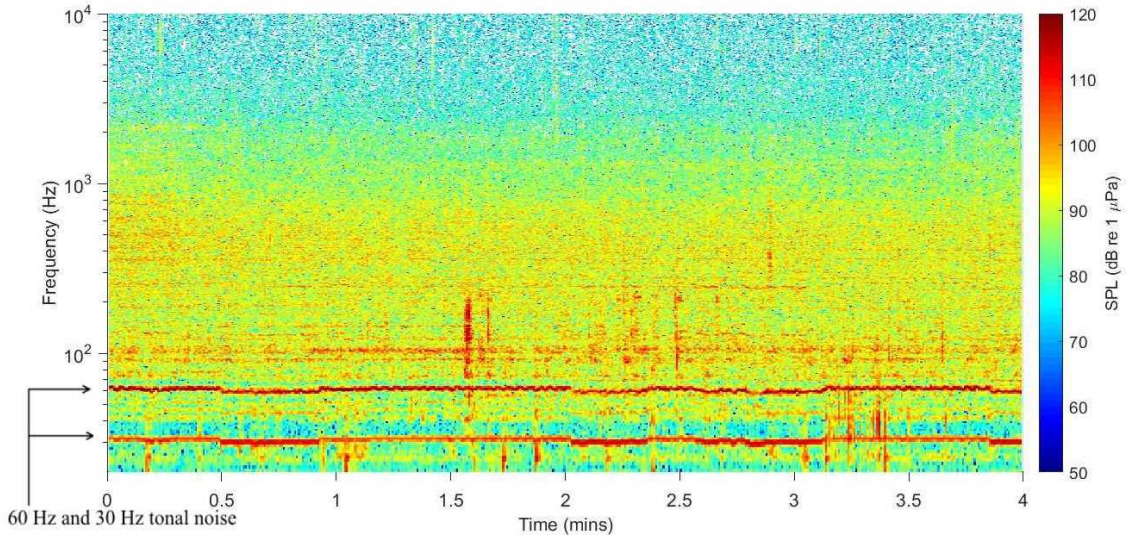

(a) Spectrogram of tonal 30 Hz and 60 Hz signal due to the PTO of *Lifesaver* (1 Hz frequency bandwidth, no overlap, flat shading).

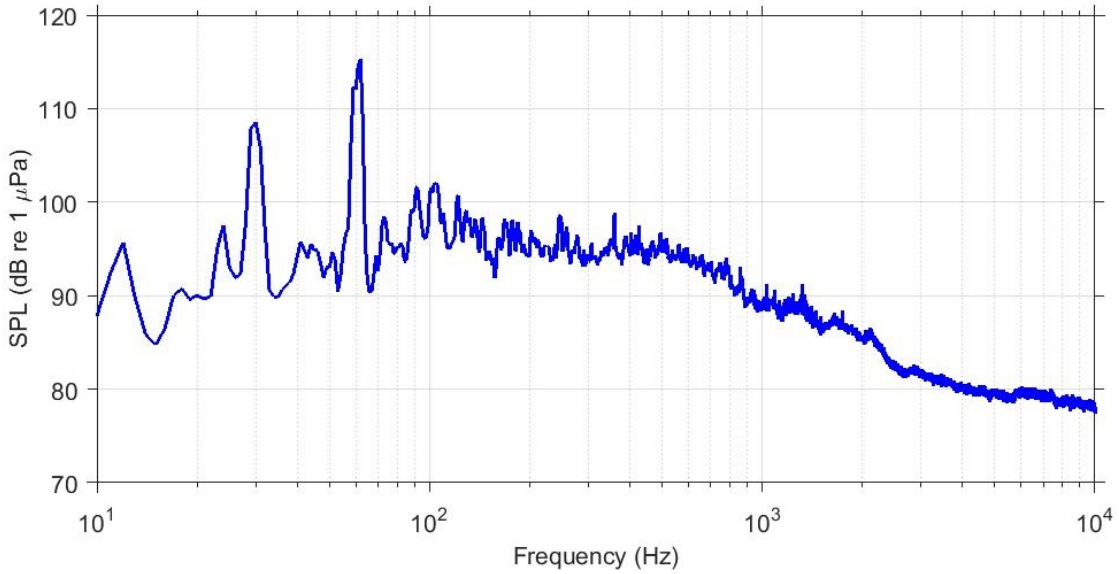

(b) PSD of tonal 30 Hz and 60 Hz signal due to the PTO of *Lifesaver* (1 Hz frequency bandwidth).

Figure 4.15: 30 Hz and 60 Hz tonal noise from the *Lifesaver* PTO.

4.3 Wave parameters and underwater acoustics

With such a large data collection spanning over months, it is interesting to consider the effect of wave parameters on the underwater acoustics detected. It is already established that as the sea state increases, the sound levels detected increase as shown in Figure 3.2 (Wenz 1962). However, with a WEC in the water, do increased wave parameters increase the sound levels further because of the increased movement of mechanical parts? This question can be approached with the data presented here.

From the data set, 38 files were selected with various wave parameters and number of PTOs active (0, 1, 2 or 3). Each of these 30-minute sound files was assessed for their mean 1-second (50% overlap) broadband SPL_{RMS} allowing each data point's acoustic properties to be described by just one number. These data files were then matched to the wave parameters at that time and the number of active PTOs from the operations log. The results of this are Figure 4.16 and 4.17 which show no obvious relationship between the wave parameters presented, the number of active PTOs at the time, and the sound pressure level presented.

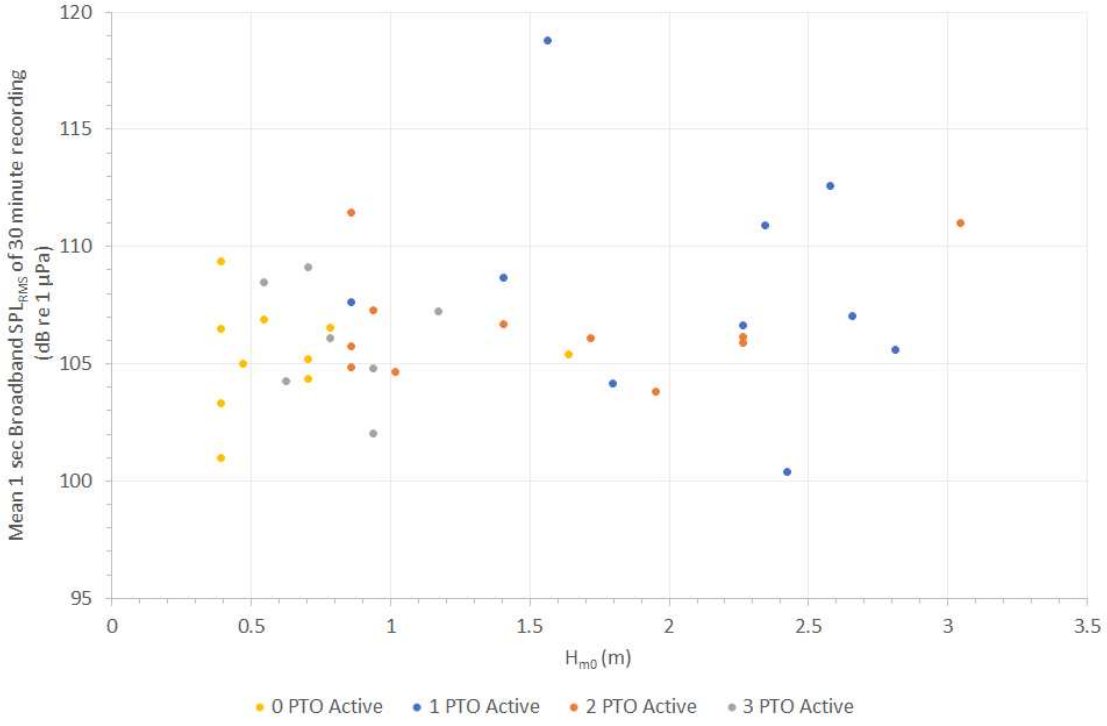

Figure 4.16: Mean 1-second broadband SPL_{RMS} of 38 30-minute files and associated Spectral Specific Wave Height, H_{m0} and number of active PTOs.

4.4 Discussion

Both methods of analysis, using short and long timescale analysis were able to identify tonal elements in the WEC signal. In Figure 4.1, the *differences* between operational and non-operational median PSD show contributions from frequencies

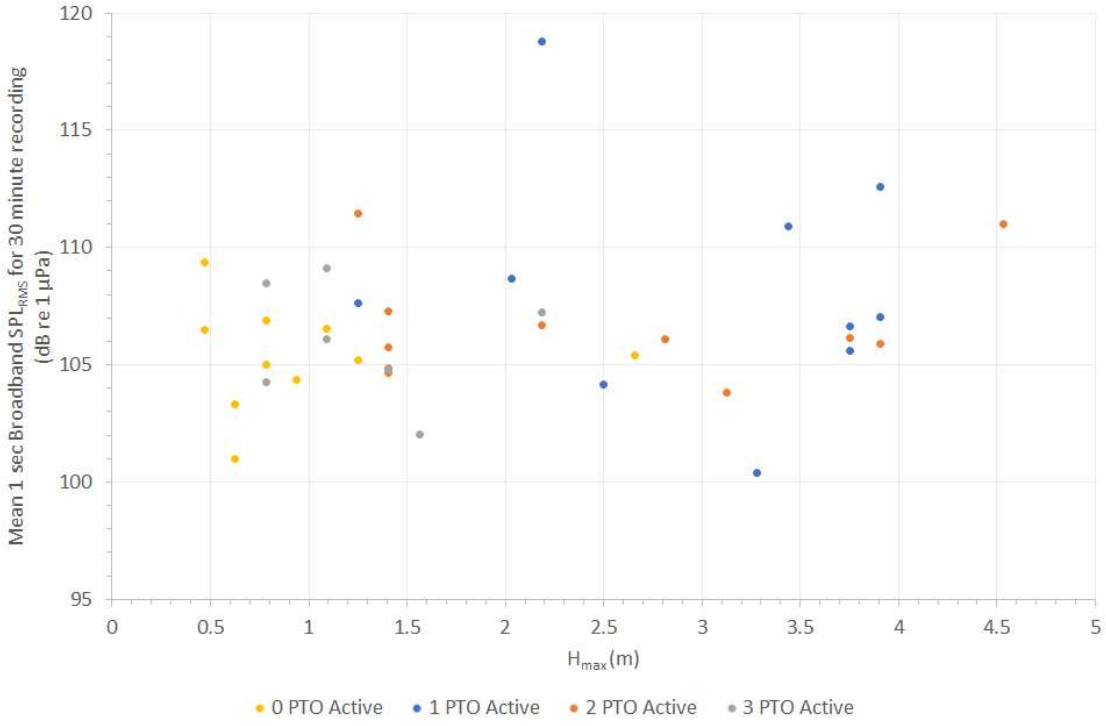

Figure 4.17: Mean 1-second broadband SPL_{RMS} of 38 30-minute files and associated Maximum Wave Height, H_{max} and number of active PTOs.

30 to 100 Hz up to 1 dB re 1 μPa^2 Hz^{-1}. However, Figure 4.15b captures individual tonal elements within the same frequency range contributing up to 115 dB. This is believed to be associated with the WEC generator.

This is not the first case of relatively low-frequency noise elements being detected from WEC engineering components (Robinson and Lepper 2013). Tougaard (Tougaard 2015) reported a 150 Hz tonal noise at 121 to 125 dB during the start and stop of the converter caused by the hydraulic pump of *Wavestar WEC*, although data was collected for the short time period of one day. In this study, tonal noises were not just identified during the start and stop of the converter, but throughout recordings. In case of the *SeaRay* WEC, increased spectral levels below 1 kHz were noted, consistent with the WEC torque and shaft speed in the fore generator (Bassett et al. 2011). In this study, the tonal noise key frequencies identified were 30 Hz, 60 Hz, and 100 Hz.

Time-frequency analysis revealed AE signatures of the active PTO system up to 120 dB at 200 m in the frequency range 100 Hz - 1 kHz that could be related to the fine scale dynamics of the PTO system and sea state. This gives a direct link into the engineering health of the device through its acoustics. In half of the studies of WECs, a link is drawn between the noise produced and converter operation (e.g. (Bassett et al. 2011; Garrett et al. 2016; Tougaard 2015)). Lepper and Robinson found a number of "events" related to the acoustic emissions of the *Pelamis* device (rattles, bangs, clanking) but did not draw any correlation to the mechanics of the device itself (Lepper et al. 2012). In retrospect, it was possible to link the acoustics detected

with the incorrect assembly of a WEC as part of the Lysekil project (Tougaard 2015). Unfortunately, the received level for these impulsive signals could not be confirmed due to the sensors (located 20 m from the device) being overloaded. The authors did not connect the detected acoustic emission with the possibility of condition monitoring. The underwater acoustic emission of tidal devices has also been found to provide crucial information in retrospect. *Verdant Power* deployed 6 tidal turbines that, when recorded, were generating more noise than expected, believed to be related to the blades on one of the turbines being broken, and another failing (Bassett et al. 2011).

Until now, no studies regarding the operational noise of WECs have analysed the data in view of engineering features towards exploring AE as a condition monitoring technique. This application was briefly mentioned in a very small number of reports as a future development possibility (Austin et al. 2009; Haikonen et al. 2013; Lepper et al. 2012; Robinson and Lepper 2013) and has been recently trialled for a tidal energy deployment (Elsaesser et al. 2015). This Chapter has explored the acoustic data of a WEC while operating at sea and identified engineering component signatures that could be used for condition monitoring purposes in the future.

The development of such condition monitoring will be of benefit to environmental impact assessments, allowing the identification of device components that are particularly noisy or faults that produce elevated noise levels than typical operations. The results presented in this initial study give confidence that this method is feasible.

By considering the wave parameters at the time of a selection of recordings and matching this information to the number of PTOs active, Figures 4.16 and 4.17 were generated. When considering each set of data (number of active PTOs) there appears to be no relationship between the number of PTOs active, and the noise produced. Indeed, there also appears to be no tangible relationship between the wave parameters and the noise produced. This confirms the results of Garrett, 2015 in which no significant increase in sound levels is found to occur due to the presence of the WEC in question (Garrett 2015). One interesting data point occurs at H_{m0} = 1.55 m (H_{max} = 2.2 m)and mean SPL_{RMS} = 119 dB re 1 μPa. It has a much larger sound level than the other data points. On inspection of the file in question, it was found that the signature of a passing ship was found, which would explain the overall increased sound level and suggests that marine traffic governs the sound emission levels (Garrett et al. 2016).

A practical challenge is the amount of acoustic data recorded, meaning that efficient data acquisition, signal processing techniques and the storage and/or transmission of data will be vital to the success of a remote and continual monitoring systems in the offshore environment.

In this study, another limitation was the use of only one hydrophone. The use of multiple hydrophones would have allowed the identification of the direction

(bearing) of the sound source locations through time-of-arrival triangulation. This would be of particular interest when considering device arrays, to detect one device among many. One concern regarding commercially available airborne AE systems is the "false alarm" rate (May and McMillan 2013). The use of multiple sensors would allow for a more accurate decision as to the reality of a signal by comparing multiple recording of the same acoustic signature.

The possibility of this method of condition monitoring is not confined to just the *Lifesaver* WEC, as shown by the numerous examples of acoustic signatures discovered in other studies ((Lepper et al. 2012; Robinson and Lepper 2013; Tougaard 2015)). Acoustic signatures will be dependent upon device design and components. There is a large variety of device designs in the industry that include different moving elements, mooring and anchoring systems and locations within the water column. However, this could be overcome with bespoke signal processing looking for abnormalities in a received signal, and through individual testing for the more commonly used components. Hence, this could also be transferable to tidal stream devices and other offshore developments.

In conclusion, systematic high-resolution short-time analyses of these long-term acoustic measurements near the *Lifesaver* WEC in Falmouth Bay show that:

- The ambient levels exhibited negligible average difference between operational and non-operational periods, although there were regular differences in the 30 - 100 Hz range.
- Detailed time-frequency analyses show the AE signature of the active PTO system during WEC operation (0.5-s bursts up to 120 dB re 1 μPa^{2}Hz^{-1}, mostly between 100 Hz and 1 kHz).
- The three peaks in this signal correspond to vibrations in the primary mooring system induced by high sea states.
- Tonal components at 30, 60, 80 and 100 Hz, reaching 115 dB re 1 μPa^{2}Hz^{-1} were also attributed to the device generator.
- Although most AE measurements to date have focused on sensors close to the devices/components of interest, in underwater environments, it is possible to detect AE signatures 200 m away from the WEC.

Chapter 5

Acoustic Monitoring of Component Tests

This section presents the key results obtained from the experimental method outlined in the Section 3.4. Firstly, the input and output loading of DMaC are presented. The background noise of the test rig is then characterised in order to isolate the acoustic emissions from the rope specimens. The observed AE signals are then classified, the failure acoustics presented and finally, the key observations for all three rope samples are summarised. These results have been published in Bashir et al. (2017). The work presented in the paper was a joint collaboration between Walsh and Bashir, with Bashir focusing on signature identification and Walsh focusing on overall trends in the data. The experiment was designed and implemented jointly by both authors.

5.1 Test Schedule / Load Profiles

Before the AE of the testing can be considered, the good working order of DMaC must be examined. This is done through visually inspecting the input drive data for the linear actuator and the output recorded data. Figure 5.1 compares these two data sets for an example test of R1 with loading from 5 kN to 70 kN. The first 1000 s of the testing is compared in Figure 5.1a as well as a 100 s excerpt in Figure 5.1b. As can be seen there is visually good agreement between the drive signal and the recorded data. The regression plots of the Z-ram force for a representative test from each rope sample are given in Figure 5.2. Points above the ideal correlation line Y = X show that the measured force is above the value that was requested by the input drive signal and vice versa. R^2 values for each regression analysis are shown in Table 5.1. These high values confirm the visual time series conclusion that there was very close agreement between input drive data and recorded data during all tests.

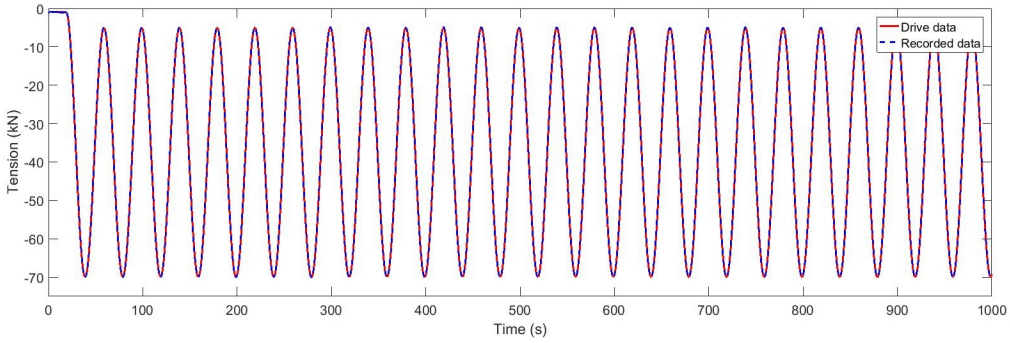

(a) First 1000s

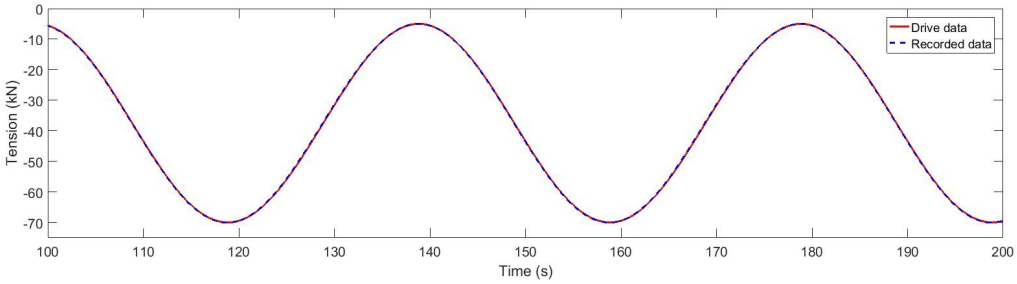

(b) Excerpt

Figure 5.1: Input drive data of linear actuator of DMaC compared to the output recorded data. Example, 5 kN to 70 kN sinusoidal drive data.

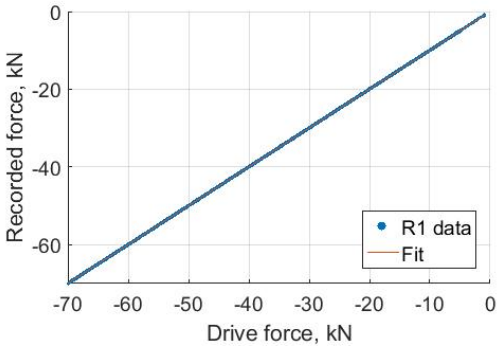

(a) Regression analysis of R1 for loading 5 kN to 70 kN.

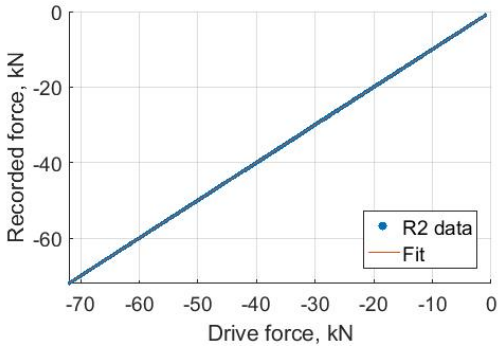

(b) Regression analysis of R2 for loading 5 kN to 72 kN.

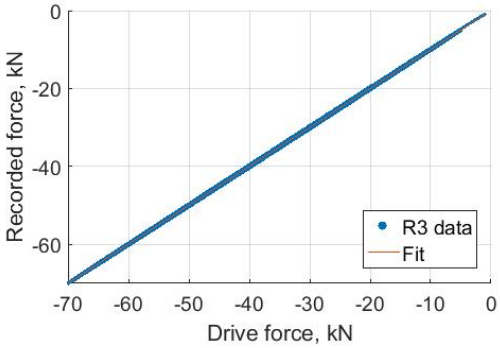

(c) Regression analysis of R3 for loading 5 kN to 70 kN.

Figure 5.2: Example regression analysis of input drive signal force to DMaC and the recorded output force for R1, R2 and R3.

Table 5.1: R^2 values for regression analysis of input drive and recorded force data.

Rope sample	R1	R2	R3
R^2	0.999994	0.999976	0.999848

5.2 Background Noise

The hydraulic test rig produces noise stemming from the hydraulic pumps, valve activity and mechanical movements. This background noise can potentially mask the AE signal from the rope specimens, and it was thus important to characterise these signals. The noise characterisation of the test rig was carried out by filling it with water and monitoring the AE signal during different cyclic loading conditions in displacement control mode. Figure 5.3a shows the time domain recording of the linear actuator hydrophone (red line); it has been superimposed with the loading cycle of DMaC (blue line). The amplitude of recorded noise and loading cycles has been normalised to allow a direct comparison.

It can be observed that the level of background noise is governed by the motion of the hydraulic actuator. Increased noise amplitudes are recorded when the actuator is moving, i.e. ramping up or down towards maximum or minimum loading. Noise levels are reduced when the loading reaches a maximum – i.e. when the linear actuator is relatively steady.

Knowledge of this acoustic behaviour allows distinction to be made between the noise produced by the DMaC facility and samples, particularly at higher loadings. The test rig produced a continuous high amplitude and low frequency tonal noise at 230 Hz. The harmonics of the tonal noise can be seen in the spectrogram along with high frequency cracking/mechanical noises due to valves and movement of the linear actuator as shown in Figure 5.3b. The headstock was held at a fixed position; therefore, the source of noise was due to the movement of the linear actuator alone. Furthermore, the AE of the test rig is very periodic, which improves the predictability of this noise source.

The amplitude of the noise produced varies in accordance with the time period of the loading cycle, i.e. it depends on the speed of linear actuator movement. The optimum loading cycle was found to be at 60 s duration where the linear actuator produces minimum noise for a given load. Thus longer cycle durations were selected to reduce the AE emissions from the test rig. It is acknowledged here that the 60-s duration load cycle is larger than what would be experienced by mooring systems of small WECs.

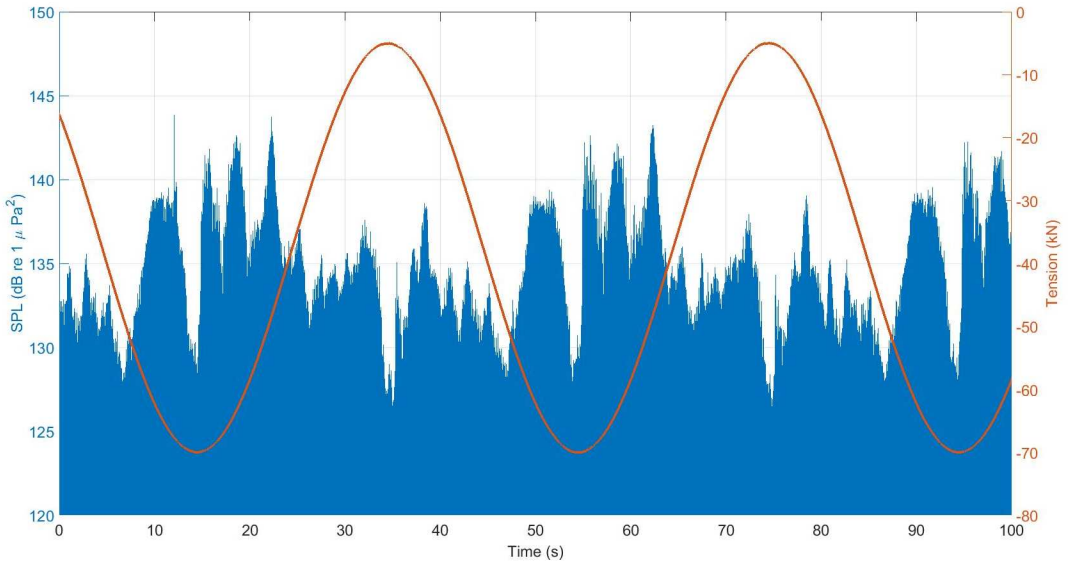

(a) Time domain recording for the hydrophone placed close to linear actuator (Z-ram, blue line) in dB re 1 μPa^2, with superimposed loading cycles (red line) in kN.

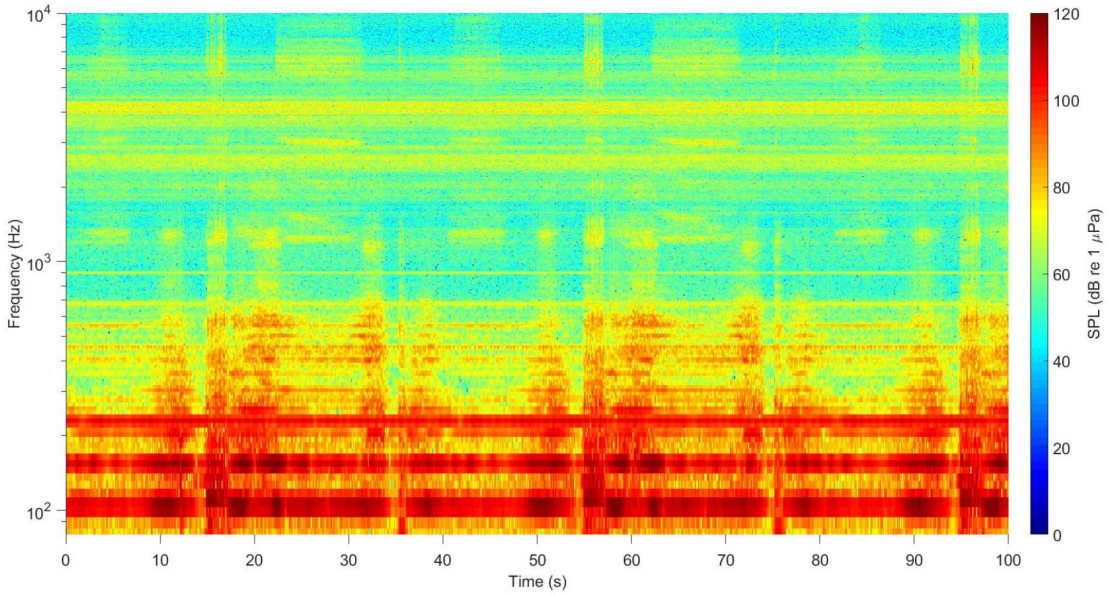

(b) Spectrogram plot of DMaC background noise.

Figure 5.3: Time domain and spectrogram of DMaC background noise - 100 s segment.

5.3 AE Signatures

The polyester rope samples subjected to cyclic loading produced a variety of AE. All of the AE signatures detected from the rope specimens were bursts of sound lasting for a very short period of time in the order of 0.5 ms, which are henceforth referred to as "signals". Impulsive signals are distinct acoustic signals separate in time while continuous signals contain a combination of indistinguishable individual waveforms. During testing a number of different signals were detected and hence the introduction of some descriptive language will help to classify them (Table 5.2). Each signal has been classified by considering its amplitude (both qualitatively and

quantitatively), ranging from 90 to 125 dB re 1 μPa, and frequency, ranging from 0.01 to 48 kHz.

Table 5.2: Classification of AE signatures due to loading on polyester rope during the DMaC acoustic testing.

Classification	**Amplitude (qualitative)**	**Amplitude (quantitative) (dB re 1 µPa)**	**Frequency Range (kHz)**	**Example figure**
Low-to-high frequency signal	Low	100	0.05 - 10	Figure 5.4
Low-amplitude signal	Low	90	10 - 20	Figure 5.5
Medium-amplitude signal	Medium	110	0.5 - 48	Figure 5.6
High-amplitude signal	High	125	0.01 - 48	Figure 5.7

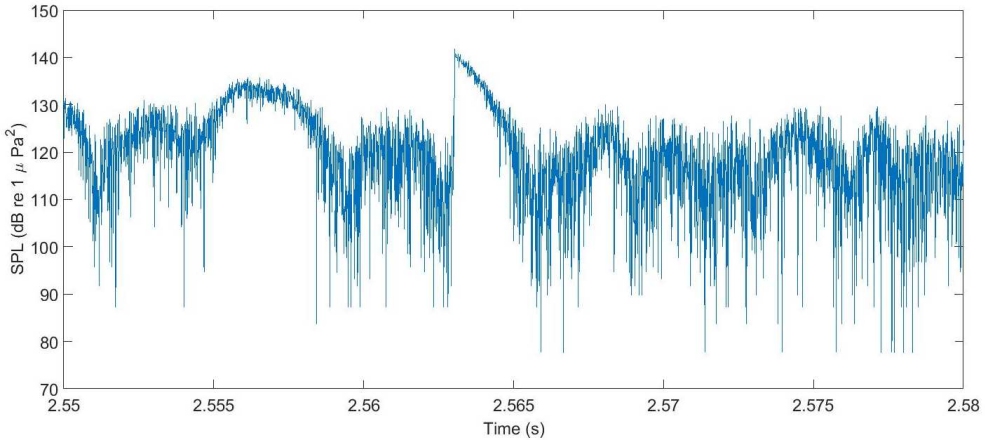

(a) Time domain SPL of a low to high frequency signal.

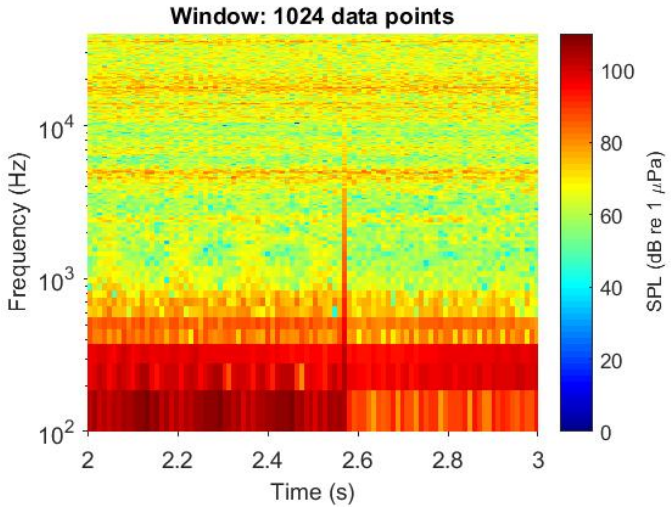

(b) Spectrogram of a low to high frequency signal, window size 1024 data points.

Figure 5.4: Representative example of a low to high frequency signal.

Figure 5.4a shows the time domain plot for a low-to-high frequency acoustic signal and 5.4b gives the corresponding spectrogram. This acoustic signal spans from 50 Hz to 10 kHz and appears for very short periods of time. The measured amplitude for these signals was between 90 and 100 dB re 1 µPa. They are few in number, typically one or two signals were detected for each rope sample studied.

Figure 5.5a shows the time domain plot for a low amplitude acoustic signal and Figure 5.5b gives the corresponding spectrogram. The acoustic signature for the low amplitude signals is fairly narrow-band as compared to the other acoustic features described later. The signature appears within the frequency range of 10–20 kHz. The measured amplitude for these signals was around 90 dB re 1 μPa. The observed acoustic signatures for the low amplitude signals were very consistent in all three ropes and produced more or less an identical signature.

The medium amplitude signal is broadband with a frequency band between 500 Hz to 48 kHz. Time-domain and spectrogram representations of a typical medium signal are shown in Figure 5.6. The measured amplitude was between 110 and 120 dB re 1 μPa. In Figure 5.6b four window sizes are used to generate the spectrogram to highlight the differences in the appearance of the signal with a change in window size. While a window size of 1024 data points gives detail in the higher frequencies with time, the low frequency tonal elements are lost, while the opposite is true for a window size of 8192 data points.

Figure 5.7a shows the time domain plot for a high-amplitude acoustic signal and Figure 5.7b gives the corresponding spectrogram. The high-amplitude signal spans the entire frequency range measured, i.e. 10 Hz to 48 kHz as the hydrophone's sampling frequency was set to be 96 kHz. The spectral content and time domain waveforms of the large AE signal are identical to what was observed in all rope samples. The measured amplitude for high amplitude signals was between 120 and 130 dB re 1 μPa. The time domain waveform of high amplitude signals show multiple hits (i.e. each peak is counted as one hit). An average of up to thirty hit counts has been found in a high amplitude AE signal. Again, Figure 5.7b shows the comparison of multiple window sizes for comparison.

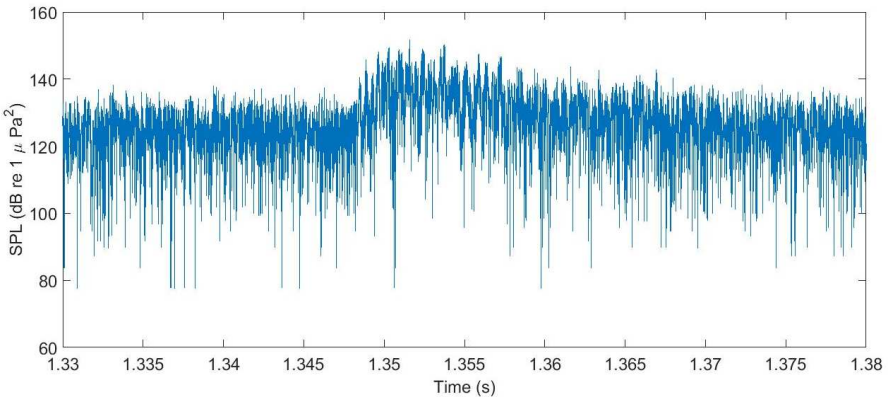

(a) Time domain SPL of a low amplitude signal.

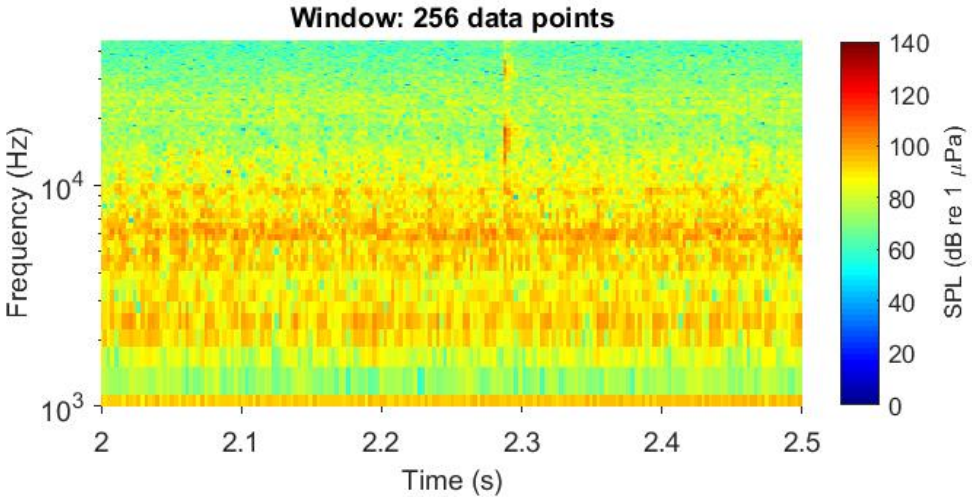

(b) Spectrogram of a low amplitude signal, window size 256 data points.

Figure 5.5: Representative example of a low amplitude signal.

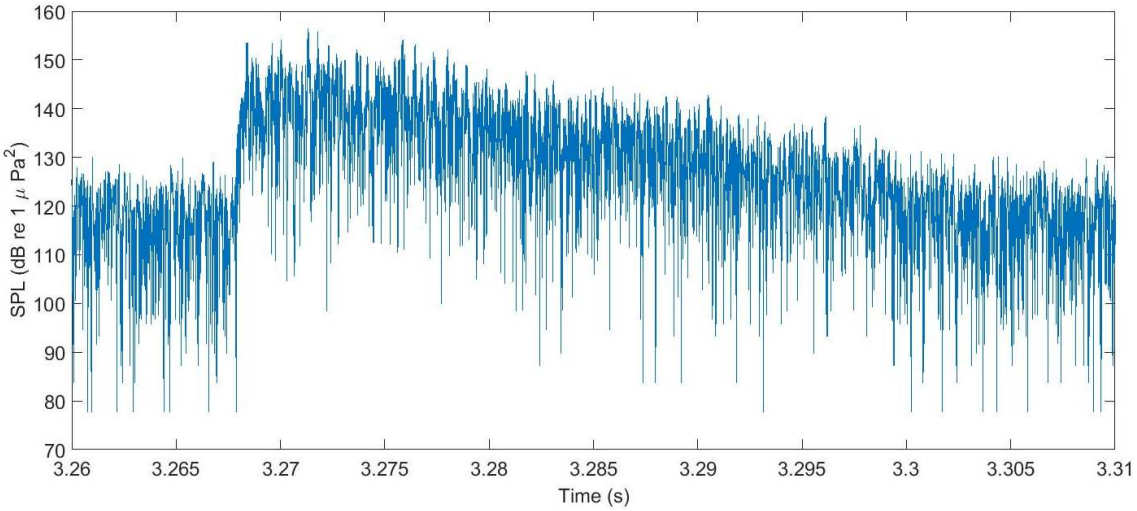

(a) Time domain SPL of a medium amplitude signal.

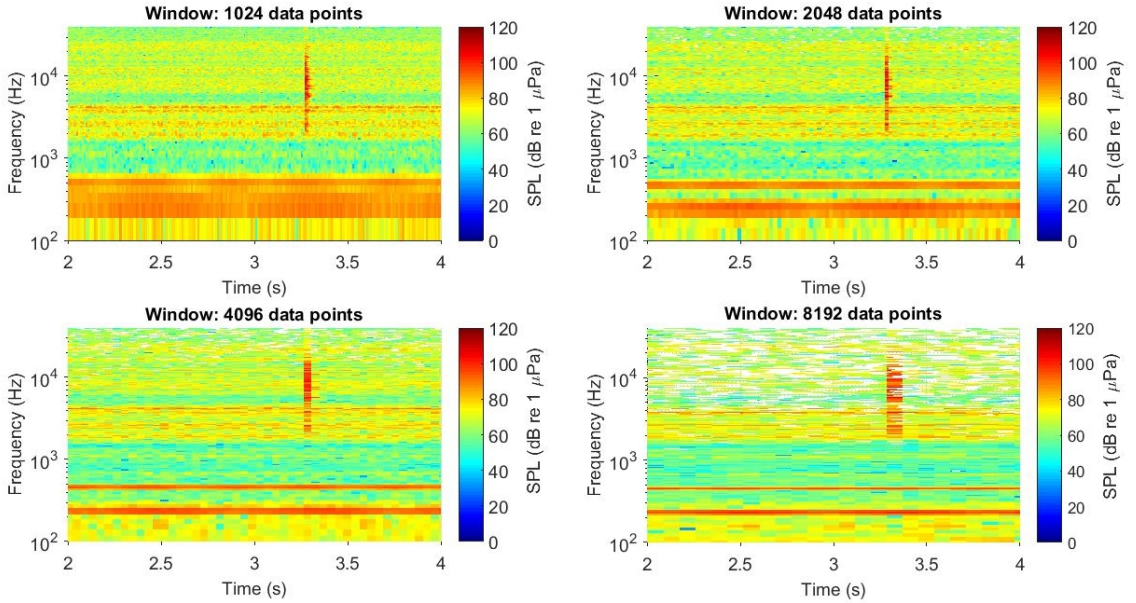

(b) Spectrogram of a medium amplitude signal showing multiple window sizes (1024, 2048, 4098 and 8192 data points).

Figure 5.6: Representative example of a medium amplitude signal.

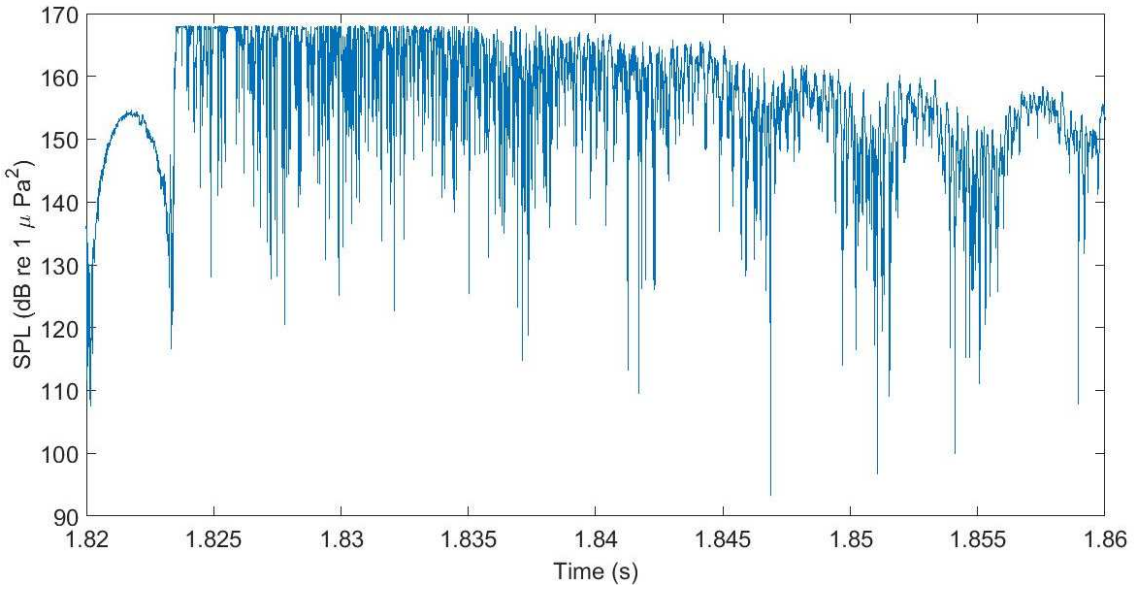

(a) Time domain SPL of a high amplitude signal.

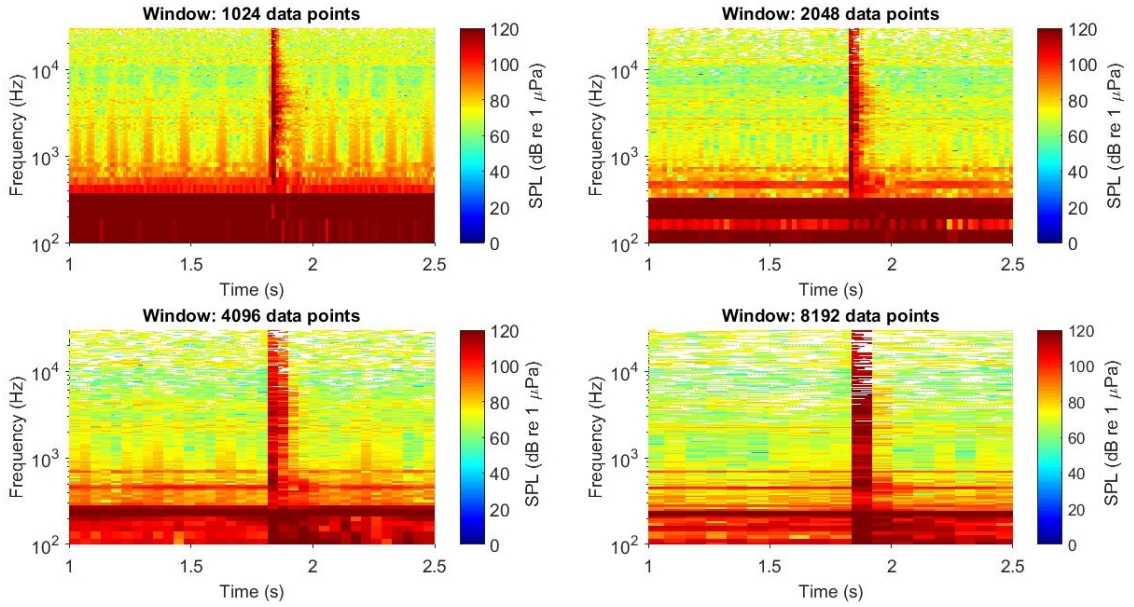

(b) Spectrogram of a high amplitude signal showing multiple window sizes (1024, 2048, 4098 and 8192 data points).

Figure 5.7: Representative example of a high amplitude signal.

5.4 Sample Failure

Each rope sample failed at a different breaking load close to a splice either located at the z-ram or headstock. The origin splice of the AE signatures could be determined due to the synchronisation of the hydrophone array. In Figure 5.8 the synchronised signals from the 2 hydrophones are shown for 2 high amplitude signals. At this time resolution, it is impossible to determine which of the two hydrophones recorded the signal first, and hence determine which splice the AE originated form. However, increasing the time resolution as in Figure 5.9 shows that the signal originated from closer to the z-ram hydrophone as that signal was recorded $0.0008s$ sooner. Over a distance of 1.21 m, this corresponds to a sound speed of 1500 ms^{-1}, the speed of sound in water. This technique was used to determine the origin location of all significant signatures, including the failure locations.

Rope 1 failed at 98 kN (76% MBL) near the z-ram. The acoustic signature of this failure is shown in Figure 5.11 and the sample failure is shown in Figure 5.10a. Three high amplitude signals are seen within 0.3 s of each other at 9 s. There are then two significant "failure" signals shown at 9.4 s and 10 s which are assumed to be the core failure and cover failure respectively.

Rope 2 failed at 98.5 kN (77% MBL) near the headstock. The failure of this sample included the core failing first (shown in Figure 5.12), DMaC being shut off after assuming to be a completely failed sample, and upon visual inspection the cover was still intact. Therefore, the cover was then a second failure (shown in Figure 5.13). The sample failure is shown in Figure 5.10b.

Rope 3 failed at 112 kN (87% MBL) near the headstock. The acoustic signature of this failure is shown in Figure 5.14 and the sample failure is shown in Figure 5.10c. Unlike the other two samples, there was no separate failures for the core and cover. However, there was a high amplitude signal 10 s before failure.

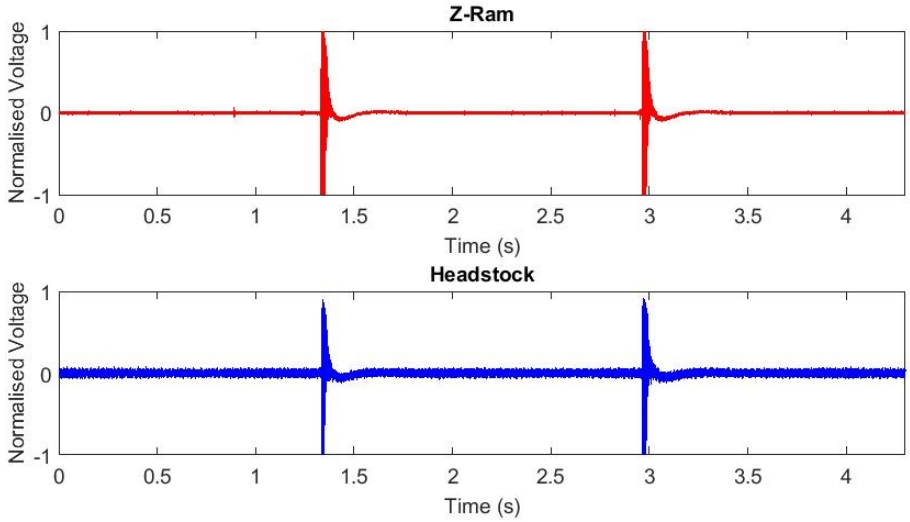

Figure 5.8: Two synchronised time domain signatures of two high amplitude signals. Red is from the Z-ram hydrophone, blue is from the headstock hydrophone.

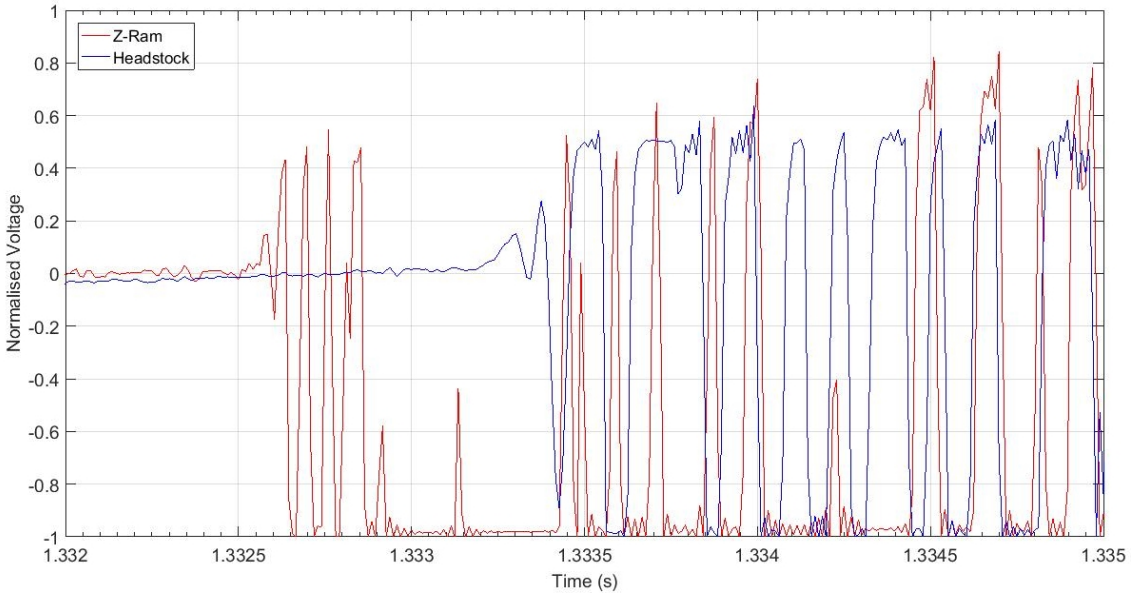

Figure 5.9: Zoomed-in synchronised time domain signature of a high amplitude signal. Red is from the Z-ram hydrophone, blue is from the headstock hydrophone.

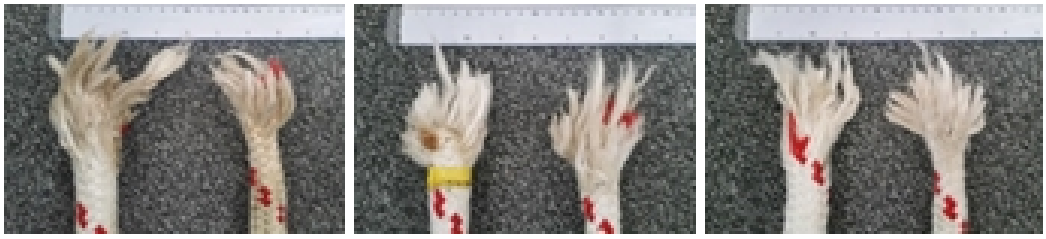

(a) Photo of rope 1 failure. (b) Photo of rope 2 failure. (c) Photo of rope 3 failure.

Figure 5.10: A summary of the failure information for the 3 synthetic fibre rope samples.

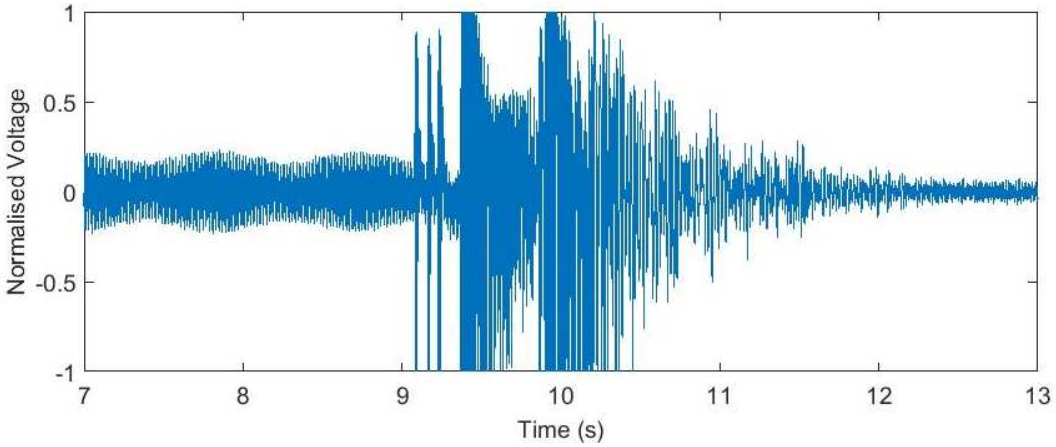

(a) Time Series with normalised voltage.

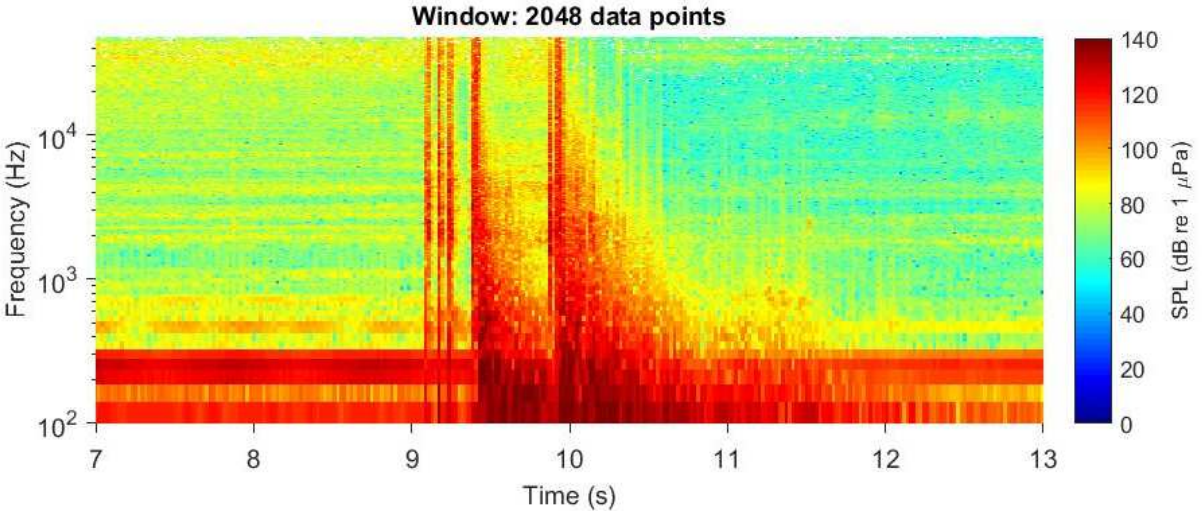

(b) Spectrogram with window size of 2048 data points.

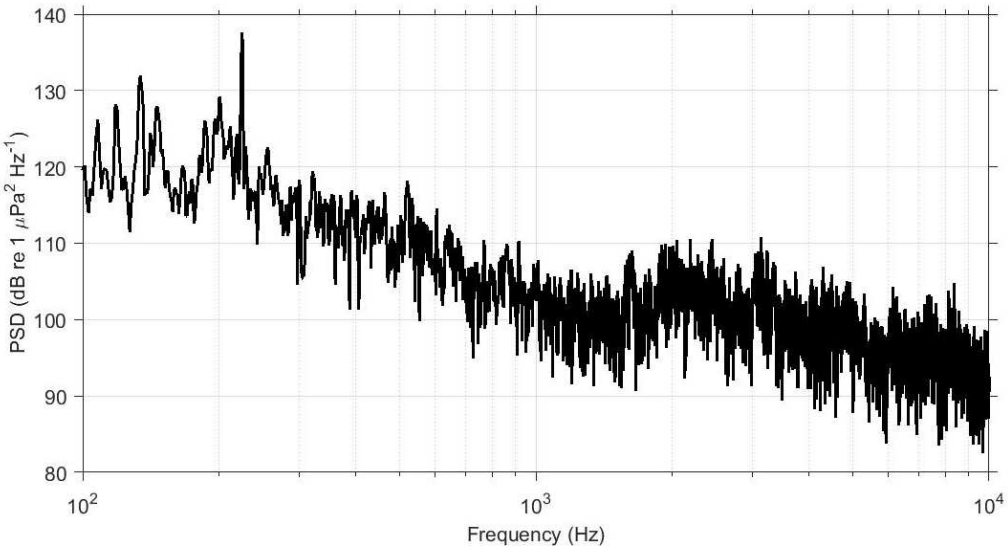

(c) PSD with 1 Hz frequency resolution.

Figure 5.11: Rope 1 failure at 98 kN.

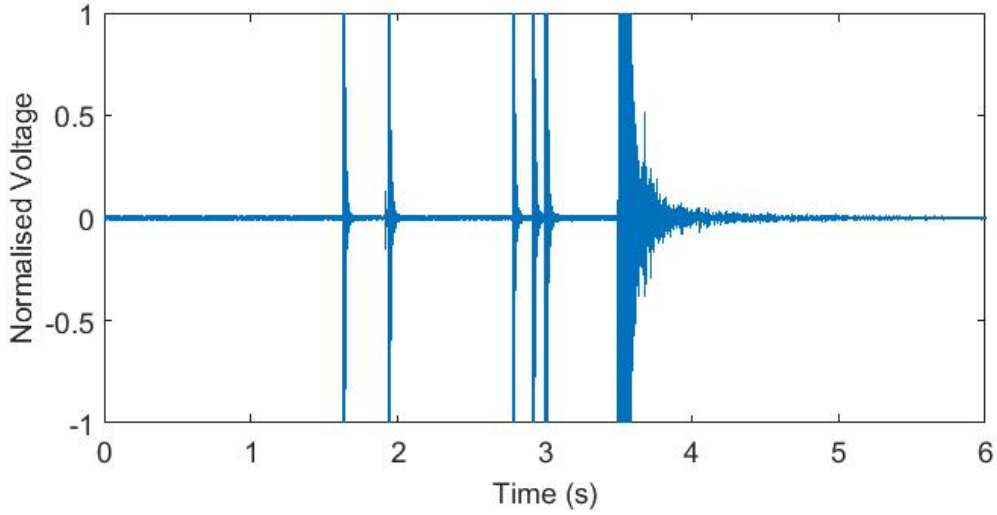

(a) Time Series with normalised voltage.

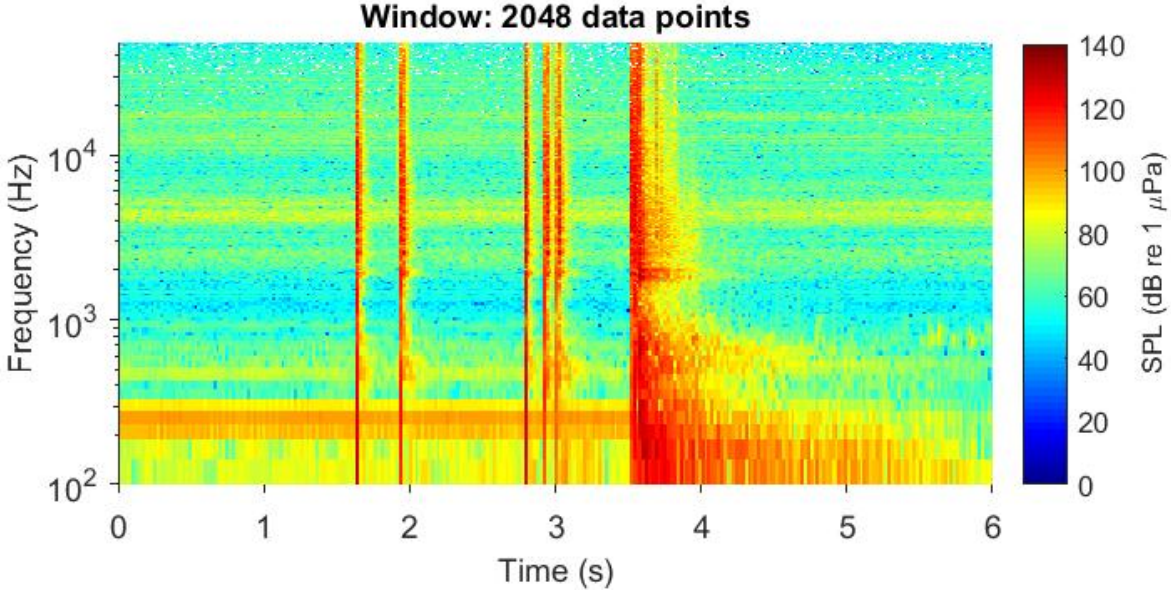

(b) Spectrogram with window size of 2048 data points.

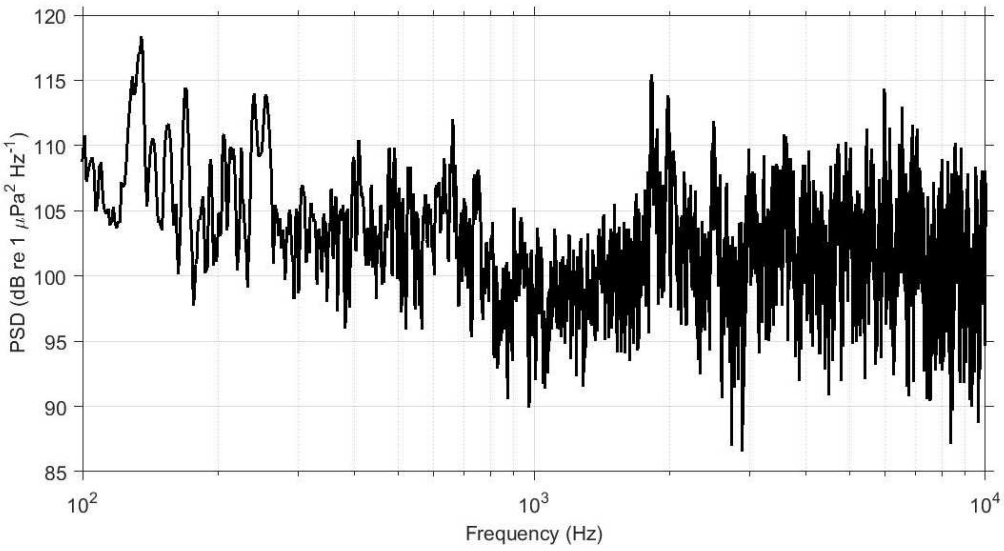

(c) PSD with 1 Hz frequency resolution.

Figure 5.12: Rope 2 core failure at 98.5 kN.

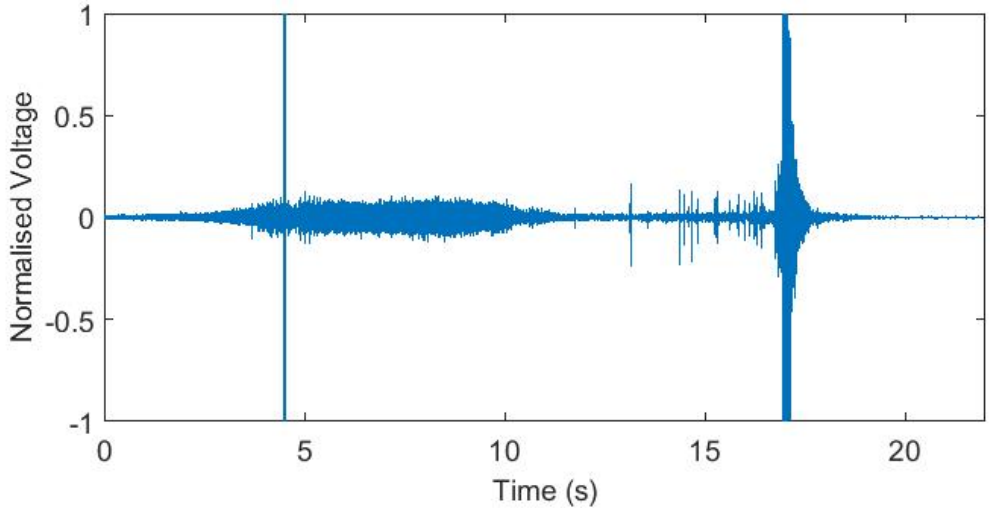

(a) Time Series with normalised voltage.

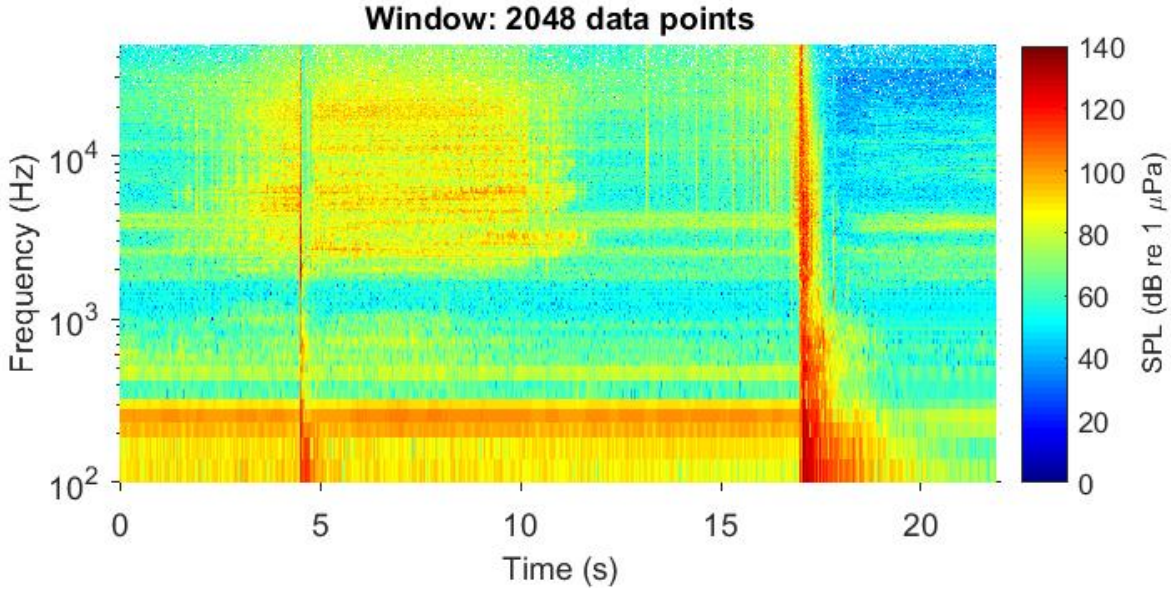

(b) Spectrogram with window size of 2048 data points.

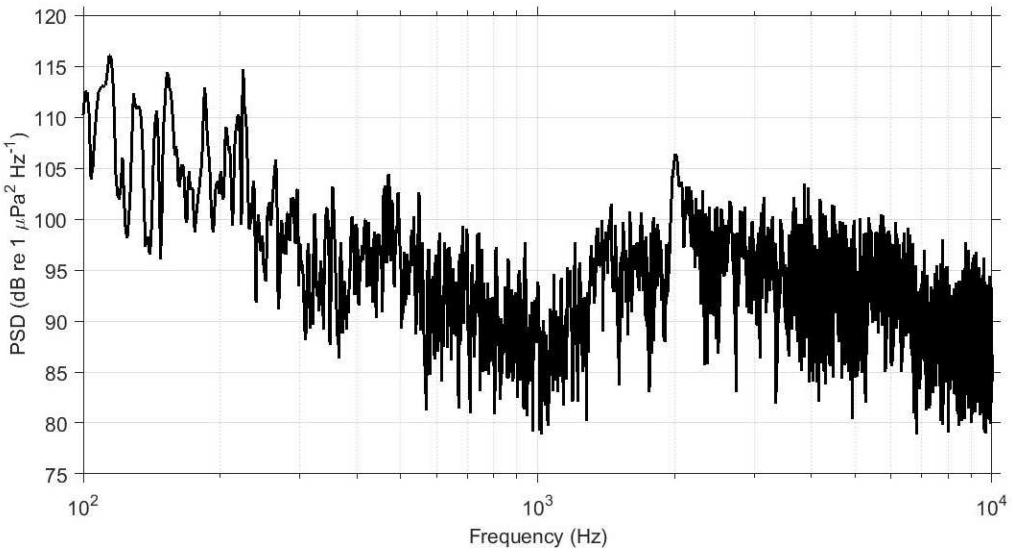

(c) PSD with 1 Hz frequency resolution.

Figure 5.13: Rope 2 cover failure at 98.5 kN.

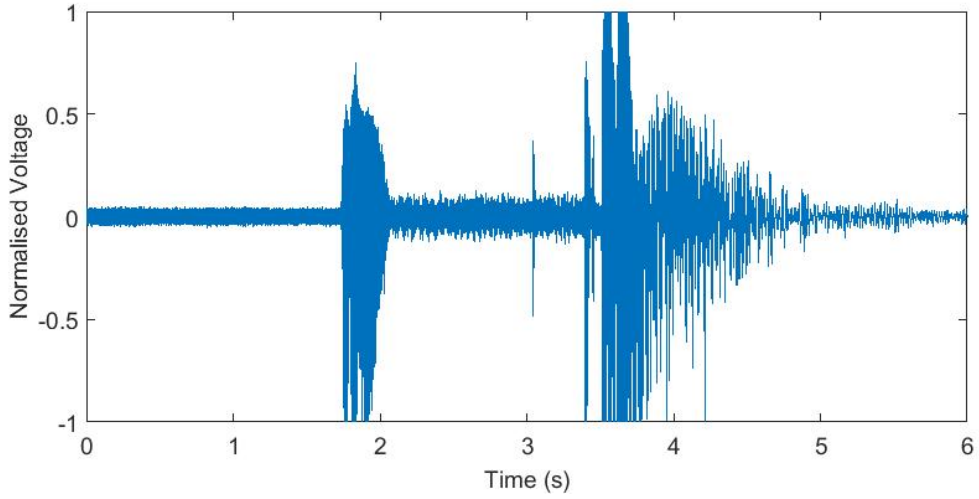

(a) Time Series with normalised voltage.

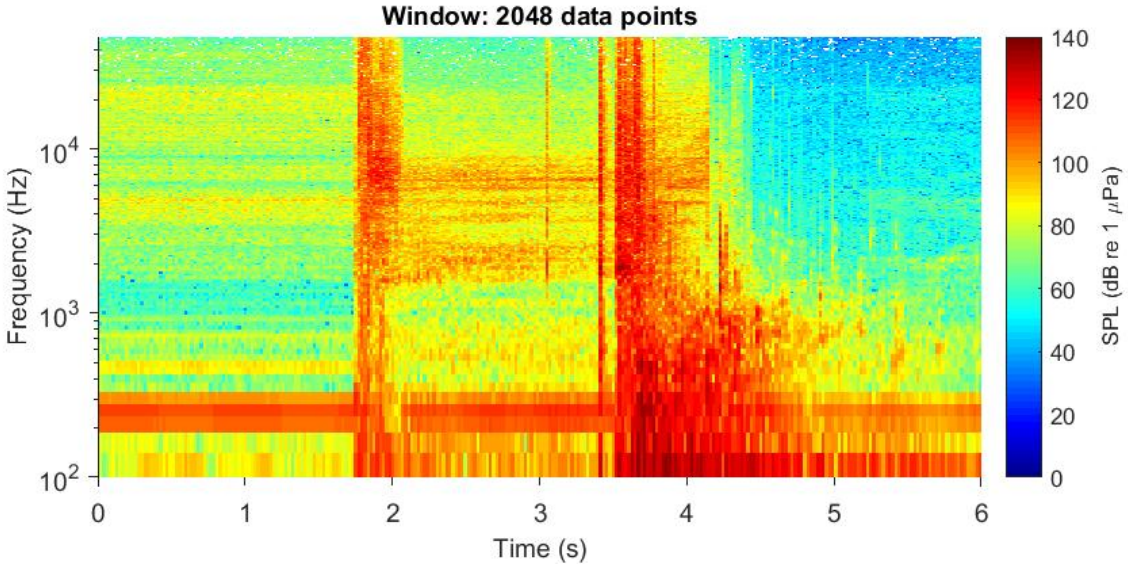

(b) Spectrogram with window size of 2048 data points.

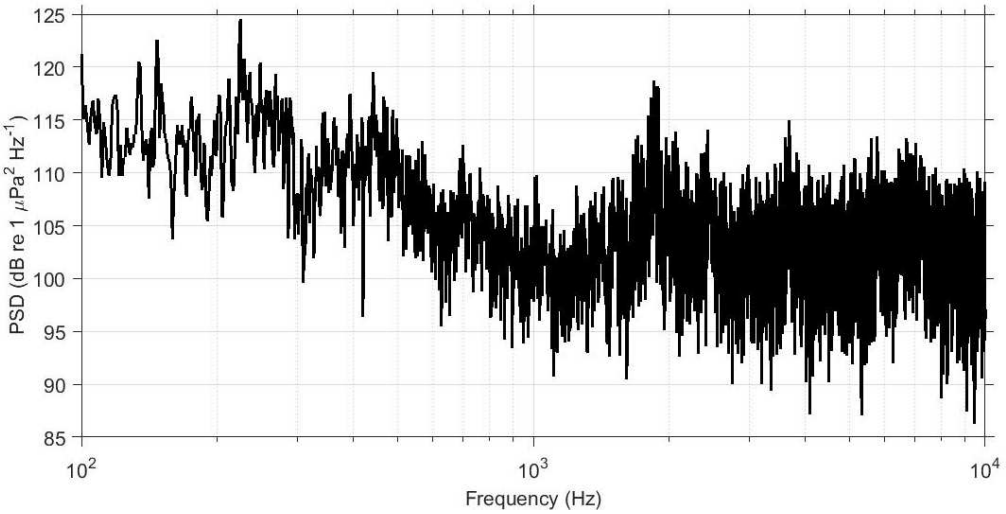

(c) PSD with 1 Hz frequency resolution.

Figure 5.14: Rope 3 failure at 112 kN.

5.5 Full Testing Cycle Results

When considering the rope testing for each sample, it was important to use the classification system outlined in Section 5.3 to understand the progression of the AE emitted. AE in synthetic ropes was detected as low amplitude signals when the cyclic loading was increased to more than 50% MBL (64.5 kN). As the loading increased beyond 70% MBL (90.3 kN), the rope samples entered into a new AE regime and started producing more frequent high-amplitude AE signals. Figure 5.15 shows the total number of AE signals recorded against the maximum applied loading force for each rope sample respectively. For R2 and R3 the origin of these signals are also distinguished.

With the increase in cyclic loading force, the rope samples produced a series of high-frequency AE signals. As the mean load was increased more high-frequency noise along with a series of high amplitude signals were produced followed by internal core and subsequent outer core failure. All rope samples failed before the rope was loaded to the MBL specified by the manufacturer i.e. the rope samples R1, R2 and R3 failed at 76% MBL, 77% MBL and 87% MBL respectively. The failure location was identified by the time difference of arrival measured with the hydrophone array.

Figure 5.15 shows the accumulative AE signals observed under cyclic loading for all 3 rope samples. Figure 5.15a details the loading for R1 where there is no AE activity until loading of up to 75 kN. The first high amplitude click was detected at maximum loading of 90 kN (70% MBL). The number of AE signals steadily increased until a maximum loading of 93 kN where there was a quiet period. Maximum loading of 97 kN and 98 kN then saw a combined total of 15 medium or high amplitude signals and sample failure occurred at 98 kN after 23 AE signals were detected, 17 of which were medium amplitude or high amplitude.

A similar result was recorded for R2 as shown in Figure 5.15b. No AE activity was detected until 70 kN where a low amplitude signal was detected from both the headstock and Z-Ram splice. The first high amplitude signal was detected at 93 kN (72% MBL) from the headstock splice. A quiet period occurred from 81 kN to 92.5 kN loading. Between 97.5 kN loading and failure, 13 high amplitude clicks originated from the headstock splice, and 1 from the Z-Ram splice. At 98.5 kN the sample failed at the headstock splice. In total 46 AE signals were detected, 23 of which were medium or high amplitude signals.

Finally, the progression of AE in R3 is presented in Figure 5.15c. The first AE signal was detected at 71 kN (55% MBL) at the Headstock. No other activity was detected at either splice until 80 kN where a number of low amplitude and broadband signals were detected. A quiet period then occurred between 85 kN and 102 kN. The first high amplitude signal was detected from the headstock splice at 104 kN (81% MBL) shortly followed by a high amplitude signal at the Z-ram at 105 kN. Between 104 kN and sample failure 4 high amplitude signals were detected from

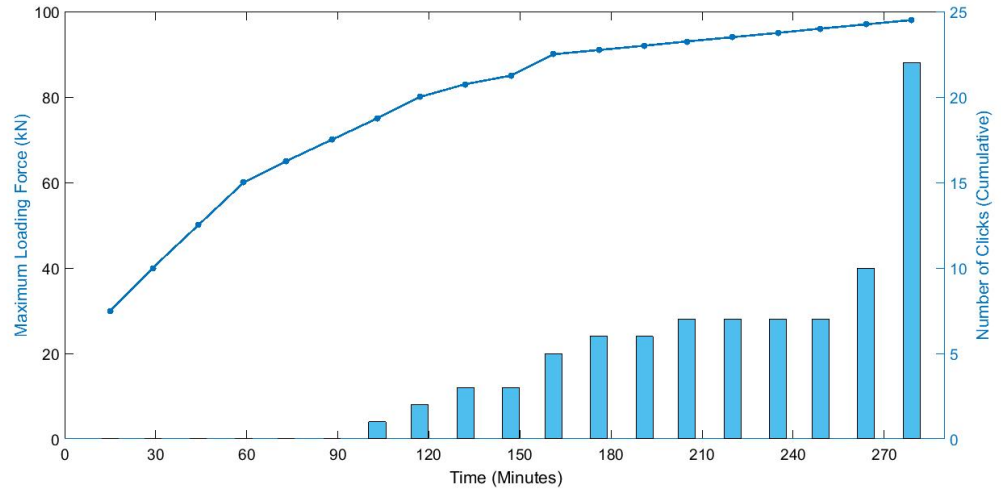

(a) Rope 1.

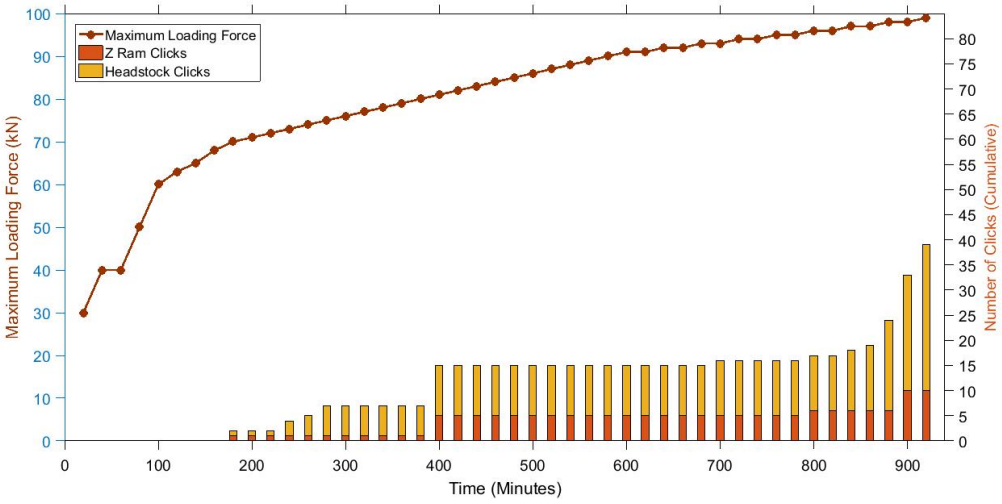

(b) Rope 2.

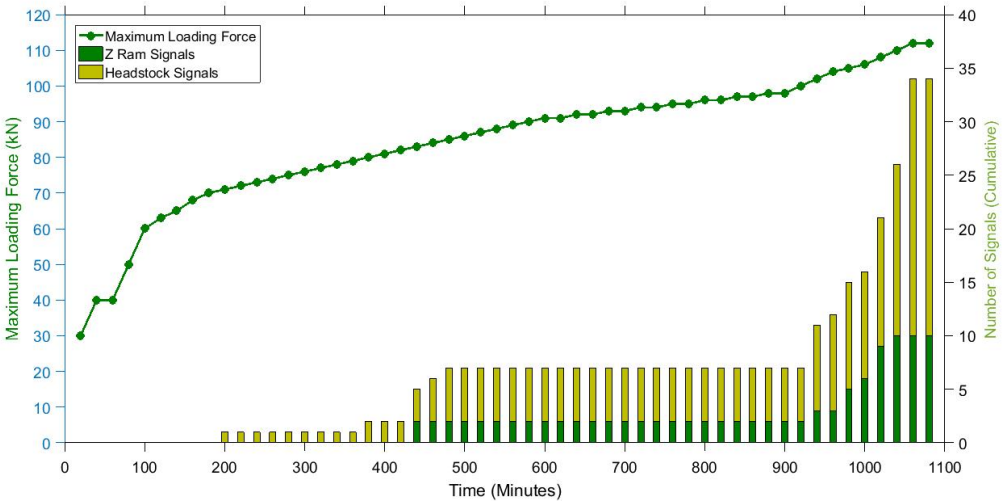

(c) Rope 3.

Figure 5.15: Total number of AE signal vs maximum loading force (kN) with respect to the cyclic loading (minutes) applied on each rope sample.

the Z-ram and 11 from the headstock. At 112 kN the sample failed at the headstock splice. In total, 34 AE signals were detected from R3, 20 of which were medium or high amplitude signals.

5.6 Discussion

This discussion is divided into two subsections to distinguish between the new methodology presented and the results from the experimental testing.

5.6.1 Experimental Methodology

Chapter 3 presented a new methodology for the identification and recording of underwater AE monitoring within offshore component testing at the DMaC test facility. Overall, the designed setup provides a suitable method for submerged AE testing of synthetic mooring ropes. However, it is acknowledged that there are some limitations to the experimental method if compared to the AE that would be measured offshore.

The selected ropes are small in diameter and short in length compared to mooring lines at used at sea. These experiments are carried out by shortening the length of the rope as it is not possible to test full length ropes in most tension-tension test rigs and furthermore it is standard practice to test short samples (Weller et al. 2014). The mooring ropes used in these tests are of similar material and construction, therefore the test results are deemed to be representative. Similarly, the loading has been carried out using accelerated testing with the assumption that the damage accumulates over the lifetime of the ropes (Thies et al. 2016). The correlation between the accelerated rope testing for synthetic ropes under controlled laboratory conditions (DMaC test rig) has been compared with real sea data (Rodríguez et al. 2015). The comparison between two tests and numerical simulation concluded that it might be possible to carry out accelerated testing on ropes by accumulating failures modes (Rodríguez et al. 2015). In this study the number of samples are limited; however, all samples produce very consistent and similar results.

The use of multiple hydrophones allowed for the localisation of underwater AE with good results. However, this could be further improved with the inclusion of a third hydrophone, with varied depth, to allow for 3-D localisation of the underwater AE. This could then be tested as a technique before use in arrays of WECs. Synchronising the DMaC data loggers to the recording equipment would allow for exact correlation between the loadings experienced and AE produced, which could provide further evidence regarding the physical phenomenon behind the AE produced. At this time, it is only known that the AE is produced when the loading is at a maximum (of the loading schedule) but not if it is just prior to the maximum, on the maximum, or just after the maximum during relaxation.

One similar experiment was presented in ABS Consulting (2015). In this work, underwater and in-air Acoustic Emission Testing (AET) was conducted for chain and wire ropes. Fatigue testing was conducted on a full size mooring chain with sensors mounted onto the chain links and 2 of the 4 chains submerged in a seawater tank. Sensors were resonant based sensors with 150 kHz resonant frequency, operation range of 80 - 300 kHz and used in a passive manner. The results of this work showed that AET is a promising technique for mooring chain and wire rope monitoring, with the possibility of detecting crack initiation, propagation and fracture. The work presented in this thesis differs in a number of ways. We test synthetic polyester mooring rope, not chain or wire rope. The experiment presented here is fully submerged, with hydrophone sensors placed 10 to 15 cm away from the sample whereas ABS Consulting (2015) present partially submerged testing with traditional AE sensors placed on the chain links. The work presented in ABS Consulting (2015) does however give confidence that the type of testing being conducted in this thesis is of similar nature to commercially conducted work.

5.6.2 Experimental Results

Underwater AE measured during loading of mooring ropes has been studied at the DMaC test facility. Multiple AE signatures were recorded from the 3 samples tested. The measurements obtained indicate that the AE signals could be related to different physical phenomena such as bedding in, fatigue, slippage and failure.

Initially low amplitude signals were detected which might be produced due to realignment or rubbing of the fibre threads in the rope (Weller et al. 2014). Previous work focused on several different kinds of damage mechanisms in ropes and studied the performance and durability of a rope deployed for 18 months at sea (Weller et al. 2014). The study reasoned that wear occurring due to friction between the moving fibres or yarns, accelerated by the ingress of particles into the rope structure, was a likely cause of altered rope properties including a lower measured MBL. Friction occurring between the fibres will cause localised heating of the rope and could cause AE. The low-amplitude signals recorded provide some indication of the possible initialisation of weak points in the rope as all ropes failed in the proximity of where these signals had been detected first. The low-amplitude signals could be evidence of early macrocrack growth 2.4.

With the progressive application of load cycles, the rope samples started producing high-amplitude signals. The spectral content and time domain waveforms of the high amplitude AE signals are identical to what was observed for all rope samples. Therefore, it is likely that a similar physical phenomenon is producing these signals. The hypothesis is that the high-amplitude AE signals might have been generated by the fatigue and failure of load bearing elements in the rope (i.e. fibres, yarns and/or yarn assemblies) possibly caused by abrasion between contacting

elements (as reported in Weller et al. 2014). These failures might also be the result of unequal load sharing in short rope sample. Therefore, the rope failed on either end near the splice. The partial failure of Rope 2 where the core failed, and then upon further loading the cover, further endorses this hypothesis.

The time of arrival at the hydrophones for these high amplitude signals was used to locate the weak point in the rope. It was concluded that all observed high amplitude signals were more or less originating from single or multiple weak points identified earlier in the rope. Counting the number or the intensity of high amplitude signals could be used to monitor the condition of mooring ropes in-situ. AE can be potentially used to predict imminent rope failure to avoid a catastrophic incident.

All rope samples failed at different breaking loads at, or close to, a splice. Figure 5.15 plots the accumulative AE signals for all 3 rope samples. All rope samples failed at the splice that first created a high amplitude signal which could be a significant result for the detection of weak points (as evidence of fatigue) and their progression into failure. However, the restriction to only 3 samples because of time constraints limits the reliability of the hypothesis.

Considering Figure 5.15 it was considered that each of the bar charts potentially showed a logarithmic relationship. Further investigation led to Figure 5.16. The maximum load data was normalised to the failure loading for each rope (R1: 98kN, R2: 98.5 kN and R3: 112 kN), hence on the x-axis in Figure 5.16, 100 represents sample failure. The cumulative number of high amplitude signals was converted to the number of high amplitude signals per second, using knowledge of the length of one cyclic loading cycle. This enabled a logarithmic relationship to be shown for all three samples. The R^2 values for each logarithmic fit are 0.806, 0.741 and 0.995 respectively. If further tested and confirmed, this could be used as a predictive tool for estimating the loading at which a rope would fail, rather than relying upon manufacturer MBL specifications. However, the small sample size means these interpretations should be used with caution.

This work acts as a baseline and there is a clear need to carry out more testing for identical samples under identical loading conditions. Such experimental data could then be used to develop an empirical derivation for continuous monitoring and the prediction of imminent mooring rope failures.

The AE signals were produced over various frequency bands with varying amplitude. Table 5.2 summarises the frequency ranges and corresponding amplitudes. For AE monitoring, it is important to understand how far away the AE signals could be detected. The measured amplitudes for the low- and high-amplitude signals were around 90 dB re 1 μPa and 125 dB re 1 μPa respectively. These amplitudes can be regarded as source amplitudes, measured at a distance of 0.1 m from the source in a controlled laboratory environment. Ignoring other factors for transmission loss spherical spreading can be used to approximate sound attenuation

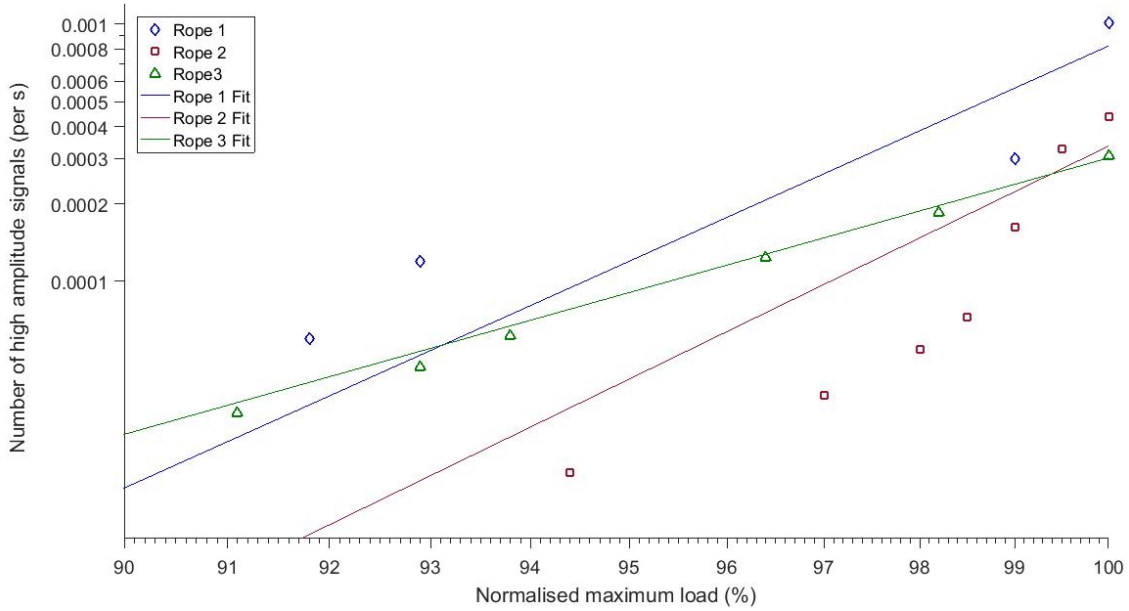

Figure 5.16: Logarithmic relationship between normalised maximum loading (as a percentage of failure loading) and the number of high amplitude signals per second for all 3 samples.

over a distance from the source. The spherical spreading transmission loss for respective distances of 200 m, 500 m and 1 km are 46 dB, 53 dB and 60 dB respectively. The sound attenuation in the sea is also dependent on the frequency of its propagation. The absorption due to seawater at 1 kHz, 10 kHz and 50 kHz is 0.06 dB/km, 0.76 dB/km and 12.77 dB/km (Francois and Garrison 1982). Background noise in the ocean is usually high, with low frequencies dominated by shipping noise and higher frequencies with wave and wind noise (Wenz 1962). High frequencies also experience more attenuation; therefore an AE signal with a broadband frequency spectrum is more likely to be detectable.

The existing monitoring methods for mooring lines have limited applications. The most commonly used method is visual inspection, which is challenging and potentially hazardous for divers, and also damage can occur to the mooring lines. The accumulation of marine growth can also restrict the effectiveness of visual inspections. Direct and indirect in-line tension monitoring technology exists to detect failures. Similarly, other techniques include inclinometers which detect failures through mooring line angle, load cells which use load monitoring and Global Positioning System (GPS) systems monitoring differential displacement of mooring ropes. All these methods are capable of only detecting an already-failed mooring system.

The proposed technique in this work points towards a technique that allows the continuous monitoring of mooring ropes including the detection of developing failures, located away from the dynamic mooring ropes themselves. This would also enable the monitoring of several ropes (or indeed components across multiple WECs in an array) simultaneously. The use of multiple hydrophones would allow for 3-D

failure localisation as partially demonstrated here in 2-D in DMaC testing.

Chapter 6

Propagation Modelling

This Chapter investigates the propagation of the WECs AE and how it changes and evolves through the WECs life cycle. A comparison is made between the effectiveness of both propagation modelling with Bellhop and simple cylindrical spreading calculations for propagation of signals in a WEC environment like FaBTest. It leads to a novel quantification of the effect of the WEC on the local soundscape with consideration to the amount of useful electricity generated. These results have been published in (Walsh et al. 2017b).

6.1 Acoustic Metric Results Summary

Key underwater acoustic metrics from each period of the underwater acoustic life cycle (pre-installation, installation, operational & non-operational, condition based monitoring, decommissioning) are presented in this section. These are found within (Garrett 2015), except for condition-based monitoring, found within (Walsh et al. 2017a).

Pre-Installation

The study of the *Lifesaver* WEC began with a "baseline period" that lasted 2 weeks, before the installation of the device at FaBTest. It was found that mean 30-minute sound levels ranged from 34 dB re 1 μPa^2 Hz^{-1} at 47,964 Hz to 113.4 dB re 1 μPa^2 Hz^{-1} at 76 Hz (Garrett 2015).

Results from (Garrett 2015) suggested that Falmouth Bay (classed as having high anthropogenic activity), is overall *quieter* than other similar published sites, which could be due to reduced contribution from distant shipping given the shape of Falmouth Bay. Sources of noise were attributed to shipping, sonar-like sounds and snapping shrimps during the 2-week pre-installation period.

Installation

The "installation period" lasted 5 days and included all activities associated with

the installation of the WEC at FaBTest, including, but not limited to the presence of work vessels and the laying of anchor chains. No drilling or pile driving was required, and no power cables to shore were installed. Therefore the WEC is classed as having minimal installation requirements, being a prototype, without a cable connection to shore. This technique is typical for attenuator/point absorber devices that float on the sea surface (Austin et al. 2009). Installation activity was noticeable during 20% of the recording time during the 5-day installation period.

Mean broadband SPL_{RMS} during installation was 117.2 dB re 1 μPa (Garrett 2015). Installation activity was found to increase sound levels by a mean 6.9 dB from pre-installation activity, in the frequency range 10 Hz - 48 kHz (comparing like for like data in terms of wave conditions) (Garrett 2015). The lowest frequency range (10 – 100 Hz) was found to exhibit the greatest difference (nearly 20 dB) between pre-installation and installation periods, but the loudest received levels were recorded in the frequency range of 100 Hz - 1 kHz (Garrett 2015).

Operational and Non-Operational Periods

The WEC was inactive during low wave conditions, i.e. significant wave heights $H_s = 0.4 - 0.6\ m$ (Sjolte 2014). The WEC survived and operated in rough wave states up to $H_s = 5.1\ m$ (Sjolte 2014).

Acoustic metrics during these periods were calculated in (Garrett 2015) over long time periods (either a single period of AMAR recording, for up to 90 days or several successive periods). Comparing operational and non-operational values of broadband SPL_{RMS} does not lead to clear conclusions, with some louder overall levels during operational activity and some during non-operational activity. This indicates that there is no overall effect of the WEC on the broadband SPL_{RMS} values at this location, most likely due to the many other sources of noise in Falmouth Bay (Garrett 2015). From 10 Hz to 32 kHz, the mean difference between median PSD levels during operational and non-operational activity was just 0.04 dB (this is negligible, achievable in ± 1 dB operational accuracy best practice (Robinson et al. 2014)). However, this was higher between 10 Hz - 100 Hz, where the mean difference was greater than 0.46 dB (but still below ± 1 dB).

This low level difference had been previously noted for *Wavestar* and attributed to moving parts being located above the sea surface (Tougaard 2015), although this particular conclusion was drawn from only 57 minutes of data. It should also be noted that most operations of the *Lifesaver* used only 1 or 2 PTOs concurrently (Garrett 2015).

Acoustic Emissions

Condition-based monitoring consists of associating different acoustic signatures to modes of operation and (most often) the noise produced by moving parts, in

the WEC or in its moorings. In this context, broadband measurements of periods of operation were analysed (Walsh et al. 2017a). The operational status and engineering "log book" from the device developers were matched to the 30-minute acoustic recordings acquired in each mode of operation, enabling the comparison of acoustic signatures with particular modes or tests of the WEC. The specific details are commercially confidential and cannot be published, but the most notable are acoustic "bursts" (e.g. (Walsh et al. 2017a)). These "bursts" last 0.5 s on average, with SPL values up to 120 dB re 1 μPa^2 Hz^{-1}, mostly between 100 Hz and 1 kHz (Walsh et al. 2017a). They are attributed to vibrations in the primary (active) mooring system, induced by high sea states. Their period is approximately 6 s, matching the period of oscillations in the primary mooring. Tonal components at 30, 60, 80 and 100 Hz, reaching 110 dB re 1 μPa^2 Hz^{-1} are also attributed to the device generator (Walsh et al. 2017a).

Once detected, these signatures were found throughout the operation of the WEC by detailed time/frequency analyses of the data, inspected visually. This signature was only detected when averaged measured wave heights were above 0.9 m.

Decommissioning

Although the data considered here does not include any recordings from the decommissioning period of the WEC at FaBTest, it can be assumed to be similar to the installation period in terms of ship activity (and type of ship). The decommissioning of the WEC took place between 30th May – 4th June 2014, when it was disconnected from its moorings and towed to the neighbouring Falmouth Docks (Falmouth Harbour Commissioners 2014). This phase of activity was followed by the removal of the moorings (Falmouth Harbour Commissioners 2014). Although funding constraints and equipment availability meant there were no long-term recordings available for this period, the decommissioning period was very similar to the installation period of the WEC. Similarities included the length of time required, the numbers and types of vessels used, and how equipment was moved. Therefore the acoustic signatures produced during the decommissioning period can be assumed to be very similar to those produced during the installation period.

6.2 Sound Propagation Modelling Results

The sound levels presented have all been measured at locations slightly different for each AMAR deployment (although they were at very similar ranges from the WEC). Each deployment may have been affected differently by changes in the properties of the shallow waters of Falmouth Bay depending on the season and the weather. It may therefore necessary to reference them to as close to actual SL as possible. This will be important to relate acoustic footprints to different stages in the life

cycle of the WEC, and this will greatly facilitate the comparisons with studies of other WECs, done in different conditions and in different water depths. However with continually changing environmental properties, it may be difficult to obtain accurate results.

For its computational efficiency and general adequacy, the sound propagation model Bellhop was selected as described in Chapter 3. This ray/beam tracing propagation model was developed by Michael B. Porter at the Naval Ocean Systems Center (now SPAWAR) as part of the Effects of Sound on the Marine Environment (ESME) project (Porter 2011a). The model predicts acoustic pressure fields in ocean environments and its beam tracing structure leads to what the author describes as "a particularly simple algorithm" (Porter 2011a). The model allows for the input of range-dependent parameters such as sound speed profile and bathymetry and considers interaction with the seafloor along the propagation path. The outputs of the model can include transmission loss, eigenrays, arrivals and received time-series.

In this thesis, Bellhop was selected as the model of choice compared to the alternatives described in Chapter 3 because of its range-dependant bathymetry input, its suitability to be used for shallow waters at high frequencies, its ease of use within MATLAB and computational efficiency. Its reduced accuracy at low frequencies (dependant upon water depth) was considered, but not deemed significant as there is a large amount of contaminating shipping noise in the area already affecting low frequencies.

Two propagation scenarios were created, one with idealised conditions of a flat seafloor, flat sea surface and ideal reflector, and the other including a local bathymetry profile and actual sediment information for a more accurate modelling environment. These are shown schematically in Figure 6.1. In the ideal case, the water depth was kept constant at 40 m (the local bathymetry varies instead between 40 and 60 m). The speed of sound in the water column was in both cases kept constant (1,500 m s^{-1}) because of the small variations seen during the winter months, associated with increased mixing from the weather (Garrett 2015). For the same reason, the water density was kept constant (1,024 kg m^{-3}). For the ideal case, the seafloor was given the default AcTUP values (sound velocity of 1,749 m s^{-1} and sediment density of 1,941 kg m^{-3}). For the more detailed conditions, a sediment sound speed was used (Etter 2013), with the density of wet, packed, sand (The Engineering Toolbox 2010), corresponding to a sound velocity of 2,000 m s^{-1} and a sediment density of 2,082 kg m^{-3}. Both models were run for the reference frequency of 1 kHz, with the source 5 m below the sea surface (based on the WEC dimensions).

Figure 6.2 shows transmission loss calculations for both the idealised and detailed propagation models considering both range and depth for a 1 kHz signal. Although this figure gives a good visual overview of the entire water column, it is difficult to

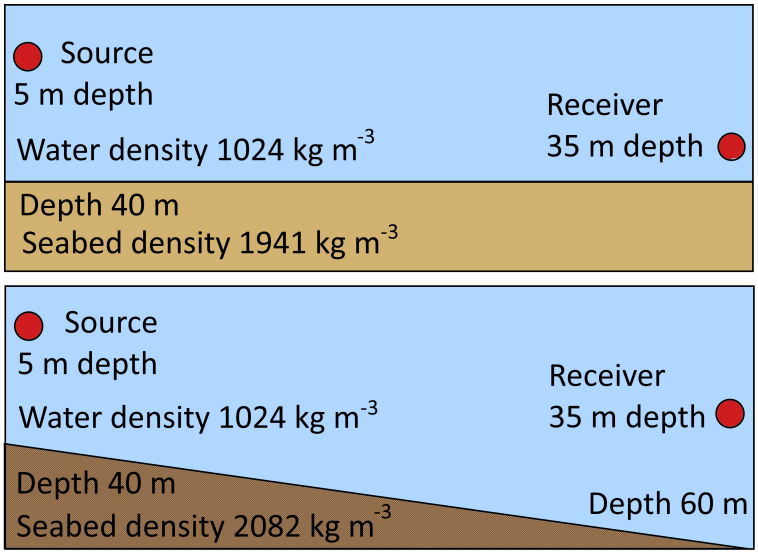

Figure 6.1: Schematic of the Bellhop model parameters and boundaries for idealised conditions (top) and detailed conditions (bottom).

interpret the results at any depth of interest.

Figure 6.3 shows the same data only at 35 m depth (the approximate depth of the receiver in the associated study) for both a 1 kHz signal and a 10 k Hz signal. The red line corresponds to the idealised conditions and the blue line is as described in Figure 6.1. The differences between the idealised and detailed conditions are significant: multi-path propagation in this shallow environment creates considerable variability in the transmission loss, especially sensitive to position (range) as well as input model parameters. Moving the receiver by just a few meters (which is highly possible between deployments, or during a deployment because of changes in mid-water currents) could create variations in the transmission loss of up to 20 dB. This variability is much higher than the expected experimental uncertainty of $\pm$ 1 dB (Robinson et al. 2014). To compare with the spherical spreading calculations, these are included in Figure 6.3 and they provide a conservative limit to the Bellhop model results.

It is also interesting to consider the changes in these results with frequency. Because of the depth of the water column, any calculations with a frequency less than 750 Hz should be considered cautiously. For this reason, the frequencies 1 kHz, 2 kHz, 5 kHz and 10 kHz were considered. While the PTO signature found from the *Lifesaver* device only reaches 1 kHz, other signals, such as those discovered during the DMaC mooring rope testing, do reach 10 kHz and beyond. The model results are shown in Figure 6.4. While it only shows the results of the idealised environment, is it evident that the results are highly variable in TL with respect to range.

Because exact back-propagation is limited by the high potential variation of environmental parameters, it was decided instead to use the accepted approximations for spherical spreading as described in Chapter 3. The SL in dB of

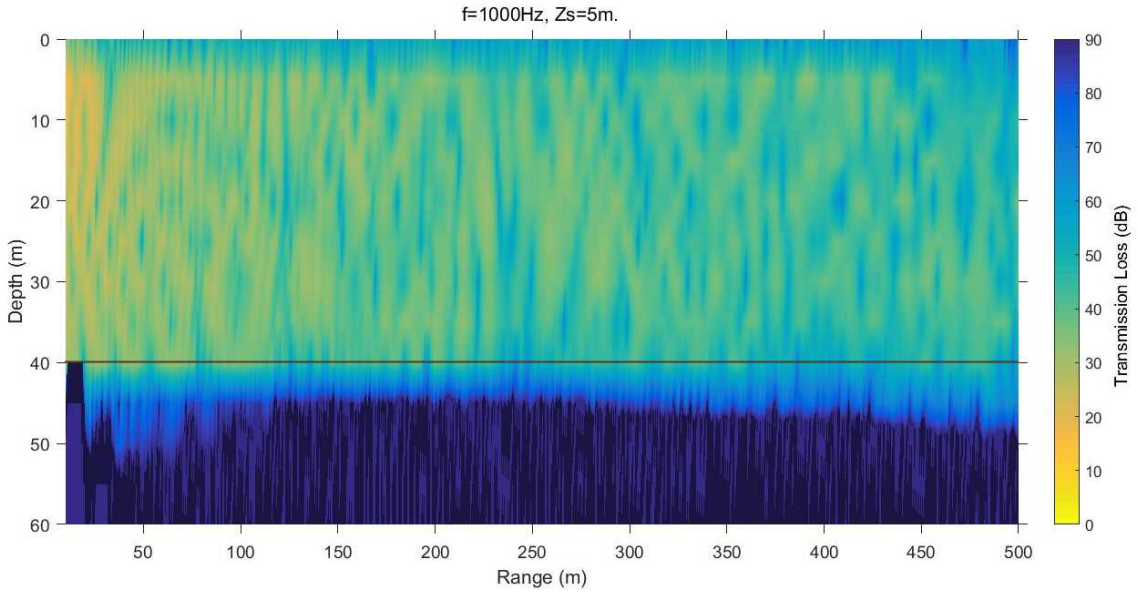

(a) Spectrogram of TL for an idealised (simple), flat environment of 40 m depth.

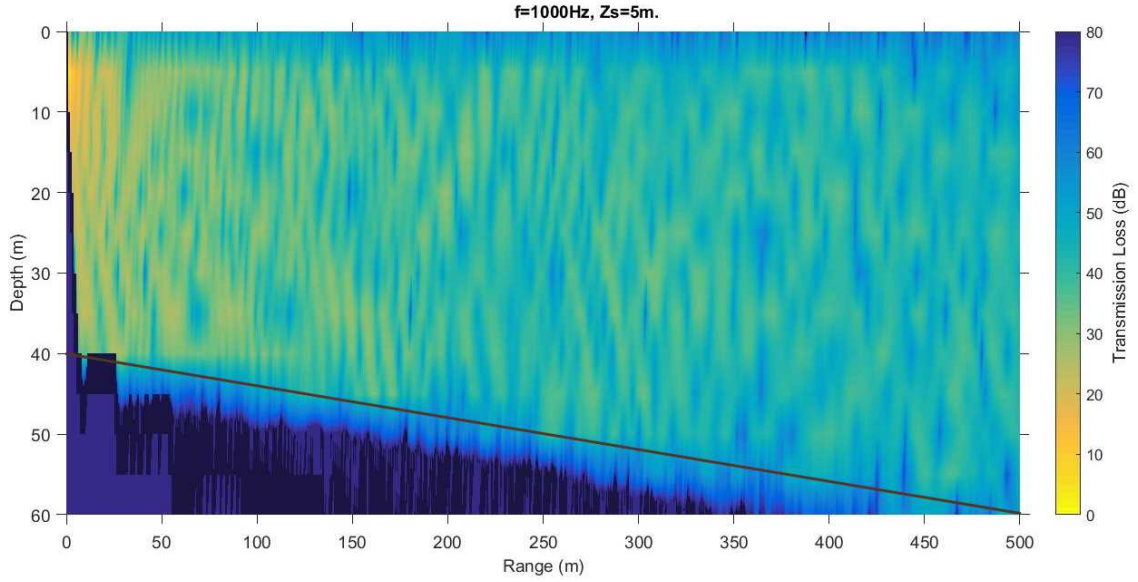

(b) Spectrogram of TL for a detailed, sloped sandy environment of 40 m to 60 m depth.

Figure 6.2: Comparison of the TL (in dB) calculated with Bellhop for a 1-kHz signal through idealised (top) and detailed (bottom) propagation environments at source depth of 5 m. The brown lines show the seafloor boundary of the model.

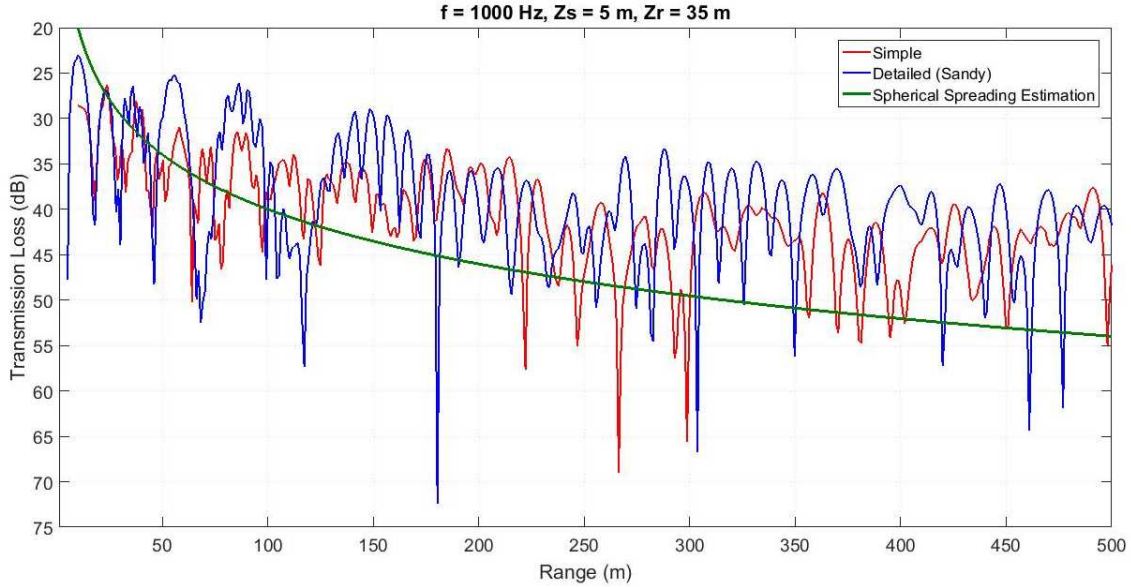

(a) TL calculations for a 1-kHz signal using Bellhop.

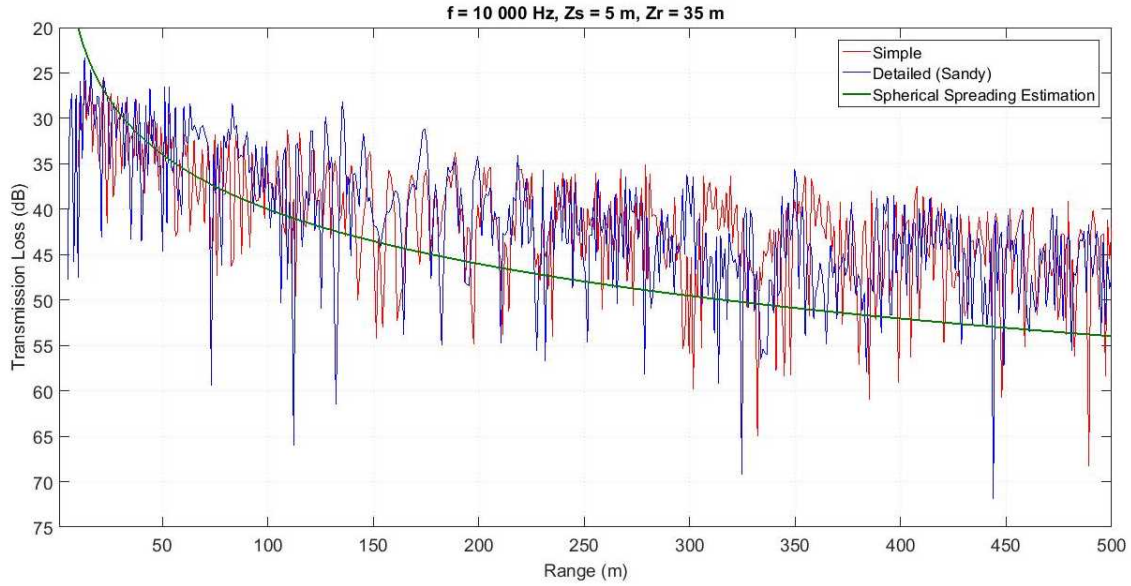

(b) TL calculations for a 10-kHz signal using Bellhop.

Figure 6.3: Comparison of the TL (in dB) calculated with Bellhop for a 1-kHz and 10-kHz signal through idealised and detailed propagation environments at source depth of 5 m and at a receiver depth of 35 m (i.e. close to the seabed). The spherical spreading estimation is also shown.

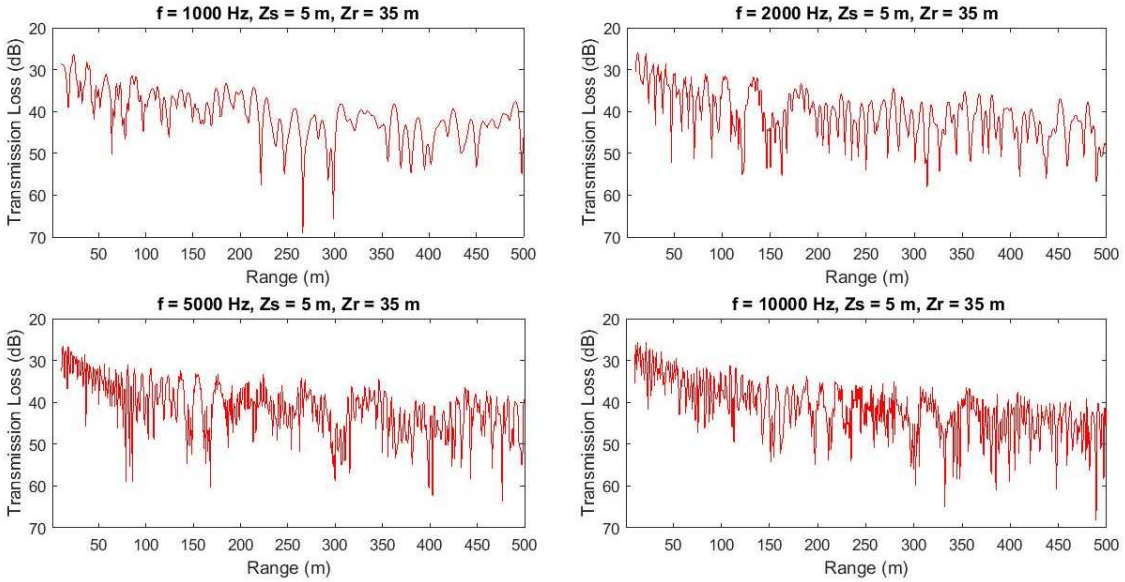

Figure 6.4: TL calculation of a 1 kHz, 2 kHz, 5 kHz and 10 kHz signal in an idealised environment over a range of 500 m. Source depth is 5 m and receiver depth is 35 m.

Table 6.1: Maximum average SLs during different periods of the WECs life cycle using both spherical and cylindrical spreading calculation.

Life Cycle Period	**Averaging Particulars**	**RL** dB re 1 μPa at 200 m	**Spherical SL** dB re 1 μPa at 1 m	**Cylindrical SL** dB re 1 μPa at 1 m
Pre-Installation	Mean 30-min RL at 76 Hz	113	159	136
Installation	Mean 10-min RL at 175 Hz	118	164	141
In-Situ/Operational	Median broadband SPL_{RMS} (1-s window, 50% overlap)	107	153	130
Condition Based Monitoring	SPL 0.5 s at 1 kHz	120	166	143

the WEC during the periods of its underwater acoustic life cycle are presented in Table 6.1. The RLs in Table 6.1 are based on the loudest average received levels during each period of the underwater acoustic life cycle (averaging particulars are detailed within the table). The loudest average received level is considered to provide the worst-case scenario for each period. Depending on the most appropriate data processing technique during that period, the received levels are recorded as differing in averaging time periods and frequency ranges, with some being recorded at a single frequency. This again highlights the importance of considering each period of the WECs life cycle individually.

Notwithstanding where exactly the receivers are located, and independently of local variations in their exact deployments, it is then possible to use these measurements of RLs, estimate the most likely SLs averaged over up to 30 minutes, and forward propagate them over different ranges to assess the WEC's influence on local sound maps. Figure 6.5 shows the SPL sound maps estimated for each period of the underwater acoustic life cycle assessment. The centre of each figure is the source point from which the acoustic emissions propagate. The colour bar indicates the estimated RL at any point as an SPL and the black dashed circle highlights the distance at which the RL was originally measured (200 m). The addition of frequency - dependent absorption in these calculations were negligible at the range of 10 Hz to 1 kHz considered.

When comparing the spherical and cylindrical spreading results, it is helpful to consider both Table 6.1 and Figures 6.5 and 6.6. Cylindrical spreading calculations of the SL are 23 dB re 1 μPa less than the spherical spreading calculations of the SL. As a result, the sound maps shown in Figures 6.5 and 6.6 show that at any distance from the source, the received SPL is lower for cylindrical spreading. While neither calculation can be said to be the actual spreading, in this work the spherical spreading calculation was used as a more cautious estimation of the SL. In some work, (such as Garrett 2015), an estimate between cylindrical and spherical spreading is used with the equation $TL = 15log(R)$. Justification of choosing either spherical or cylindrical spreading has been much debated in the literature and the consensus remains unresolved.

6.3 Discussion

It is a fine line between using a simple model for estimating a calculation and it requiring little time or resources, and inputting variables for a full modelling solution which is costly, but gives a more accurate and/or precise result. Here the discussion focuses around the use of simple SL estimation using spherical spreading and the use of the Bellhop propagation model to calculate TL and hence SL for multiple frequencies.

While Figure 6.2 provide a good aid to visualising the sound field in the area and water column considered, it is difficult to understand the variability of the transmission loss. Figure 6.3, however, shows the transmission loss at 35 m depth (the approximate depth of the receiver in the associated study) for both the idealised and detailed propagation models.

Figure 6.3 clearly shows that multipath propagation in such a shallow environment creates considerable variability in the TL that is especially sensitive to position (range and depth) as well as being sensitive to input model parameters. The movement of the receiver by just a few meters through the range could create

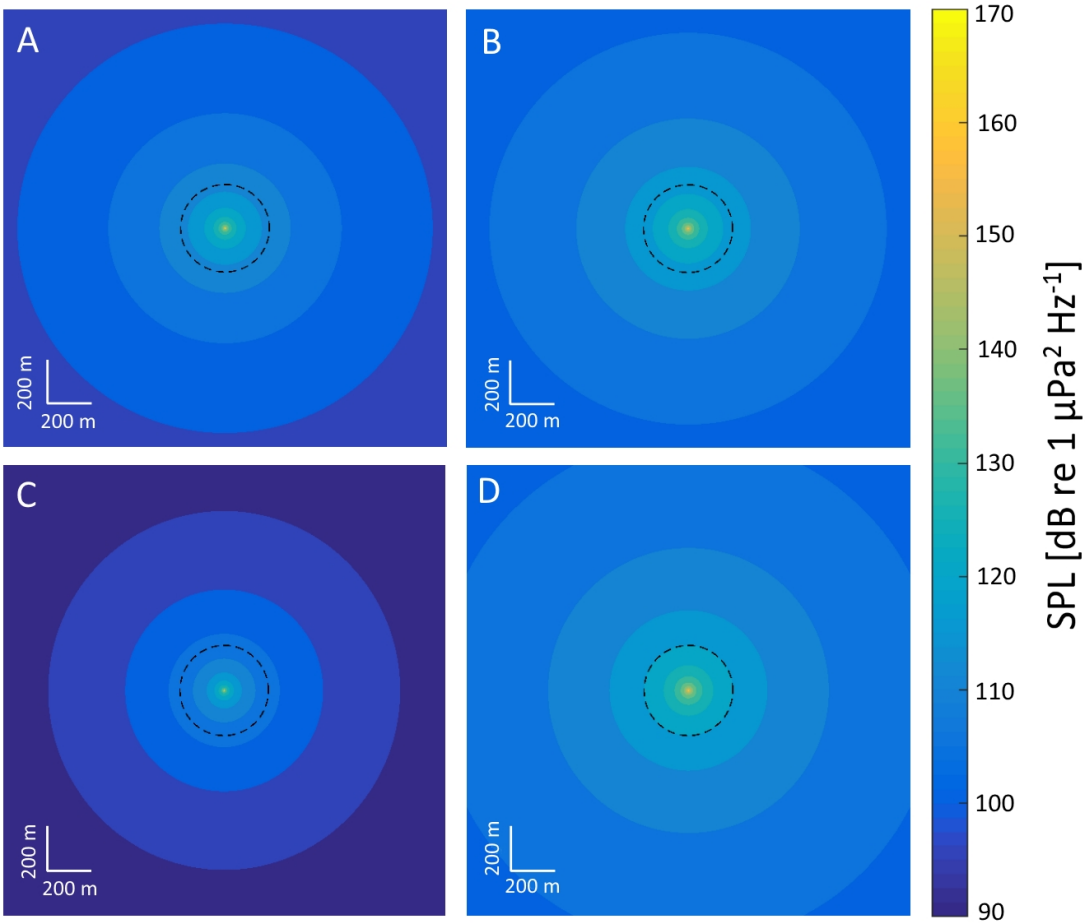

Figure 6.5: Sound maps of SPL relating to periods of the WECs life cycle via spherical spreading estimations: (A) Baseline, (B) Installation, (C) In-Situ/Operational and (D) Condition-Based Monitoring. The dashed line shows the distance at which received levels were measured (200 m).

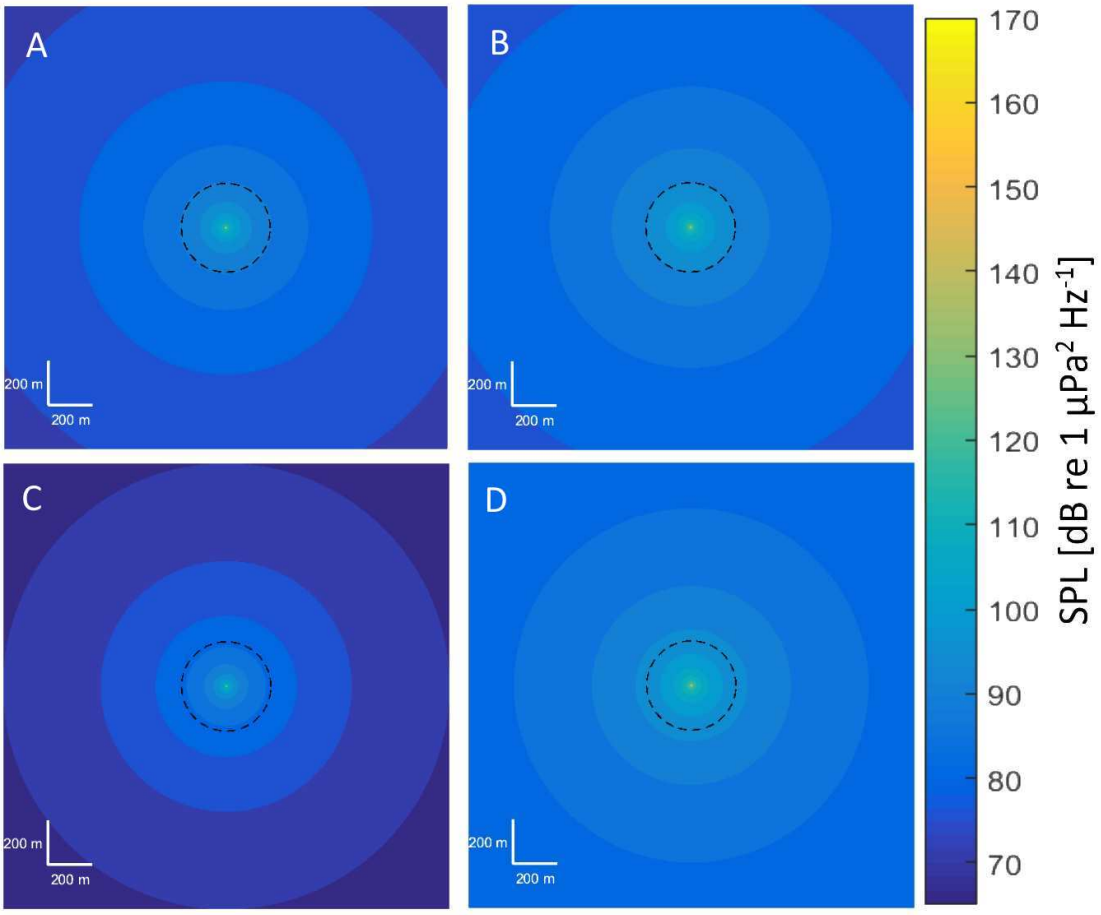

Figure 6.6: Sound maps of SPL relating to periods of the WECs life cycle via cylindrical spreading estimations: (A) Baseline, (B) Installation, (C) In-Situ/Operational and (D) Condition-Based Monitoring. The dashed line shows the distance at which received levels were measured (200 m).

variations in the transmission loss of up to 20 dB. This variability is much higher than the expected experimental uncertainty of ± 1 dB (Robinson et al. 2014) and has a number of consequences.

Firstly, when such large variations exist, the ability to use back-propagation to calculate a source's effective SL is near impossible. This has recently been considered in detail within the specific domain of Environmental Impact Assessment (EIA) (Farcas et al. 2016), with similar conclusions. Received Levels, if appropriately documented (Merchant et al. 2015; Robinson et al. 2014), should however be most useful when comparing different MRE devices.

Secondly, from a more practical point of view, the marine environment is extremely dynamic, meaning that both source and receiver will move around their assumed positions. WECs will move with winds, waves, currents and forces acting on their moorings to the seabed. Acoustic receivers will move due to underwater currents. Both types of influences can create variations in known relative positions of the source and receiver of tens of meters. This in turn will impact upon any propagation model results with variations of up to 20 dB in TL.

Another significant result from Figure 6.3 highlights that there are significant areas where a large TL is accumulated over a significant range. For example, in Figure 6.3a, between 100 m and 125 m for the idealised environment, there is a sustained transmission loss of 45 – 50 dB. Information such as this could inform the position of acoustic receivers when a specific frequency or signal is of importance, such as tonal noises from generators. These are generally low-frequency signals, and would need more modelling with a more appropriate model to confirm these "quiet zones" exist at lower frequencies.

Finally, Figure 6.3 shows that at 200 m range, there is a 5 dB difference between the two input model parameters. This highlights the importance of using the most accurate environment description, along with the exact frequencies to be considered. Accurate modelling, to back-propagate from RL to SL would therefore require constant monitoring of the source/receiver positions (in the same way that the receiver would move through water with currents and tides, the source WEC would also move slightly around its mooring, based on surface currents, tides and wave action). Knowledge of the properties along the propagation path would also require regular measurement of water column properties, at space and time scales commensurate with the expected variations. This is generally not practical or cost-effective in long-term monitoring of ORE deployments, where the focus is on operational parameters (e.g. wave heights, energy extracted). Even if this could be achieved, the comparison with other ORE deployments would be limited as it would require them to know propagation paths between sources and receivers to similar accuracies.

Further work following on from this could look to compare the outputs of all

sound propagation models across the AcTUP library. However, each model has its own parameters for good use, and as expected, no two models are good under the same parameters. The models are outlined in Table 3.1. Bellhop was chosen here for its range dependant results and use in shallow water across high frequencies. The other appropriate propagation modelling methods to use in shallow water would have been the Normal Mode and the Parabolic Equation, both of which were not considered due to their computationally expensive nature. As the aim of this chapter was to consider sound propagation across the different stages of the acoustic life cycle of the WEC, a comparison of one model (Bellhop) and the already recognised estimate of spherical spreading was considered sufficient.

In a situation where realistically, only an indication of the RLs are needed to appropriately place sensors near to WECs, spherical spreading offers a conservative estimate to the answer, saving both time and effort in the use of relatively detailed propagation models such as Bellhop. Model appropriateness is further discussed across multiple publications, e.g. (Etter 2013; Farcas et al. 2016; Wang et al. 2014). However, as other underwater acousticians have also already pointed out, SL is not ideal at comparing the impact of WECs (Farcas et al. 2016).

Chapter 7

Discussion and Concluding Remarks

7.1 Discussion of Results

Most of the chapters in this thesis included a discussion subsection. Here a clear link will be drawn between the research questions raised as a result of reviewing relevant literature (Section 2.5), and the results presented across Chapters 4, 5 and 6.

7.1.1 Underwater AE Component Testing

Two distinct methods were used in understanding the underwater AE emitted by WECs and their components: sea trials and laboratory testing. Each provided valuable results toward the solidification of underwater AE as a monitoring technique for WECs, but there were also limitations to each method.

Sea Trials

Access to data previously collected at sea for environmental monitoring purposes (Garrett 2015) enabled a feasibility study to be conducted in the early stages of this work. The data successfully enabled the discovery of the PTO resonance signal (Figure 4.14) and generator tones (Figure 4.15) which could both be linked directly to the engineering components of the WEC in question. These results gave confidence that it was possible (in an ocean environment) to detect signals from the WEC relating to its engineering. While other studies have also been able to do the same (Bassett et al. 2011; Haikonen et al. 2013; Robinson and Lepper 2013; Tougaard 2015; Wilson et al. 2014), this was evident through a data-set spanning 18 months, and was the first to link the result to underwater AE condition monitoring.

There are some limitations to this study in need of attention. Firstly, the data collection experiment was not designed with underwater AE condition monitoring in mind and hence a number of improvements could be made for future sea trials of this nature. The use of multiple recording devices with appropriate time syncronisation would enable the localisation of the signal's origin, particularly useful for WECs

with multiple complex components or an array of MRE devices.

The busy port environment of Falmouth Bay means that there was relatively little impact upon overall sound levels in the area (Garrett 2015). However, vessel activity close to the WEC or other background noise could have masked important AE events. This would need to be considered carefully for future sea trials. The inability to distinguish WEC sound levels from background noise and hence non-operational and operational modes has been noted in a number of other studies (Robinson and Lepper 2013; Tougaard 2015). The 1/7th scale *SeaRay* WEC was unable to estimate the source level of the device due to local shipping (Bassett et al. 2011). This could be subject to change when arrays of devices are deployed, as the noise from multiple devices in an array would combine (Tougaard 2015).

In industry, the lack of real time data would be problematic and data processing techniques would need to be developed to reduce the need for time consuming data collection and interpretation. The transmission of data in real or near-real time would take this concept to an industry ready solution. This has also been noted by ABS Consulting (2015).

The most obvious limitation was that underwater acoustic monitoring did not occur during the decommissioning period of the WEC life cycle. A complete data set (installation to decommission) would have been very valuable to life cycle assessment research.

Laboratory Testing

An experiment was designed and conducted to test whether AE signals from components could be collected in a laboratory setting. As it had not been done before, this was approached by taking the set up for a component loading test, and adding the data collection equipment for underwater acoustic recording to create the novel experiment.

Three 12-strand double-braided polyester rope samples were tested successfully, with significant results being discovered regarding the AE emitted by the rope under cyclic tension loading. AE signals could be classified by their frequency range and amplitude, with the most significant result being the high amplitude signals (amplitude: 125 dB re 1 μPa, frequency range: 0.01 - 48 kHz). These signals were detected toward the later end of the testing, under high loading, detected more frequently the closer to failure the sample was. While the exact physical phenomenon behind the signal requires further investigation, it is strongly believed to be the failure of strands within the rope braid. This would indicate the rope becoming less able to cope with high tension and could act as an indication of the remaining lifetime of a mooring rope.

This study has demonstrated that it is in principle feasible to detect mooring line failures with underwater AE monitoring techniques.

This testing was the first of its kind and hence a number of limitations exist. Firstly, the only sample tested was the 12-strand double-braided polyester rope and hence testing different types of rope or other components would improve the understanding of AE from multiple components, not just this one rope. On the same topic, only 3 rope specimens (6 splices) were tested. More sample specimens need testing to show statistically significant results. This was not completed due to its time/cost constraints.

It is noted that the rope samples may not have been completely bedded-in, an important process in ensuring that between manufacturing and use the fibres and strands have had sufficient time and load exposure to settle. This could have produced AE, especially at low maximum loading, that were not attributed to failures or fractures, but to bedding-in. If the sample was not sufficiently bedded in, it may have affected the performance of the rope sample as reported in Weller et al. (2014). As this testing was not concerned with the detail of the loading specifics, it was not detrimental to the experiment. However, it should be considered with more caution in future testing.

The loading schedule used was slow and gentle compared to what a component may experience in an offshore environment. This was needed to ensure that AE signals could be detected over the noise of the DMaC hydraulic test rig. However, it limits the claims that can be made about the transferring of the progression of these AE signals to an offshore environment. This was also noted by ABS Consulting (2015) as it may be "possible for defects to go undetected altogether if the loading is not high enough to cause an acoustic event". Figure 5.15 discusses a relationship between time through the testing and the number of AE signals detected. This would only be applicable in a laboratory setting where loading was incrementally increased rather than offshore where loading is not structured in that way.

Finally, the hydrophones used in this testing were placed very close to the sample. This was because of the limited size of the test rig. The ability to do this testing in a larger body of water would enable the propagation of the signal and hence the recorders would not have been saturated by the high amplitude signals.

The ability to locate the origin of the AE was also confirmed and led to the ability to locate the weak point in the rope samples. It is concluded that AE monitoring can be used to potentially predict the location of failure as well as imminent failures. The acoustic features observed in controlled laboratory environment are surprisingly consistent.

The novelty of this method means that it is still being developed and tested. The identification of component AE needs to occur through more component testing, and the feasibility of this system in practise and in the field needs to be further explored.

7.1.2 Effect Upon Local Soundscape

Previous work around the underwater noise produced by WECs (and other MRE devices) has focused around the impact to marine life (e.g. Garrett 2015; Malinka et al. 2018; Tougaard 2015). The present work however has focused upon the insight that can be gained into the engineering health of the devices that are being monitored.

To investigate how AE from the WEC propagates in shallow water, tested and bench marked propagation modelling techniques and spherical spreading estimations were compared for their suitability. The propagation model Bellhop was used to create 2 environments: a simplified idealistic model of FaBTest and a more realistic model of FaBTest.

The results showed a large variability (± 20 dB) by the propagation model Bellhop with both range and between the 2 environments. With such variability, back-propagation to actual SLs becomes highly inaccurate and RLs, properly documented, are the best way forward for accurate documentation of WEC AE. This variability in shallow water is sensitive to environmental parameters such as bathymetry and sediment properties. It is therefore concluded that using spherical spreading for condition monitoring purposes is suitable as an estimation of TL due to its simple implementation and easy to interpret results.

The use of Bellhop or other similar propagation models should only be used when all environmental data is known exactly, and precision is important. For example, this could be used to calculate shadow zones in a proposed bathymetry around an array of WECs important for sensor placement. The claims made that spherical spreading estimations could be the best way to calculate propagation of AE in shallow water environments should be used in non-precision calculations and with the caution that it could be an oversimplification of a complex problem.

The limitations of this study, which are important to consider for the conclusions are the following: The only model that was tested was Bellhop. Testing other models but with different frequencies, depths and ranges, such as RAMGeo or Kracken would remove the assumption that all models produced similarly variable results. The detailed environment used in Bellhop was not exact. It would have been more accurate to input actual bathymetry data from the deployments and locations rather than create a simple sloped environment to represent FaBTest.

The results presented here should be used within the context of a shallow water environment within the frequency range of 1 - 10 kHz. More modelling is needed to test the outcomes outside of these parameters.

After deciding that spherical spreading was adequate in calculating the propagation of AE in shallow water environments, it was then important to consider this during each period of the WECs life cycle. The installation period had the most impact upon the local soundscape, however, this was a relatively short period of the

overall life cycle.

The effect of the WEC working in-situ was negligible to the local soundscape in the noisy Falmouth Bay. However, results of AE events were significant. Hence, over the lifetime a WEC as it becomes degraded or faulty, the AE emitted would be increased. Therefore, it is important to maintain devices as a mitigation of increased sound pollution into the local environment.

This work would have benefited from the same acoustic quantities being quoted for each period of the WECs life cycle. However, given that this work regard each period as a separate entity needing different processing techniques, it aligns that different metrics would be quoted in each instance. The worst case scenario was used in each period.

7.1.3 Acoustic Life Cycle Assessment

Life cycle assessment has been identified as a potential measure in seeking a method of assessing the overall impact of a WEC on a local soundscape and an ability to compare this with other WECs and submerged offshore structure. Traditional life cycle assessments often seek to provide an impact factor for the entire life cycle of the system in question (Gerbinet et al. 2014). In this case, one would seek to measure the effect of the underwater life cycle of the WEC on the local soundscape. This thesis proposes to estimate the acoustic energy transferred to the environment at each stage of the WECs life cycle. This can be done using the average RLs at different periods of the WEC life cycle and converting from relative dB values to absolute energies in Watts as described in Equation 3.4. We assume $\rho = 1,023\ kg\ m^{-3}$ is the density of seawater (Kaye & Laby Online 2008) and $c = 1,500\ m\ s^{-1}$ is the approximate speed of sound in sea water (Kaye & Laby Online 2005). The total energy transferred, E, in Joules, is then calculated as described in Equation 3.5 where t is the time spent in each life cycle period and j is the index of the life cycle period.

In this case, there are three periods in the life cycle where the underwater acoustics contribute to the local soundscape: installation, operational / non-operational and decommissioning. The baseline is excluded because it is not relevant. Condition based monitoring is also excluded as an independent underwater acoustic life cycle period as it is incorporated into the operational mode of the WEC.

The 30-minute period on 22$^{\text{nd}}$ September at 23:00 was selected as an operational / non-operational activity case study in (Garrett 2015) and hence this is used as a representative recording during operational / non-operational periods. Due to the absence of a vessel in transit it can be assumed that the underwater acoustics exhibited in this recording were from the WEC only (1 PTO active). Table 7.1 details the calculation results for assessing the underwater acoustic energy over the WEC life cycle using Equations 3.4 and 3.5 by calculating the energy contribution

from the installation, operation and decommission periods. Time periods are detailed from the device developer (Fred Olsen 2016).

Table 7.1: Underwater acoustic life cycle assessment energy calculations for *Lifesaver* WEC at FabTest.

	Installation Period	**Operation Period**	**Decomm. Period***	**Underwater AE Total**	**WEC Total**
RL (at 200 m) [dB re 1 μPa]	117.2	102.3	117.2		
t [hrs]	24	4,267	24	4,315	
E [J]	14,853	85,453	14,853	115,159	
E [kWh]				0.032	9,401

*Assuming that decommissioning and installation would be equal in underwater AE contribution.

By converting to kWh, a ratio can be made between the underwater acoustic energy from the WEC and the useful energy produced by the WEC over its lifetime. Therefore, the ratio of underwater acoustic energy per MWh electricity produced by the WEC is 3 Wh underwater acoustic energy per MWh electricity. If the same calculations are completed for other WEC deployments, or other offshore stuctures such as wind turbines, then they can be directly compared as to how efficient the underwater acoustic emission is toward electricity generation.

Authors have previously noted the difficulty in quantifying the overall effect of the underwater acoustics produced by a WEC (Lepper et al. 2014; Robinson and Lepper 2013). By summing the underwater acoustic energy over each period of the life cycle of the WEC, an estimate of the underwater acoustic energy input into the local environment could be made. By then comparing it to the amount of useful electrical energy produced by the WEC an efficiency ratio could be made. Both of these quantities (the overall underwater acoustic energy and the ratio) could be calculated for other WECs and offshore devices to compare the impact.

The underwater acoustic life cycle assessment ratio could be improved by selecting a representative recording for each deployment of the AMAR, and using deployment specific parameters to create a more accurate calculation of the underwater energy. This new technique has not yet been tested with any other WECs or offshore devices, therefore it is not yet possible to compare underwater acoustic efficiency ratios.

7.2 Conclusion

For MRE to become a competitive industry in the renewable energy market, the cost of energy must be reduced. This can be achieved via condition-based monitoring using techniques such as underwater AE to monitor the health of an MRE device. Underwater acoustic propagation modelling can be used to better understand the effect of a device on the local soundscape. This work has proved the feasibility of such a technique and designed and implemented a laboratory experiment for the classification of underwater AE signals for components. While each WEC is different, many are comprised of similar components and the author believes that this work will be applicable to other WECs and offshore devices.

7.2.1 Key Results

The key results from this thesis, linking to the research questions raised from Section 2.5 are:

- What AE is emitted underwater by individual components of WECs?

Through sea trials, the AE emitted by the *Lifesaver* WEC was recorded. This included AE from the PTO system (high amplitude events up to 120 dB re 1 μPa at a distance of 200 m lasting 0.5 s spanning frequencies between 100 Hz and 1 kHz) as well as tonal signals from the generator (most significantly at 115 dB re 1 μPa at a distance of 200 m at 60 Hz). This was linked to the resonance of the PTO belt system, linking the AE and performance of the WEC together.

It was also possible to detect component AE through laboratory testing. A novel experiment using an array of hydrophones was conducted to record AE emitted from a 12-strand double-braided polyester mooring rope under sinusoidal tensile loading. Successfully, a range of signals were detected, varying in amplitude and frequency, when the sample was placed under tensile stress. The most significant of these signals was the "high amplitude signal" (125 dB re 1 μPa at a distance of 0.1 m spanning frequencies of 0.01 to 48 kHz) which is discussed as being linked to the failure of significant strands within the rope structure (although this has not been explicitly proved in this work). It was possible to locate the origin of the AE events using time of arrival techniques. AE always originated from either of the 2 eye splices that connected the sample to DMaC.

- How does the AE from WECs propagate in a shallow water environment?

It is possible to calculate the propagation of underwater acoustics in a shallow water environment using propagation modelling techniques. However, the results of this modelling is highly dependant upon input model parameters (up to 5 dB difference between 2 input scenarios in this work), and is highly variable with small

changes in range (up to 20 dB with a change in distance of 5 m). This is not practical for condition monitoring of WECs where there is variation in the location of recording equipment and the WEC itself due to currents and wave action.

The other method considered for the calculation of AE propagation in this thesis was spherical spreading estimations. While spherical spreading produces a less precise result than propagation modelling, it is more practical for the purpose of condition monitoring of WECs. It does not require specialist knowledge of propagation modelling, is a simple calculation to perform and can be easily interpreted.

The propagation of AE from 4 periods of the WECs life cycle was considered - baseline, installation, in-situ/operational and condition-based monitoring. The AE emitted from the baseline and in-situ/operational periods were found to propagate the least in the local environment hence having the least impact on the local soundscape. The propagation of AE from condition monitoring was found to have the largest propagation range. However, because it had the shortest time period the it does not have the largest impact on the local soundscape. The propagation of sound from the installation period was found to therefore have the largest impact on the local soundscape.

Directly comparing the underwater acoustics emitted by WECs has previously been conducted through calculation of the SL of each WEC. In this thesis the underwater acoustic energy emitted by the WEC from each period of its lifetime is totalled over the entire lifetime of the WEC. A ratio is then created between the total underwater acoustic energy and the useful energy output of the device. This will enable the direct comparison between WECs and other offshore devices by considering the value of the noise pollution produced by the device. For the *Lifesaver* WEC, this is 3 Wh of underwater acoustic energy per MWh electrical energy.

7.2.2 Implications

This work has a number of implications for research, industry and regulators.

Research

There is significant research in the field into the underwater acoustics produced by WECs (and other submerged structures) to understand the impact upon the local environment including mammals and fish. This data can be re-analysed for the purpose of considering engineering features of the WECs they were recording, as was conducted here for *Lifesaver*. This would produce new results without the need for more sea trials, which are costly and time consuming.

The novel laboratory testing presented in this thesis has produced significant results. Underwater acoustic testing of marine components for AE signature

identification is possible and can be used by others to understand the AE of other marine components. The identification of the energy produced by underwater acoustics may also enable a better understanding into the energy transfer processes of those components.

Finally, propagation modelling methods used in the shallow water environment have been shown to produce highly variable results. Research into how to best create precise*and* accurate propagation calculations needs to be conducted. It is also important for researchers to consider the individual periods of the WECs life cycle when processing data and discussing results.

Industry

This work has proved the feasibility of using underwater AE to monitor the condition of a partially submerged WEC. Condition monitoring techniques are known to reduce the cost of O&M activities through better planning and understanding of the health of devices. If industry partners were to implement such a method of condition monitoring alongside existing monitoring systems it has the potential to reduce the need for human intervention an unneeded inspections.

Regulators

There is a number of implications of this work for regulators within the MRE sector. The first is related to the need for regulators to not only consider the effect of AE produced by a WEC but the consideration needs to be made for each individual period of the WEC life cycle - baseline, installation, operational, in-situ and decommissioning.

Secondly, regulators often look to understand if a project is polluting to the environment, but also if there is a benefit to the reason for pollution. The use of the ratio of underwater acoustic energy to useful electrical energy will enable regulators to understand the "value" of the noise pollution. If a WEC is particularly noisy and produces very little electricity then the electricity produced is not worth the pollution entered into the soundscape. On the other hand, if a device is noisy but produces a large amount of electricity, it may worth the extra pollution. This still needs further development but could provide a measure for regulators to understand the balance between wanting to reduce noise pollution in the ocean and increasing renewable energy outputs.

7.3 Further Work

During this thesis, a data set was used that was collected with the original purpose of environmental monitoring of the *Lifesaver* WEC. While the adaptation of the data processing to underwater AE monitoring was successful, it would be logical

for the next step to be a dedicated experiment specifically for developing the use of underwater AE monitoring of WECs. This could include:

- Multiple sensors to test time of arrival localisation.
- Real (or near-real) time data transfer to enable meaningful condition monitoring that can influence maintenance schedules.
- Development of automatic data processing techniques.
- Monitoring an array of devices to understand the impact of multiple sources of AE.

There is a need within the industry for long-term monitoring studies. Results regarding the impact of AE from WECs so far published have not covered long periods of time (e.g. Tougaard 2015). The impact of a WEC cannot be justified in just 30 minutes of recording. Long term continual monitoring will enable an understanding of the effect of sea state, weather, season and shipping traffic on AE results. While this study was able to consider the majority of the WEC life cycle, the decommissioning period was not recorded. It is important to asses the impact of the decommissioning of a WEC along with its installation and operation. In this work, it was assumed to be similar to that of installation, this cannot be said for sure until further data is collected.

The component testing here was the first of its kind, and hence more needs to be done to improve the testing. More samples of 12-strand double-braided polyester rope should be studied to increase data points and confirm the conclusions of this thesis. Different samples of rope also need to be considered - different braiding, sizes, lengths and splices. Changing the type of loading the rope is subjected to could also be of interest: if it is still possible to hear AE over increased DMaC noise then it may be possible to subject the samples to offshore conditions for a more realistic testing regime. It would also be of great important to understand the physical phenomenon that is creating the AE signals detected.

The signals of more components (PTOs, generators, etc.) need to be tested and documented, either through sea trials or laboratory testing. By gathering more component signals, a database of appropriate signals could be created as a basis for cross-correlation signal processing within real-time data analysis.

Other further work should consider comparing multiple propagation models with that presented here to confirm the assumption that all propagation models will create highly variable results. Specifically, the inclusion of bathymetry is of particular importance when trying to locate shadow zones for avoiding during sensor placement.

Finally, as WEC development moves toward commercialisation, more research by both academics and industry needs to be done towards the implementation of meaningful and effective operation and maintenance techniques. Underwater AE is

just one example of how the cost of O&M can be reduced. More sharing needs to be done between MRE and offshore wind, who are more developed an industry and therefore more experienced. This could mean that initial O&M activities are better prepared and hence cost less to execute. The ocean is a harsh environment, and investments need to be protected in order to prove that MRE can make a significant contribution to the renewable energy industry.

Appendix A

Sample Eye Splice Procedure

The creation of the eye splices used to attach the 12-strand double-braided polyester rope samples to DMaC was conducted by the author and the procedure is outlined below.

1. From the end of the rope, 1 fid length is measured and marked as point A. From A the length of the eye is marked as point B and finally a stop knot is placed in the rope at a further 5+ fid lengths.

2. At point B the core of the rope is extracted from the cover. The core is milked to ensure it is the correct length and then at the point at which the core meets the cover, the core is marked as point C.

3. The core is pulled out of the cover further. From point C, a short fid length is measured and marked as D and then a further 1.5 fid lengths is marked as point E. The end of the cover is tapered to reduce its size.

4. The fid is inserted into the core at point D and exits at point E. The end of the cover is put through the fid so it is fed through the core and exits at point E. The fid is removed and a knot is tied in the end of the cover to stop it from feeding back through.

5. The fid is now inserted into the cover at point A and exits a few inches past point B. The end of the core is then fed through the fid to the exit of the cover. The fid is then removed. The rope is held at the crossover and the end of the core is pulled tight. The point at which it emerges from the cover is marked point F. The core is cut at point F and tapered. The cover end is also tapered. The ends are milked into the rope so that they disappear.

6. The rope is fixed to a location. A hard pole is put into the eye of the slice and a constant force is applied to the rope to slip the core into the cover. If the splice becomes stiff, it is worked and snapped to allow more movement.

7. Once the cover has completely disappeared the eye splice is complete.

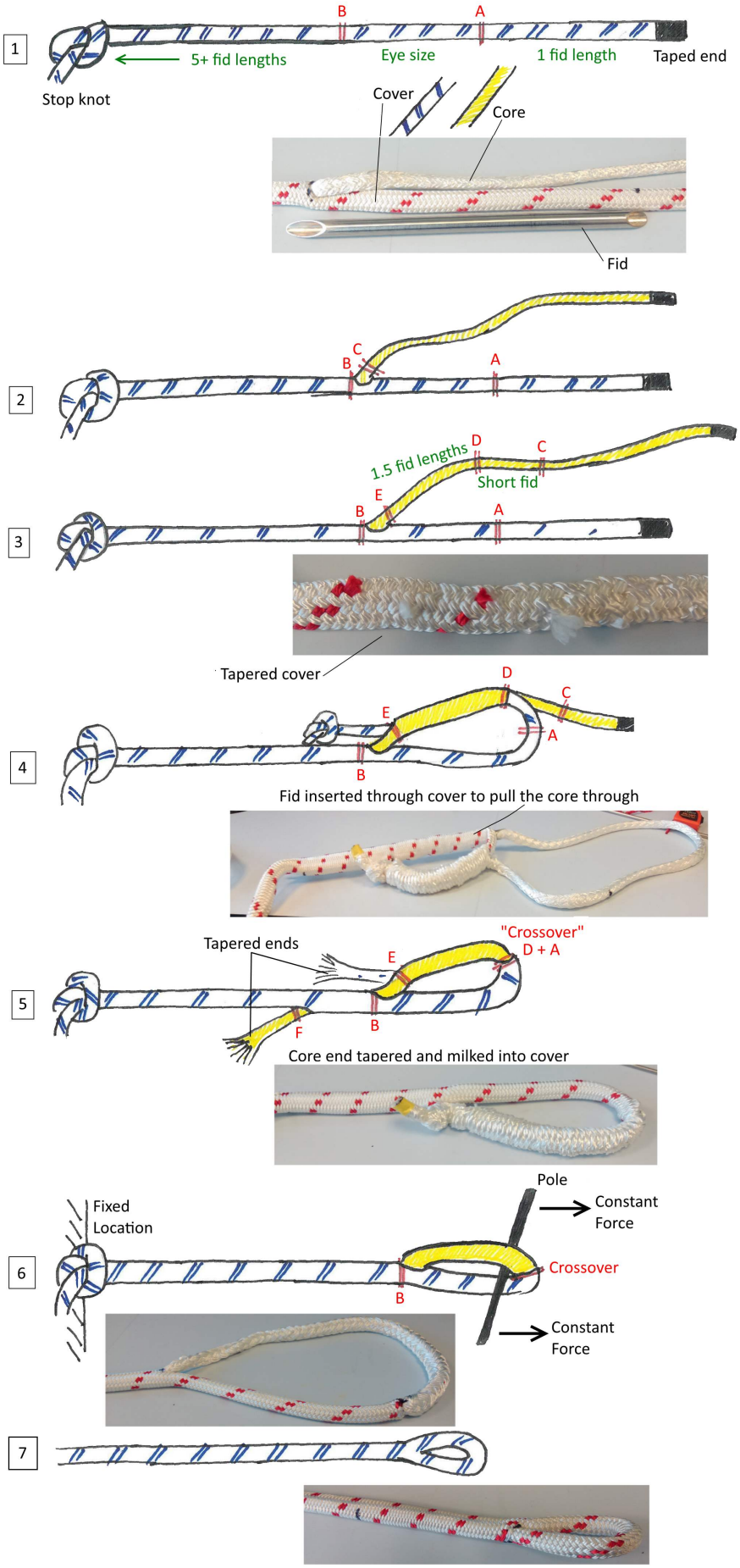

Figure A.1: Step by step instructions on creating an eye splice in a double braided rope.

Appendix B

Hydrophone Specifications

B.1 JS-B100-C4DS-PA Hydrophone Specification

SEA (2011). *Wideband Spherical Sensor*. URL: https://www.sea.co.uk/media/1610/mardef-021-0717-wideband-spherical-sensor.pdf (visited on 04/15/2018)

Wideband Spherical Sensor

The Wideband Spherical Sensor (JS-B100-C4DS-PA) is a cutting edge, high quality, high-performance solution to a wide and varied range of underwater acoustic measurement applications.

Key Features

- High sensitivity, wideband output
- Low noise, low power, high gain, differential pre-amplification
- Acceleration cancelled response
- Minimal directivity variation
- Robust, long term operational reliability and stability
- Excellent tolerance to environmental variation
- Simple electrical and mechanical system integration options
- Wide environmental condition tolerance

The Wideband Spherical Sensor combines a high sensitivity, acceleration cancelling, wideband spherical hydrophone element with an internally mounted, miniature low noise, low power, high gain differential pre-amplifier.

The Wideband Spherical Sensor is one of a family of high-quality spherical transducers; polyurethane moulded for standalone applications or epoxy resin coated for internally integrated applications.

The Wideband Spherical Sensor is supplied as standard with 2m of cable and conductor flying leads for user self-termination. Alternative cable lengths and factory fitted and moulded underwater mateable connector options are available upon request.

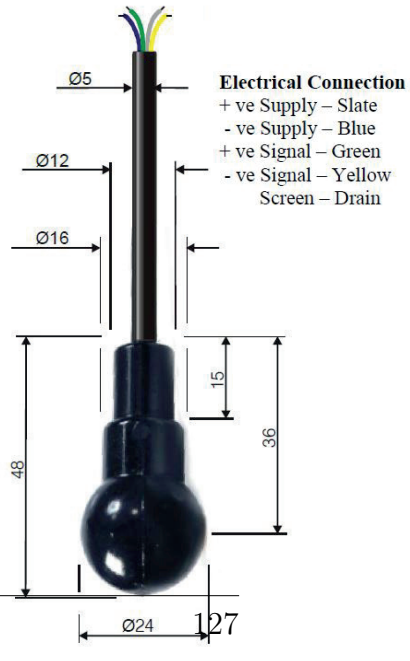

Wideband Spherical Sensor

Parameter	Qualification	Nominal Specification
Receive Voltage Sensitivity	Nominal [diff. O/P] Low Freq. (100 Hz)[diff. O/P]	-168 dB re. 1V/uPa -166 +/- 2 dB re. 1V/uPa
Frequency Response	Flat +/- 1.5 dB Flat +/- 3 dB	<50 Hz to >20 kHz <25Hz to >100 kHz
Noise Floor	10kHz	<28 dB re.1uPa√Hz
Linear Dynamic Limit	Max Acoustic Pressure	168 dB re. 1uPa
Directivity Response	Radial Plane at 100 kHz Axial Plane at 100 kHz	Omni +/- 1.5 dB 300° +/- 2 dB
Current Consumption	5 V dc supply (3V – 5.5V range)	<10 mA
Max. Depth	Operational >3000m Survival	>3000m >4000m
Diameter	Maximum	24.0 mm
Length	Overall (not inc. cable)	48 mm
Mass	In air (inc. 2m leads)	90g
Electrical Connection	Prepared for customer self termination	Tinned flying lead ends – shorted together for delivery.
Mounting Options (Mechanical)	1) Self Suspension 2) External Clamping	1) Support self weight on cable 2) Ø12 x 15 rear axial shank

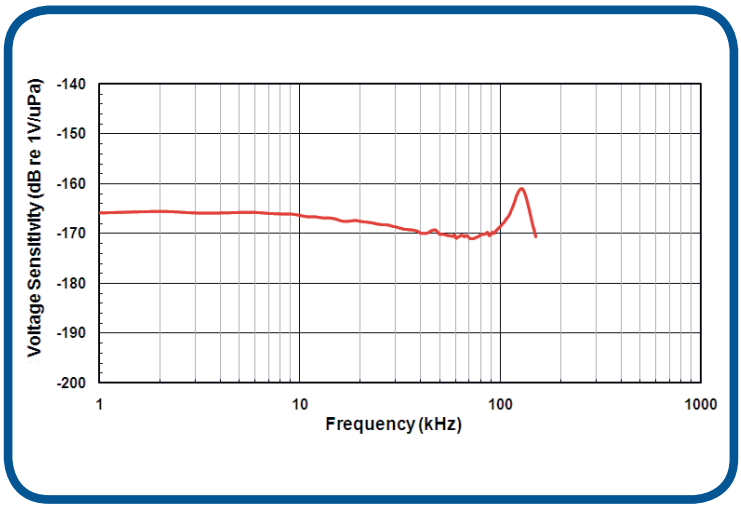

SEA
17 Castle Corner
Beckington, Frome
Somerset
BA11 6TA

Telephone: +44 (0) 1373 852000

Email: info@sea.co.uk

www.sea.co.uk

B.2 SQ26-08 Hydrophone Specification

Cetacean Research Technology (2017). *SQ26-08 Hydrophone*. URL: https://www.cetaceanresearch.com/hydrophones/sq26-08-hydrophone/index.html (visited on 04/15/2018)

SQ26-08 Hydrophone

The Sensor Technology SQ26-08 has a very slick, compact design, and is a component in several **Cetacean Research™** hydrophone systems, and is also sold separately.

The SQ26-08 is a general purpose hydrophone ideal for whale watching, full audio-band signal detection, and mobile underwater recording; except that it can NOT be used as a stand-alone hydrophone.

The SQ26-08 hydrophone **must be used with a recording device or preamplifier** that has a bias powered (a.k.a. plug-in powered) microphone input, and thus is included in the following **Cetacean Research™** underwater recording systems:

- **SQ26-H1** compact portable hydrophone system
- **µRUDAR-mk2™** autonomous underwater recording system

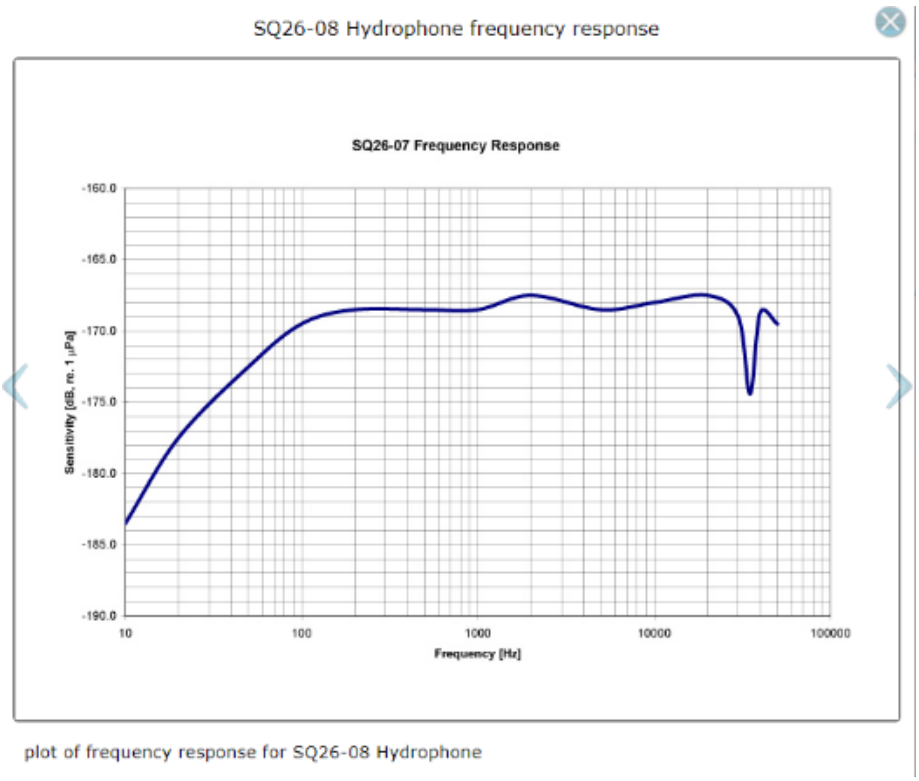

plot of frequency response for SQ26-08 Hydrophone

SQ26-08 Hydrophone specifications	
Frequency Range [kHz]	0.020 to 50
Transducer Sensitivity* [dB, re 1V/µPa]	-194
Preamplifier Gain [dB]	25
Effective Sensitivity* [dB, re 1V/µPa]	-169
SPL Equiv. Self Noise at 1kHz [dB, re 1µPa/√Hz]	44
Power Requirement [Vdc]	2 to 5
RMS Overload Acoustic Pressure [dB, re 1µPa]	154
Maximum Operating Depth [m]	100
Operating Temperature Range [°C]	-25 to 60
Dimensions [mm]	70 L x 32 dia.
Shielded Cable Length [m] **cable includes 3.5mm stereo phone plug**	10 or 30
Directionality	omnidirectional below 10kHz
Battery / Connector box	N/A **

* Transducer Sensitivity + Preamplifier Gain = Effective Sensitivity.
** powered by most of the plug-in powered microphone inputs, such as the Zoom H1 digital flash recorder

The SQ26-08 **must be used with a recording device or preamplifier** that has a bias powered (a.k.a. plug-in powered) microphone input, such as the Zoom H1 used in our **SQ26-H1 system** or it's **SQ26-H1B** base.

Applications

- Kayaking
- Recreation
- Tourism
- Environmental science
- General cetacean research
- Educational outreach programs
- Contact microphone
- Geophone
- Capturing the sounds of the natural underwater environment for eco-art
- Adding underwater sound to video recordings

Bibliography

ABS Consulting (2015). *Study on mooring system integrity management for floating structures*. Tech. rep. Submitted to BSEE, p. 116. URL: https://www.bsee.gov/sites/bsee.gov/files/tap-technical-assessment-program//730-aa.pdf (visited on 04/04/2018).

Al Thobiani, F. (2011). "The non-intrusive detection of incipient cavitation in centrifugal pumps". PhD thesis. University of Huddersfield, p. 237.

Alfayez, L., D. Mba, and G. Dyson (2005). "The application of acoustic emission for detecting incipient cavitation and the best efficiency point of a 60 kW centrifugal pump: Case study". In: *NDT E Int.* 38.5, pp. 354–358. DOI: 10.1016/j.ndteint.2004.10.002.

Aquaret (2009). *Aquaret images and illustrations*. URL: http://www.aquaret.com/indexea3d.html?option=com%7B%5C_%7Dcontent%7B%5C&%7Dview=article%7B%5C&%7Did=203%7B%5C&%7DItemid=344%7B%5C&%7Dlang=en (visited on 02/28/2017).

Ashton, I. G. C., J-B. Saulnier, and G. H. Smith (2013). "Spatial variability of ocean waves, from in-situ measurements". In: *Ocean Eng.* 57, pp. 83–98. DOI: 10.1016/j.oceaneng.2012.08.010.

Atargis Energy Corporation (2012). *Cycloidal wave energy conversion at a glance*. URL: http://www.atargis.com/Tech%7B%5C_%7DCycWEC.html (visited on 11/19/2017).

Austin, M., N. Chorney, J. Furguson, D. Leary, C. O'Neill, and H. Sneddon (2009). *Assessment of underwater noise generated by wave energy devices*. Tech. rep. Oregon Wave Energy Trust, p. 58. URL: http://ir.library.oregonstate.edu/concern/technical%7B%5C_%7Dreports/ng451p108 (visited on 02/05/2018).

AW Energy (2012). *Waveroller concept*. URL: http://aw-energy.com/about-waveroller/waveroller-concept (visited on 02/02/2018).

Bashir, I., J. Walsh, P. R. Thies, S. D. Weller, Ph. Blondel, and L. Johanning (2017). "Underwater acoustic emission monitoring – Experimental investigations

and acoustic signature recognition of synthetic mooring ropes". In: *Appl. Acoust.* 121, pp. 95–103. DOI: 10.1016/j.apacoust.2017.01.033.

Bassett, C., B. Polagye, M. Holt, and J. Thomson (2012). "A vessel noise budget for Admiralty Inlet, Puget Sound, Washington (USA)". In: *J. Acoust. Soc. Am.* 132.6, pp. 3706–3719. DOI: 10.1121/1.4763548.

Bassett, C., J. Thomson, B. Polagye, and K. Rhinefrank (2011). "Underwater noise measurements of a 1 / 7 th scale wave energy converter". In: *IEEE Ocean. 2011.* Kona, Hawaii. DOI: 10.23919/OCEANS.2011.6107283.

Bombora Wave Power (2016). *mWave*. URL: http://www.bomborawave.com/mwave (visited on 11/19/2017).

Bridon (2011). *Fibre rope catalogue*. URL: http://www.bridon.com/x/downloads/fibre/Fibre.pdf (visited on 01/30/2018).

Brown, A., S. Muller, and Z. Dobrotkova (2011). *Renewable energy markets and prospects by technology*. Tech. rep. IEA, p. 66. URL: https://www.iea.org/publications/freepublications/publication/Renew%7B%5C_%7DTech.pdf (visited on 02/05/2018).

Canadian Transportation Agency (2011). *Railway noise measurement and reporting methodology*. Tech. rep., p. 68. URL: https://otc-cta.gc.ca/eng/railway%7B%5C_%7Dnoise%7B%5C_%7Dmeasurement (visited on 04/04/2018).

Carbon Trust (2006). *CTC601 Future marine energy*. Tech. rep. URL: https://www.carbontrust.com (visited on 01/01/2018).

Carbon Trust (2009). *CTS153 Checkmate Seaenergy rubber snakes seek to slash cost of wave power*. Tech. rep. URL: http://www.checkmateukseaenergy.com/wp-content/uploads/2010/09/carbon-trust-Innovations-Case-Study.pdf (visited on 02/05/2018).

Carbon Trust (2011). *CTC797 Accelerating marine energy*. Tech. rep. URL: https://www.carbontrust.com/media/5675/ctc797.pdf (visited on 02/05/2018).

Carroll, J., A. McDonald, and D. McMillan (2016). "Failure rate, repair time and unscheduled O&M cost analysis of offshore wind turbines". In: *Wind Energy* 19, pp. 1107–1119. DOI: 10.1002/we.1887.

Casey, N. F., K. M. Holford, and J. L. Taylor (1987). "The acoustic evaluation of wire ropes immersed in water". In: *NDT Int.* 20.3, pp. 173–176. DOI: 10.1016/0308-9126(87)90406-8.

Casey, N. F., H. White, and J. L. Taylor (1985). "Frequency analysis of the signals generated by the failure of constituent wires of wire rope". In: *NDT Int.* 18.6, pp. 339–344. DOI: 10.1016/0308-9126(85)90164-6.

Catapult Offshore Renewable Energy (2014). *Financing solutions for wave and tidal energy*. Tech. rep., p. 21. URL: https://ore.catapult.org.uk/documents/10619/150618/pdf/6d8ad914-ecc4-43e1-b4a9-55082d77fb04 (visited on 03/06/2018).

Cetacean Research Technology (2017). *SQ26-08 Hydrophone*. URL: https://www.cetaceanresearch.com/hydrophones/sq26-08-hydrophone/index.html (visited on 04/15/2018).

Chapman, N. R. and A. Price (2011). "Low frequency deep ocean ambient noise trend in the Northeast Pacific Ocean". In: *J. Acoust. Soc. Am.* 129.5, pp. 161–165. DOI: 10.1121/1.3567084.

Choudhury, A. and N. Tandon (2000). "Application of acoustic emission technique for the detection of defects in rolling element bearings". In: *Tribol. Int.* 33, pp. 39–45. DOI: 10.1016/S0301-679X(00)00012-8.

Christensen, L., E. Friis-Madsen, and J. P. Kofoed (2005). "The wave energy challenge: The wave dragon case". In: *Proc. POWER-GEN 2005 Eur. Conf.* Milan, Italy, p. 20. URL: https://www.researchgate.net/publication/242114457%7B%5C_%7DTHE%7B%5C_%7DWAVE%7B%5C_%7DENERGY%7B%5C_%7DCHALLENGE%7B%5C_%7DTHE%7B%5C_%7DWAVE%7B%5C_%7DDRAGON%7B%5C_%7DCASE (visited on 02/05/2018).

Christopher, S. and S. Kumaraswamy (2013). "Identification of critical net positive suction head from noise and vibration in a radial flow pump for different leading edge profiles of the vane". In: *J. Fluids Eng.* 135.12. DOI: 10.1115/1.4025072.

Clarke, A. (2016). *Rethinking the environmental impacts of renewable energy: mitigation and management*. Routledge, p. 274. ISBN: 0415722187.

Coe, R. G. and V. S. Neary (2014). *Review of methods for modeling wave energy converter survival in extreme sea states*. Tech. rep. URL: https://vtechworks.lib.vt.edu/handle/10919/49221 (visited on 02/05/2018).

Crabtree, C. J., D. Zappala, and S. I. Hogg (2015). "Wind energy: UK experiences and offshore operational challenges". In: *Proc. Inst. Mech. Eng. Part A J. Power Energy*, pp. 1–20. DOI: 10.1177/0957650915597560.

DECC (2013). *Wave and tidal energy: Part of the UK's energy mix - detailed guidance*. Tech. rep. URL: https://www.gov.uk/wave-and-tidal-energy-part-of-the-uks-energy-mix (visited on 11/13/2014).

DECC (2014). *Renewable energy in 2014*. Tech. rep., p. 45. URL: https://www.gov.uk/government/uploads/system/uploads/attachment%7B%5C_%7Ddata/file/437953/Renewable%7B%5C_%7Denergy%7B%5C_%7Din%7B%5C_%7D2014.pdf (visited on 02/05/2018).

Dong, L. and H. Dong (2014). "Bellhop – A modeling approach to sound propagation in the ocean". In: *Proc. 36th Scand. Symp. Phys. Acoust.* Geilo, Norway, pp. 1–4.

Duncan, A. J. and A. L. Maggi (2006). "A consistent, user friendly interface for running a variety of underwater acoustic propagation codes". In: *Proc. Acoust. 2006*. Christchurch, New Zealand, pp. 471–477. ISBN: 9781627480017.

Elforjani, M. and D. Mba (2010). "Accelerated natural fault diagnosis in slow speed bearings with acoustic emission". In: *Eng. Fract. Mech.* 77, pp. 112–127. DOI: 10.1016/j.engfracmech.2009.09.016.

Elsaesser, B., M. Coffin, J. Hood, and R. Starzmann (2015). "Field testing a full-scale tidal turbine part 3 : Acoustic characteristics". In: *Proc. 11th Eur. Wave Tidal Energy Conf.* Pp. 1–7.

EMEC (2012). *Wave devices*. URL: http://www.emec.org.uk/marine-energy/wave-devices/ (visited on 01/28/2015).

EMEC (2017). *Wave developers*. URL: http://www.emec.org.uk/marine-energy/wave-developers/ (visited on 03/02/2017).

Erbe, C. (2010). *Underwater acoustics: Noise and the effects on marine mammals*. URL: http://oalib.hlsresearch.com/PocketBook%203rd%20ed.pdf.

Esteban, M. and D. Leary (2012). "Current developments and future prospects of offshore wind and ocean energy". In: *Appl. Energy* 90, pp. 128–136. DOI: 10.1016/j.apenergy.2011.06.011.

Etter, P. C. (2013). *Underwater acoustic modeling and simulation*. Fourth Ed. CRC Press, p. 554. ISBN: 9781466564930.

European Commission (2010). *Europe 2020: A strategy for smart, sustainable and inclusive growth*. Tech. rep., p. 34. URL: http://eur-lex.europa.eu/legal-content/en/ALL/?uri=CELEX%7B%5C%%7D3A52010DC2020 (visited on 11/11/2014).

FaBTest (2014). *FaBTest overview*. URL: http://www.fabtest.com/ (visited on 11/09/2017).

Falmouth Harbour Commissioners (2014). *Decommissioning of a wave energy converter from Falmouth Bay*. Tech. rep., p. 2. URL: https://

www . falmouthhaven . co . uk / wp - content / uploads / 2014 / 07 / PORTNOTICETOMARINERS1514%7B%5C_%7D000.pdf (visited on 11/20/2017).

Farcas, A., P. M. Thompson, and N. D. Merchant (2016). "Underwater noise modelling for environmental impact assessment". In: *Environ. Impact Assess. Rev.* 57, pp. 114–122. DOI: 10.1016/j.eiar.2015.11.012.

Faulstich, S., B. Hahn, P. Lyding, and P. J. Tavner (2009). "Reliability of offshore turbines – identifying risks by onshore experience". In: *Eur. Offshore Wind Conf. Exhib.* Stockholm, Sweden. ISBN: 9781615677474.

Faulstich, S., B. Hahn, and P. J. Tavner (2011). "Wind turbine downtime and its importance for offshore deployment". In: *Wind Energy* 14.3, pp. 327–337. DOI: 10.1002/we.421.

Fijen, T. (2017). *Tidal lagoons, from Swansea to fleet lagoons.* URL: http://www.bath.ac.uk/i-see/images/PP%7B%5C_%7D-%7B%5C_%7DTon%7B%5C_%7DFijen%7B%5C_%7DFinal%7B%5C_%7DOct%7B%5C_%7D2017.pdf (visited on 03/05/2018).

Fischer, K., F. Besnard, and L. Bertling (2012). "Reliability-centered maintenance for wind turbines based on statistical analysis and practical experience". In: *IEEE Trans. Energy Convers.* 27, pp. 184–195. DOI: 10.1109/TEC.2011.2176129.

Francois, R. E. and G. R. Garrison (1982). "Sound absorption based on ocean measurements: Part I: Pure water and magnesium sulfate contributions". In: *J. Acoust. Soc. Am.* 72.3, pp. 896–907. DOI: 10.1121/1.388170.

Fred Olsen (2016). *Bolt Lifesaver at FabTest.* URL: http://fredolsen-energy.com/?nid=349842%7B%5C&%7Dlcid=1033%7B%5C&%7DWAF%7B%5C_%7DIsPreview=true (visited on 10/12/2017).

Fugro (2010). *SEAWATCH Mini II Buoy.* Tech. rep., p. 2. URL: https://www.fugro.com/docs/default-source/about-fugro-doc/ROVs/seawatch-mini-ii-buoy-flyer.pdf?Status=Master%7B%5C&%7Dsfvrsn=0 (visited on 04/04/2018).

Gaillet, L., H. Zejli, A. Laksimi, C. Tessier, M. Drissi-habti, and S. Benmedakhene (2009). "Detection by acoustic emission of damage in cable anchorage". In: *7th Int. Symp. Non Destr. Test. Civ. Eng. NDTCE-09.* Nates, France, p. 6. URL: https://hal.archives-ouvertes.fr/hal-00428635 (visited on 02/05/2018).

García Márquez, F. P., A. M. Tobias, J. M. Pinar Pérez, and M. Papaelias (2012). "Condition monitoring of wind turbines: Techniques and methods". In: *Renew. Energy* 46, pp. 169–178. DOI: 10.1016/j.renene.2012.03.003.

Garrett, J. K. (2015). "Interdisciplinary study into the effect of a marine renewable energy testing facility on the underwater sound in Falmouth Bay". PhD thesis. University of Exeter, p. 350.

Garrett, J. K., Ph. Blondel, B. J. Godley, S. K. Pikesley, M. J. Witt, and L. Johanning (2016). "Long-term underwater sound measurements in the shipping noise indicator bands 63 Hz and 125 Hz from the port of Falmouth Bay, UK". In: *Mar. Pollut. Bull.* 110, pp. 438–448. DOI: 10.1016/j.marpolbul.2016.06.021.

Garrett, J. K., M. J. Witt, and L. Johanning (2014). "Underwater sound levels at a wave energy device testing facility in Falmouth bay, UK". In: *UA2014 - 2nd Int. Conf. Exhib. Underw. Acoust.* Rhodes, Greece, pp. 309–314. URL: http://www.uaconferences.org/docs/Past%7B%5C_%7DProceedings/UACE2014%7B%5C_%7DProceedings.pdf (visited on 04/04/2018).

Gerbinet, S., S. Belboom, and A. Léonard (2014). "Life Cycle Analysis (LCA) of photovoltaic panels: A review". In: *Renew. Sustain. Energy Rev.* 38, pp. 747–753. DOI: 10.1016/j.rser.2014.07.043.

Al-Ghamd, M. A. and D. Mba (2006). "A comparative experimental study on the use of acoustic emission and vibration analysis for bearing defect identification and estimation of defect size". In: *Mech. Syst. Signal Process.* 20.7, pp. 1537–1571. DOI: 10.1016/j.ymssp.2004.10.013.

Gordelier, T., D. Parish, P. Thies, and L. Johanning (2015). "A novel mooring tether for highly-dynamic offshore applications; mitigating peak and fatigue loads via selectable axial stiffness". In: *J. Mar. Sci. Eng.* 3.4. DOI: 10.3390/jmse3041287.

Haikonen, K., J. Sundberg, and M. Leijon (2013). "Characteristics of the operational noise from full scale wave energy converters in the Lysekil project: Estimation of potential environmental impacts". In: *Energies* 6.5, pp. 2562–2582. DOI: 10.3390/en6052562.

HR Wallingford (2015). *Noise assessment tools for the marine renewable energy industry.* Tech. rep., p. 2. URL: http://www.bakerconsultants.co.uk/wp/wp-content/uploads/2015/12/HRW-brochure-high-res.pdf (visited on 01/01/2019).

IEA (2017). *World energy outlook 2017 executive summary.* Tech. rep., p. 13. URL: https://www.iea.org/publications/freepublications/publication/WEO%7B%5C_%7D2017%7B%5C_%7DExecutive%7B%5C_%7DSummary%7B%5C_%7DEnglish%7B%5C_%7Dversion.pdf (visited on 04/04/2018).

IPCC (2014). "Chapter 7: Energy systems". In: *Clim. Chang. 2014 Mitig. Clim. Chang.* URL: https://www.ipcc.ch/pdf/assessment-report/ar5/wg3/

ipcc%7B%5C_%7Dwg3%7B%5C_%7Dar5%7B%5C_%7Dchapter7.pdf (visited on 02/05/2018).

IRENA (2012). *Wind power*. Tech. rep. 5, pp. 223–242. DOI: 10.1016/B978-0-08-098330-1.00011-9.

James Li, C. and S. Y. Li (1995). "Acoustic emission analysis for bearing condition monitoring". In: *Wear* 185, pp. 67–74. DOI: 10.1016/0043-1648(95)06591-1.

Jasco Applied Sciences Ltd. (2014). *AMAR G2 user guide: Autonomous multichannel acoustic recorder user guide and technical information version 3.* Dartmouth, Canada.

Kaye & Laby Online (2005). "2.4.1 The speed and attenuation of sound, Version 1.0". In: *Tables Phys. Chem. Constants*. 16th Ed. URL: www.kayelaby.npl.co.uk (visited on 04/04/2018).

Kaye & Laby Online (2008). "2.2.1 Densities, Version 1.1". In: *Tables Phys. Chem. Constants*. 16th Ed. URL: www.kayelaby.npl.co.uk (visited on 04/04/2018).

Krewitt, W., K. Nienhaus, C. Kleßmann, C. Capone, E. Stricker, W. Graus, M. Hoogwijk, N. Supersberger, U. von Winterfeld, and S. Samadi (2009). "Role and potential of renewable energy and energy efficiency for global energy supply". In: *Clim. Chang. 18/2009*. Federal Environment Agency, Dessau-Roßlau, Germany, p. 336.

Lepper, P., E. Harland, S. Robinson, P. Theobald, G. Hastie, and N. Quick (2012). *Acoustic noise measurement methodology for the Billia Croo Wave Energy Test Site: ANNEX A: Summary of operational underwater noise tests for a Pelamis P2 system at EMEC May 2011*. Tech. rep., p. 39. URL: http://www.emec.org.uk/?wpfb%7B%5C_%7Ddl=67 (visited on 02/05/2018).

Lepper, P., V. Humphrey, M. Butler, and S. Robinson (2014). *Underwater acoustic monitoring at wave and tidal energy sites : Guidance notes for regulators*. Tech. rep. February. EMEC, p. 20. URL: http://www.emec.org.uk/?wpfb%7B%5C_%7Ddl=147 (visited on 04/04/2018).

Lewis, A., S. Estefen, J. Huckerby, K. s. Lee, W. Musial, T. Pontes, and J Torres-Martinez (2011). "Ocean energy". In: *IPCC Spec. Rep. Renew. Energy Sources Clim. Chang. Mitig.* Ed. by O Edenhofer, R Pichs-Madruga, Y Sokona, K Seyboth, P Matschoss, S Kadner, T Zwickel, P Eickemeier, G Hansen, S Schlömer, and C von Stechow. Cambridge University Press, pp. 497–533. ISBN: 978-1-107-02340-6.

Li, Y., S. Billington, C. Zhang, T. Kurfess, S. Danyluk, and S. Liang (1999). "Dynamic prognostic prediction of defect propagation on rolling

element bearings". In: *Tribol. Trans.* 42.2, pp. 385–392. DOI: 10.1080/10402009908982232.

Lu, B., Y. Li, X. Wu, and Z. Yang (2009). "A review of recent advances in wind turbine condition monitoring and fault diagnosis". In: *Power Electron. Mach. Wind Appl. PEMWA 2009 IEEE*. Lincoln, Nebraska, USA, p. 7. DOI: 10.1109/PEMWA.2009.5208325.

Lurton, X. (2002). *An introduction to underwater acoustics: Principles and applications*. Springer. ISBN: 9783540429678.

Luxmoore, J. F., S. Grey, D. Newsam, and L. Johanning (2016). "Analytical performance assessment of a novel active mooring system for load reduction in marine energy converters". In: *Ocean Eng.* 124. DOI: 10.1016/j.oceaneng.2016.07.047.

Maggi, A. and A. Duncan (2016). *AcTUP - Installation and user guide*. Tech. rep. Curtin University, p. 16. URL: http://cmst.curtin.edu.au/products/actoolbox.cfm (visited on 04/04/2018).

Malinka, C. E., D. M. Gillespie, J. D. J. Macaulay, R. Joy, and C. E. Sparling (2018). "First in situ passive acoustic monitoring for marine mammals during operation of a tidal turbine in Ramsey Sound, Wales". In: *Mar. Ecol. Prog. Ser.* 590, pp. 247–266. DOI: 10.3354/meps12467.

Marine Energy Corporation (2016). *Super watt wave catcher barges*. Tech. rep., pp. 1–6. URL: http://www.marineenergycorp.com/marine-energy/pdfs/super-watt-wave-catcher-barge-overview-052016.pdf (visited on 02/02/2018).

MarineTraffic (2016). *MarineTraffic: Global ship traffic inteligence*. URL: https://www.marinetraffic.com/ (visited on 11/09/2017).

Marquis, L., M. Kramer, and P. Frigaard (2010). "First power production results from the Wave Star Roshage wave energy converter". In: *3rd Int. Conf. Ocean Energy*. Bilbao, Spain. URL: http://wavestarenergy.com/sites/default/files/Wave%20Star%20Energy%20presentation%20ICOE%202010%20UPDATED%20After%20Conference.pdf (visited on 02/02/2018).

May, A. and D. McMillan (2013). "Condition based maintenance for offshore wind turbines: the effects of false alarms from condition monitoring systems". In: *ESREL 2013*. Amsterdam, The Netherlands. URL: https://strathprints.strath.ac.uk/id/eprint/54903 (visited on 04/05/2018).

Mba, D. and R. B. K. N. Rao (2006). "Development of acoustic emission technology for condition monitoring and diagnosis of rotating machines; bearings, pumps,

gearboxes, engines and rotating structures". In: *Shock Vib. Dig.* 38.1, pp. 3–16. DOI: 10.1177/0583102405059054.

McCormick, M. E. (2007). *Ocean wave energy conversion*. Dover Publications, p. 233. ISBN: 0486462455.

Merchant, N. D., K. M. Fristrup, M. P. Johnson, P. L. Tyack, M. J. Witt, Ph. Blondel, and S. E. Parks (2015). "Measuring acoustic habitats". In: *Methods Ecol. Evol.* 6.3. DOI: 10.1111/2041-210X.12330.

Merchant, N. D., M. J. Witt, Ph. Blondel, B. J. Godley, and G. H. Smith (2012). "Assessing sound exposure from shipping in coastal waters using a single hydrophone and Automatic Identification System (AIS) data". In: *Mar. Pollut. Bull.* 64.7. DOI: 10.1016/j.marpolbul.2012.05.004.

Monk, K. (2012). *A review of the Pico project 2010 to 2012 mistakes, milestones and the future*. URL: http://www.pico-owc.net/files/33/cms%7B%5C_%7De8432fb72c61c9066957124e5a420a05.pdf (visited on 02/02/2018).

Nedwell, J. and D. Howell (2004). "A review of offshore windfarm related underwater nosie sources". In: *COWRIE Rep. No. 544 R 0308*. URL: https://wild.nrel.gov/sites/default/files/howell.pdf (visited on 04/04/2018).

NewEnglandRopes (2010). *Splicing double braid [online video]*. URL: https://www.youtube.com/watch?v=UghIS9xdiDw (visited on 01/22/2018).

O'Connor, M., T. Lewis, and G. Dalton (2013). "Weather window analysis of Irish west coast wave data with relevance to operations & maintenance of marine renewables". In: *Renew. Energy* 52, pp. 57–66. DOI: 10.1016/j.renene.2012.10.021.

Park, J. M., W. G. Shin, and D. J. Yoon (1999). "A study of interfacial aspects of epoxy-based composites reinforced with dual basalt and SiC fibres by means of the fragmentation and acoustic emission techniques". In: *Compos. Sci. Technol.* 59.3, pp. 355–370. DOI: 10.1016/S0266-3538(98)00085-2.

Pazheri, F. R., M. F. Othman, and N. H. Malik (2014). "A review on global renewable electricity scenario". In: *Renew. Sustain. Energy Rev.* 31, pp. 835–845. DOI: 10.1016/j.rser.2013.12.020.

Pfaffel, S., S. Faulstich, and K. Rohrig (2017). "Performance and reliability of wind turbines: A review". In: *Energies* 10.1904. DOI: 10.3390/en10111904.

Polagye, B. (2017). "Challenges to characterization of sound produced by marine energy converters". In: *Mar. Renew. Energy*, pp. 323–332. DOI: 10.1007/978-3-319-53536-4.

Polagye, B., B. Van Cleve, A. Copping, and K. Kirkendall (2011). *Environmental effects of tidal energy development.* Tech. rep. U.S. Dept. Commerce, NOAA Tech. Memo. NMFS F/SPO-116, p. 186. URL: http://scholar.google.com/scholar?hl=en%7B%5C&%7DbtnG=Search%7B%5C&%7Dq=intitle:No+Title%7B%5C#%7D0 (visited on 11/13/2014).

Porter, M. B. (2011a). *The BELLHOP Manual and User's Guide (Preliminary Draft).* Tech. rep. Heat, Light, and Sound Research, Inc. La Jolla, CA, USA, p. 57.

Porter, M. B. (2011b). *The KRAKEN normal mode program.* Tech. rep. SACLANT Undersea Research Centre, p. 207. DOI: 10.1017/CBO9781107415324.004.

Porter, M. B. and Y. C. Liu (1994). "Finite-element ray tracing". In: *Theor. Comput. Acoust.* 2, pp. 947–956.

Price, E., A. Lees, and M. Friswell (2005). "Detection of severe sliding and pitting fatigue wear regimes through the use of broadband acoustic emission". In: *Proc. Inst. Mech. Eng. Part J J. Eng. Tribol.* 219.2, pp. 85–98. DOI: 10.1243/135065005X9817.

Price, T. J. (2005). "James Blyth — Britain's first modern wind power pioneer". In: *Wind Eng.* 29.3, pp. 191–200. DOI: 10.1260/030952405774354921.

Robinson, S. P. and P. A. Lepper (2013). *Scoping study: Review of current knowledge of underwater noise emissions from wave and tidal stream energy devices.* Tech. rep. The Crown Estate, p. 70. URL: http://www.thecrownestate.co.uk/media/151996/pfow-review-current-knowledge-underwater-noise-emissions-wave-and-tidal-stream-energy-devices.pdf (visited on 02/05/2018).

Robinson, S. P., P. A. Lepper, and R. A. Hazelwood (2014). *Good practice guide for underwater noise measurement. Good Practice Guide No. 133.* Tech. rep. The Crown Estate, p. 95. URL: http://www.npl.co.uk/upload/pdf/gpg133-underwater-noise-measurement.pdf (visited on 04/04/2018).

Rodríguez, A., S. D. Weller, J. Canedo, R. Rodríguez, V . González de Lena, P. R. Thies, and D. Parish (2015). "Performance comparison of marine renewable energy converter mooring lines subjected to real sea and accelerated loads". In: *Proc. 11th Eur. Wave Tidal Energy Conf.* Nates, France, p. 8.

Russel, K., E. Friis-Madsen, and H. C. Soerensen (2016). "Wave Dragon - 'Coldward and Stormward'". In: *Prog. Renew. Energies Offshore Proc. 2nd Int. Conf. Renew. Energies Offshore.* Ed. by C. Guedes Soares. Lisbon, Portugal: CRC Press. ISBN: 9781138626270.

Schijve, J. (2009). *Fatigue of structures and materials*. 2nd Editio. Springer, p. 621. ISBN: 9781402068072.

SEA (2011). *Wideband Spherical Sensor*. URL: https://www.sea.co.uk/media/1610/mardef-021-0717-wideband-spherical-sensor.pdf (visited on 04/15/2018).

Sims, R. E. H., R. N. Schock, J. Torres-Martínez, A. Adegbululgbe, J. Fenhann, I. Konstantinaviciute, W. Moomaw, H. B. Nimir, B. Schlamadinger, C. Turner, Y. Uchiyama, S. J. V. Vuori, N. Wamukonya, and X. Zhang (2007). "Energy supply". In: *Clim. Chang. 2007 Mitigation. Contrib. Work. Gr. III to Fourth Assess. Rep. Intergov. Panel Clim. Chang.* P. 72. ISSN: 0131-1646.

Sjolte, J. (2014). "Marine renewable energy conversion grid and off-grid modelling , design and operation". PhD thesis. Norwegian University of Science and Technology. ISBN: 9788232603503.

Tan, C. K., P. Irving, and D. Mba (2007). "A comparative experimental study on the diagnostic and prognostic capabilities of acoustics emission, vibration and spectrometric oil analysis for spur gears". In: *Mech. Syst. Signal Process.* 21.1, pp. 208–233. DOI: 10.1016/j.ymssp.2005.09.015.

Tandon, N. and S. Mata (1999). "Detection of defects in gears by acoustic emission measurements". In: *J. Acoust. Emiss.* 17.1-2, pp. 23–27.

The Engineering Toolbox (2010). *Densities of some common materials*. URL: http://www.engineeringtoolbox.com/density-materials-d%7B%5C_%7D1652.html (visited on 02/26/2016).

Thies, P. R. (2012). "Advancing reliability information for wave energy converters". PhD thesis. University of Exeter.

Thies, P. R., L. Johanning, I. Bashir, T. Tuk, M. Tuk, M. Marta, and S. Müller-Schütze (2016). "Accelerated reliability testing of articulated cable bend restrictor for offshore wind applications". In: *Int. J. Mar. Energy* 16. DOI: 10.1016/j.ijome.2016.05.006.

Thies, P. R., L. Johanning, and G. H. Smith (2011). "Towards component reliability testing for marine energy converters". In: *Ocean Eng.* 38.2-3, pp. 360–370. DOI: 10.1016/j.oceaneng.2010.11.011.

Thies, P., L. Johanning, and T. Gordlier (2013). "Component reliability testing for wave energy converters: Rationale and implementation". In: *10th Eur. Wave Tidal Energy Conf.* Aalborg, Denmark. URL: http://hdl.handle.net/10871/15923 (visited on 02/05/2018).

Thorpe, T. W. (1999). *A brief review of wave energy*. Tech. rep., p. 200. URL: http://www.homepages.ed.ac.uk/shs/Wave%20Energy/Tom%20Thorpe%20report.pdf (visited on 04/04/2018).

Tidal Energy Today (2016). *Seatricity deploys Oceanus 2*. URL: https://tidalenergytoday.com/2016/05/18/seatricity-deploys-oceanus-2/ (visited on 02/02/2018).

Tougaard, J. (2015). "Underwater noise from a wave energy converter is unlikely to affect marine mammals". In: *PLoS One* 10.7, p. 7. DOI: 10.1371/journal.pone.0132391.

Tougaard, J., P. T. Madsen, and M. Wahlberg (2008). "Underwater noise from construction and operation of offshore wind farms". In: *Bioacoustics* 17.1-3, pp. 143–146. DOI: 10.1080/09524622.2008.9753795.

Toutountzakis, Ti. and D. Mba (2003). "Observations of acoustic emission activity during gear defect diagnosis". In: *NDT E Int.* 36.7, pp. 471–477. DOI: 10.1016/S0963-8695(03)00063-X.

Twidell, J. and A. D. Weir (2006). *Renewable energy resources*, p. 601. ISBN: 0419253300.

Tyagi, V. V., N. A. A. Rahim, N. A. Rahim, and J. A. L. Selvaraj (2013). "Progress in solar PV technology: Research and achievement". In: *Renew. Sustain. Energy Rev.* 20, pp. 443–461. DOI: 10.1016/j.rser.2012.09.028.

UNFCCC (2015). *Paris Agreement*. Tech. rep., p. 32. URL: http://unfccc.int/paris%7B%5C_%7Dagreement/items/9485.php (visited on 02/05/2018).

Walsh, J., I. Bashir, J. K. Garrett, P. R. Thies, Ph. Blondel, and L. Johanning (2017a). "Monitoring the condition of marine renewable energy devices through underwater acoustic emissions: Case study of a wave energy converter in Falmouth Bay, UK". In: *Renew. Energy* 102, pp. 205–213. DOI: 10.1016/j.renene.2016.10.049.

Walsh, J., I. Bashir, P. R. Thies, L. Johanning, and Ph. Blondel (2016). "Modelling the propagation of underwater acoustic emissions for condition monitoring of marine renewable energy". In: *Prog. Renew. Energies Offshore Proc. 2nd Int. Conf. Renew. Energies Offshore*. Ed. by C. Guedes Soares. CRC Press, pp. 821–826. ISBN: 9781138626270.

Walsh, J., Ph. Blondel, J. K. Garrett, P. R. Thies, B. J. Godley, M. J. Witt, and L. Johanning (2017b). "Acoustic life cycle assessment of offshore renewables—Implications from a wave-energy converter deployment in Falmouth Bay, UK". In: *UACE 2017*. Skiathos, Greece.

Wang, L. S., K. Heaney, T. Pangerc, P. D. Theobald, S. P. Robinson, and M. A. Ainslie (2014). *Review of underwater acoustic propagation models.*

Waters, S. and G. Aggidis (2016). "A world first: Swansea Bay tidal lagoon in review". In: *Renew. Sustain. Energy Rev.* 56, pp. 916–921. DOI: 10.1016/j.rser.2015.12.011.

WavePiston (2013). *WavePiston MK I test at Nissum Bredning.* Tech. rep., pp. 1–15. URL: http://wavepiston.dk/download/Nissum%7B%5C_%7Dtest%7B%5C_%7Dreport.pdf (visited on 02/02/2018).

Weller, S. D., P. Davies, A. W. Vickers, and L. Johanning (2014). "Synthetic rope responses in the context of load history: Operational performance". In: *Ocean Eng.* 83, pp. 111–124. DOI: 10.1016/j.oceaneng.2014.03.010.

Wello (2017). *The penguin technology.* URL: https://wello.eu/the-penguin/technology/ (visited on 11/19/2017).

Wenz, G. M. (1962). "Acoustic ambient noise in the ocean: Spectra and sources". In: *J. Acoust. Soc. Am.* 34.12. DOI: 10.1121/1.1909155.

Whittaker, T., D. Collier, M. Folley, M. Osterried, and A. Henry (2007). *The development of Oyster - A shallow water surging wave energy converter.* URL: https://pure.qub.ac.uk/portal/en/publications/the-development-of-oyster--a-shallow-water-surging-wave-energy-converter(1c58a0d9-9d3e-4b70-9ac3-0631ebdb5ea7).html (visited on 02/05/2018).

Wilson, B., P. A. Lepper, C. Carter, and S. P. Robinson (2014). "Rethinking underwater sound-recording methods to work at tidal stream and wave energy sites". In: *Mar. Renew. Energy Environ. Interact. Humanit. Sea.* Ed. by M. A. Shields and A. I. L. Payne. Humanity and the Sea. Dordrecht: Springer Netherlands. Chap. 9, pp. 111–126. DOI: 10.1007/978-94-017-8002-5.

World Energy Council (2007). *2007 survey of energy resources.* URL: https://www.worldenergy.org/wp-content/uploads/2012/10/PUB_Survey-of-Energy-Resources_Interim_update_2009_WEC.pdf (visited on 04/05/2018).